C02018: Doctor of Philosophy
CRICOS Code: 036570B
January 2021

Multi-mode Stroke Rehabilitation System Using Signal-Controlled Human Machine Interface

Kairui Guo

School of Biomedical Engineering
Faculty of Engineering and Information Technology
University of Technology Sydney
NSW - 2007, Australia

Multi-mode Stroke Rehabilitation System Using Signal-Controlled Human Machine Interface

A thesis submitted in partial fulfilment of the requirements for the degree of

Doctor of Philosophy
in
Biomedical Engineering

by

Kairui Guo

to

School of Biomedical Engineering
Faculty of Engineering and Information Technology
University of Technology Sydney
NSW - 2007, Australia

January 2021

Abstract

Stroke has become one of the most devastating health problems due to post-stroke disabilities. Rehabilitation is the necessary process for stroke survivors following discharging from the intensive care units. Of those stroke survivors, 82% of them cannot regain full arm functions, in turn, their daily lives are dramatically affected since they cannot perform daily activities such as eating, dressing, or taking showers independently. In recent years, technology-assisted rehabilitation is introduced using functional electrical stimulation, robotic devices, and virtual reality. Although technology-based systems have demonstrated advantages in early research, there are numerous aspects needed to be further investigated to ensure more stable physiological analysis of the affected upper limb and broader usage in the clinical field.

This thesis proposes a complete upper-limb rehabilitation system with multimodal motor function training using neuroelectric signals. First, motion intent recognition and emotion classification is analysed using electroencephalogram (EEG) signal. The EEG-based motion intent recognises the desired motion of stroke patients before the motion is executed. At the same time, emotions of the patients are monitored to ensure safety while the patients are doing exercises. Novel designed classifiers, including hybrid Support Vector Machine and hidden Markov Model and a Fuzzy-based Support Vector Machine, are demonstrated. The EEG-based classifiers are able to achieve 78% accuracy using novel machine learning algorithms, which improves 10-15% comparing with the classical methods.

Second, electromyography (EMG) is one of the most frequently used parameters since it reveals the electrical activity of a specific muscle that is related to the muscle force. In this thesis, EMG connectivity analysis using multivariable autoregression is proposed to analyse the inter-relationship between muscles. Using EMG connectivity analysis, the paretic arm is considered as the abnormal system, and the non-paretic arm is the reference side. The rehabilitation strategy is to control the abnormal system to generate identical EMG connectivity patterns as the reference side.

After integrating the layers controlled by physiological signals, a wearable exoskeleton is built as a rehabilitation device by mimicking human-like movements. The exoskeleton guides and supports rehabilitation movements based on the patients' physiological signals. After consolidating with physiotherapists and stroke patients, features such as wireless communication, low-power consumption, touch screen user interface, etc., are implemented to promotes the ease-of-use and expand the possible applications in the clinical field. At the moment, a clinical study that has recruited nine stroke patients is

conducted regarding outcome assessment and rehabilitation prediction. Followed by this study, the developed exoskeleton will be evaluated on stroke patients.

Author's declaration

I, *Kairui Guo* declare that this thesis, submitted in partial fulfilment of the requirements for the award of Doctor of Philosophy, in the *School of Biomedical Engineering*, *Faculty of Engineering and Information Technology* at the University of Technology Sydney, Australia, is wholly my own work unless otherwise referenced or acknowledged. In addition, I certify that all information sources and literature used are indicated in the thesis. This document has not been submitted for qualifications at any other academic institution. This research is supported by the Australian Government Research Training Program.

Production Note:

SIGNATURE: Signature removed prior to publication.

[Your Name]

DATE: 13th January, 2021

PLACE: Sydney, Australia

Acknowledgments

I would first like to express my sincere gratitude to my primary supervisor A.Prof Steven Su. None of these work presented in this thesis can be achieved without his supports. I could never forget the patient and enlightening teaching and discussions we had. The domestic and international collaboration opportunities Prof Su brought have made this project become much more productive.

I wish to express my heartfelt thanks to my co supervisor Prof Joanne Tipper for her continuous support on my research throughout the years. Her experiences in collaboration with medical facilities and leadership in managing research teams have inspired me in many ways.

I would also like to thank my external supervisor A.Prof Michael Lee. He showed me the professionalism as a member of front-line medical staff. His views on the demands of the patients and communication between hospitals and research centres have made this project avoid many obstacles.

Many thanks to the School of Biomedical Engineering, Faculty of Engineering and Information Technology. The friendly and helpful staffs at the school create a great environment for the research study. The resources provided by the school and the faculty is the key of the success in the research.

I am truly appreciate the efforts from our international collaborators: Sun Yat-sen University, Shanghai Jiao Tong University and HEALTH Rehabilitation Hospital. Although we are physically thousands of kilometres away, the willingness to help patients brings us close.

I would take this opportunity to thank the funding bodies: the Australia-China Joint Institute for Health Technology and Innovation, the Lam Yuen Trust and the Australia China Economics Trade and Culture Association, John Heine Memorial Foundation International, and UTS Techcelerator. They supported my research journey not only financially but also by believing this project and giving me the opportunities to present my research to more people.

I would like to thank my colleagues for their encouragement and making the workplace a fun place to be.

Last but not least, I am grateful for having my wife and my family to support my research journey.

List of Publications and Awards

Publications :

1. K. Guo, et al., 'EEG-based Emotion Classification Using Innovative Features and Combined SVM and HMM Classifier', IEEE EMBC 2017. (Chapter 2)
2. K. Guo, et al., 'EMG-Based Robot-Assisted Stroke Rehabilitation For Upper-limb Impairment,' ABEC 2018, Australia, 2018, p. 9. (Chapter 3)
3. K. Guo, et al., 'A Hybrid Fuzzy Cognitive Map / Support Vector Machine Approach for EEG-based Emotion Classification Using Compressed Sensing', International Journal of Fuzzy Systems, S.I.: Fuzzy System Big Data Mining, 2019. (Chapter 2)
4. K. Guo, et al., 'A Hybrid Physiological Approach of Emotional Reaction Detection Using Combined FCM and SVM Classifier', IEEE EMBC 2019. (Chapter 2)
5. K. Guo, et al., 'Puzzle-based Upper Limb Functional Electrical Stimulation Strategy Using EMG Connectivity Analysis', IEEE EMBC 2020. (Chapter 3)

Awards :

1. Lam Yuen Trust and ACETCA Medical Research Award at University of Technology Sydney in 2017
2. DST Group and UTS - Student Innovation Competition, Emerging Disruptive Technology Assessment Symposium 2017
3. UTS, FEIT HDR Collaboration Experience Award 2019
4. 2019 John Heine Memorial Foundation International PhD Prize
5. 2020 UTS Techcelerator, Most Feasible Prototype Award

Table of Contents

List of Figures

List of Tables

Table **Page**

CHAPTER 1

Introduction and Literature Review

1.1 Introduction: Human Brain, Neural Signals and Measurements

The human brain is arguably the most important organ as it processes the information received from the body and the environment, and react to it internally and externally. Serving as the command centre for the body, the brain has been the core of biomedical-related study for centuries, and yet there is much we do not thoroughly understand. Nevertheless, to begin exploring the brain's intricate network, we must gain insight into the brain's structure.

The brain sits inside the cranium that is the bone structure under the scalp. The eight cranial bones and fourteen skeleton bones protect the brain from external traumatic injuries. Anatomically, the brain is divided into the brain stem, the cerebellum, the hypothalamus, the thalamus, and the cerebrum [1]. Furthermore, the different parts of the brain are closely connected during information processing and transferring, which is the nature of brain-related research difficulties. In this thesis, two issues are emphasized:

1 . How to examine and reflect the dynamic changes of the brain activity using non-invasion techniques? Moreover, with practical concerns such as cost, portability, comfortableness, etc., how to measure and decide the adequate spatial and temporal resolution in brain signal processing?

2 . How to calculate the interconnection qualitatively and quantitatively between different regions of the brain? In addition, how to accurately interpret the relationship (anatomically and functionally)?

The following paragraphs are presenting the fundamentals of brain anatomy related to the above issues. By understanding the biomedical background, we are able to gain the perspective from physiological studies, which is essential in comprehending the physiological basis of the target medical conditions, acquiring the requirements from patients and doctors, and filling the gap between medicine and engineering. Later in this chapter, we will discuss in detail the approaches to resolving the two challenges mentioned above.

First, the spatial property is one of the keys to revealing the mystery of how the brain works. The brain is analysed from three planes, coronal, sagittal and horizontal shown in Figure 1.1. Different methods are applied to discover the property in each plane and section. Here, we mainly focus on the sagittal plane. As this study is concentrating on both cognitive feedback and motor functions, the cerebral cortex becomes the centre of this research. The cerebral cortex is the folded section on the outer layer of the brain.

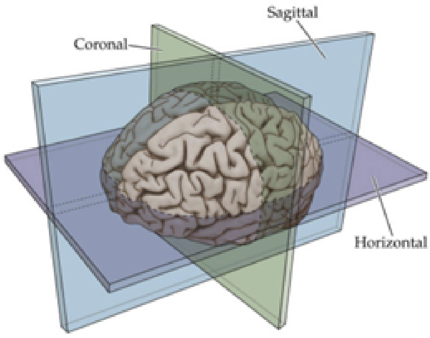

Figure 1.1: The anatomic planes of the human brain

(See: [2])

It is made of grey matter that contains millions of neurons to allow us to speak, read, and move around. The cerebral cortex consists of four lobes, as Figure 1.2 highlighted in different colours. Commonly, the frontal lobe is considered the processor for emotional reaction and controlling body movements. Parietal lobe oversees the general senses. Temporal lobe consists of the olfactory and auditory areas. Occipital lobe is responsible for visual function and spatial cognition. In this thesis, both frontal and occipital are critical in rehabilitation training. However, as we discussed earlier, the interconnection shall not be neglected, which is why other lobes are also included in the research's primary stage.

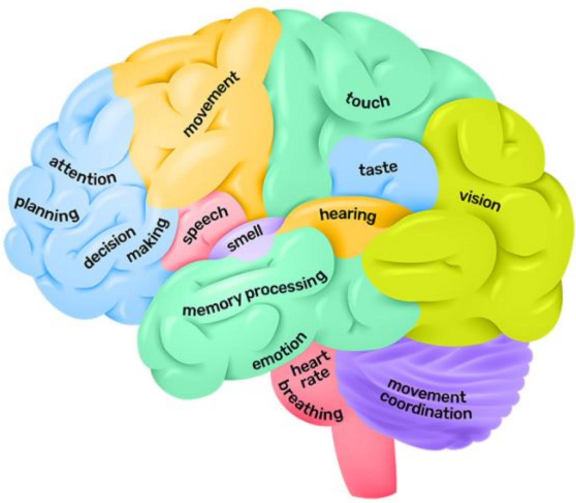

Figure 1.2: Lobes of the human brain and their functions

(See:[3])

Secondly, as we zoom into the function of emotion and cerebral cortex, it is essential to discuss further the connection between the prefrontal cortex (PFC), limbic system and the definition of human emotions. The PFC supports cognitive functions, including cognitive, affective, and integrated social behaviours. Under the frontal cortex shown in Figure 1.3, the deeper structure involving the thalamus, hypothalamus and basal ganglia form an emotion processing site, called limbic system [4]. The limbic system is commonly referred to as the functional anatomical system closely related to emotions, memory, and pathologically to psychotic conditions and cognitive defects [5].

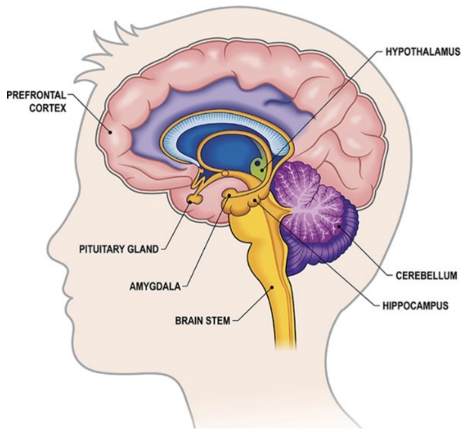

Figure 1.3: The limbic system of the human brain

(See:[4])

With the understanding of brain anatomy, we next briefly discuss the role of emotions in biomedical engineering research. To start, one must define 'emotion', which is something we experience every day, every minute and every second, and yet 'felt but cannot be explained'. In psychology, one of the broadly accepted definitions of emotion is 'episodic, relatively short-term, biologically based patterns of perception, experience, physiology, action, and communication that occur in response to specific physical and social challenges and opportunities' [6]. This definition demonstrates two critical properties of emotion, fast-changing and compounded, challenging in biomedical engineering projects. The fast-changing property presents a time-variant system, and the complex nature exposes the challenge for expressing personal and conceptual ideas using quantitative methods. Various biomedical signal processing techniques and advanced machine learning algorithms are implemented and further explained in later sections of this chapter to overcome such difficulties.

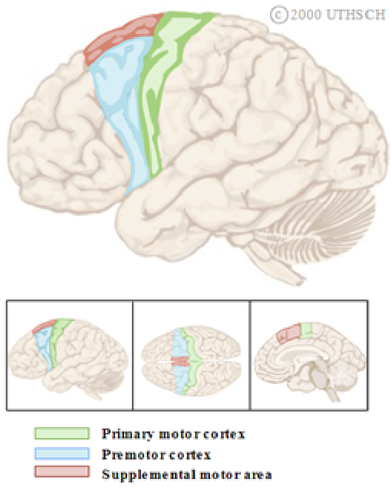

Figure 1.4: The motor cortex of the human brain

(See:[7])

Lastly, this thesis targets motor skills recovery during rehabilitation; therefore, the motor cortex plays an important role. In Figure 1.4, the motor cortex comprises primary motor cortex (green), premotor cortex (red), and supplemental motor area (green). Primary motor cortex controls simple voluntary movements [8], and the rest of the motor cortex administrates more complex functions than the primary motor cortex. Furthermore, primary cortex determines the force, direction, and speed of the movement. As the name suggested, premotor cortex selects the appropriate movement before the execution; whereas the supplemental motor area arranges the sequence of a complex movement based on experiences. Overall, each of the sections is essential to biomedical related studies, especially to rehabilitation sessions. The movement's complexity will vary at different recovery stages; therefore, by understanding the area that needs to be activated and stimulated, the recovery efficiency could be further improved.

After clearing the significance and identifying the challenges in anatomic analysis, we also need to specify the brain research's engineering aspects. In the first chapter, we begin with the most fundamental element of the analysis, data selection.

1.1.1 Computed Tomography and Positron Emission Tomography

Computed tomography (CT) uses a circular-shaped x-ray source (shown in Figure 1.5) to generate images of cross-sections of the body. Then, these cross-section images are organised together to form a three-dimensional image to understand the target area better. Comparing with traditional x-ray images, this method presents a higher spatial resolution. Also, positron emission tomography (PET) is used to measure the body's metabolic activity. PET combines nuclear and biochemical medicine to reveal the information at the cellular level. CT coupled with PET, shown in Figure 1.6, can present the metabolic processes of the brain structures embedded deeply under the frontal and temporal lobes [9].

Figure 1.5: An example of a computed tomography machine

(See:[10])

In brain-related conditions, PET/CT is a widely used neuroimaging technique in practical due to its speed, availability, and low-cost [11], which is commonly considered as an early diagnosis test. PET/CT's limitations are first keeping the patient at a stationary position during the acquisition that can take 10 – 20 minutes. Movements during this period reduce the resolution of the image dramatically. Furthermore, attenuation correction of the photons emitted by the patient's brain and position can also impact the quality of the measure [9]. In stroke rehabilitation training, patients are hardly in a stationary position for an extended period; therefore, the dynamic requirement of this thesis prevents us from choosing this neuroimaging technique. Another concern of such method is that these methods are nuclear medicine imaging. The radiation exposure for patients and health care workers can be a severe risk [12] if we are going to use these methods for long-term rehabilitation treatment. In this thesis, PET/CT is used for emergency evaluation of acute stroke.

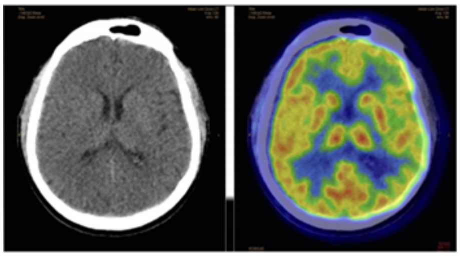

Figure 1.6: CT (left) and PET/CT (right) images of the human brain

(See:[9])

1.1.2 Magnetoencephalography

Magnetoencephalography (MEG) measures the magnetic fields generated by the electrical activity of neurons [13]. The magnetic fields generated in the brain is small (femto-tesla to pico-tesla), and the collection process can be interfered by the earth's relatively stronger magnetic field [13]. To overcome such issue, as demonstrated in Figure 1.7, MEG machine uses superconductors in an extremely low-temperature environment to pick up the small signal. Also, the acquisition is taken in a magnetically shielded room to reduce noises.

Figure 1.7: An example of the MEG machine

(See:[13])

MEG has a high temporal resolution as it can reach 1000 Hz sampling frequency. The cortical activity patterns can be clearly presented as illustrated in Figure 1.8. Nevertheless, as the restrictions stated above, the preparation and collection time is usually up to 2 hours. Together with the high cost of the overall set-up, this method becomes inappropriate for movement-induced analysis.

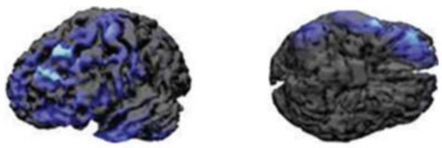

Figure 1.8: MEG scan images of the human brain

(See:[14])

1.1.3 Magnetic Resonance Imaging and Functional Magnetic Resonance Imaging

Since the early 1980s, Magnetic Resonance Imaging (MRI) has become one of the most fascinating and innovative neuroimaging techniques in recent years [15]. First, we shall understand the basis of MRI technology and its associated technique, function Magnetic Resonance Imaging (fMRI). MRI machine generates a strong magnetic field that changes the body tissue's energy state at the atomic level. Then, a pulse of magnetic energy is introduced that causes the atoms to resonate. After the pulse is removed, the atoms return to lower energy level and release the energy. This energy emitted and time taken to restore to the original state is the primary information collected, further analysed later to determine the type of tissue. In turn, MRI presents a clear anatomical structure of the targeted area, whereas fMRI focuses on the metabolic function, which is measured based on the blood oxygenation level dependent (BOLD) effect. The fMRI machine processes the difference between oxygenated and deoxygenated haemoglobin.

Nowadays, fMRI is combined with conventional MRI to generate a standard brain image in both clinical and research fields. First, the MRI image is formed by stacking the signal slices; then, fMRI is taken and placed on the MRI image. Therefore, both the anatomic structure in high spatial resolution and metabolic activities are illustrated in the same image. Since the invention and recent development of software and hardware, fMRI technology shows an increasing number of studies in almost all brain-related studies [17]. This trend is due to many behavioural and observational theories in cognitive research are further explored using the data-based approach. Nevertheless, as the diagram of MRI set-up shown in Figure 1.9, fMRI requires the participant to stay at specific positions in a specialised confined space that can cause anxiety and claustrophobia for some patients. This exposes a serious concern when we are going to study a dynamic

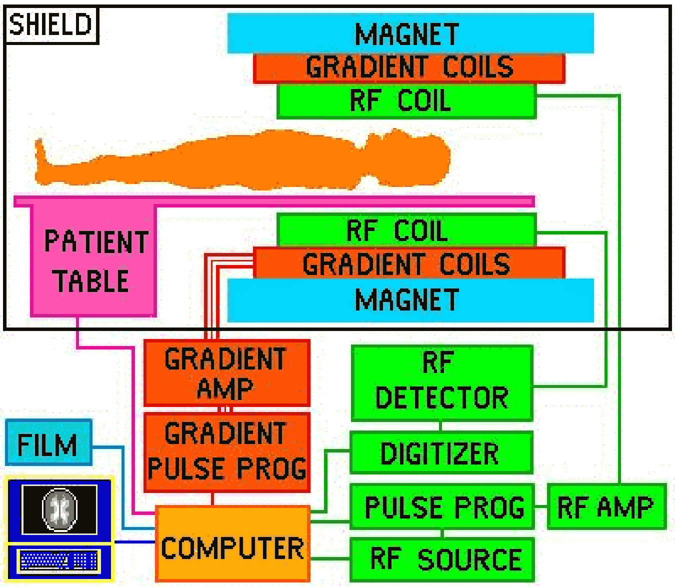

Figure 1.9: An overview of the MRI system

(See: [16])

motor system on post-stroke patients. Another challenge using fMRI method is the issue of cost. In Australia, post-stroke rehabilitation is often conducted at the rehabilitation clinics, where equipment such as fMRI systems cannot be installed due to the lack of professional human resources, specialised facilities, and financial capabilities. In the pilot studies and clinical trials involved in this thesis, fMRI is used in the hyperacute, acute and subacute phase to examine the brain's infarcted tissue for diagnosis purposes [15]. This information is later used to categorise the experiment participants into more detailed groups for further analysis.

1.1.4 Functional Near-infrared Spectroscopy

A new approach, functional near-infrared spectroscopy (fNIRS), using NI light to detect the concentration changes in brain-related biomedical engineering research is proposed since the early 2000s [18]. When the photons from the NI wave passes through the oxygenated and deoxygenated haemoglobin, fNIRS sensors pick up this information to determine the blood flow changes over time. One example of the fNIRS images is shown in Figure 1.10, where the activation intensity and cortical oxygen level are presented using a colour bar and a simple line chart.

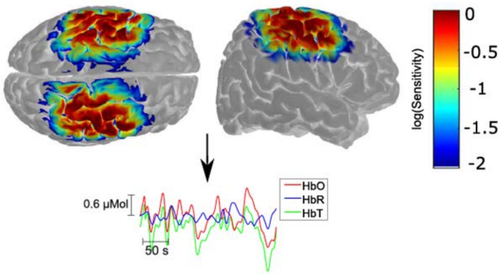

Figure 1.10: An fNIRS image showing the oxygenated and deoxygenated haemoglobin levels

(See: [19])

This new approach demonstrates several benefits of stroke-related cognitive and motor function studies. Since fNIRS uses the optical imaging technique, it would not induce health risk compared to nuclear imaging methods (e.g., CT and PET). This method has also shown high feasibility in cognitive and motor function studies [20]. The low cost, easy to use, and portable properties are also suitable for fundamental and innovative research projects. We are currently conducting a joint clinical study between Australia and China, shown in Figure 1.11, to investigate the cognitive and learning rehabilitation for post-stroke patients using fNIRS. Nonetheless, at around 100 Hz, the sampling frequency would create a problem for event-related potential research, often used in the cognitive analysis. Therefore, fNIRS is often used in combination with high temporal resolution methods such as electroencephalography (EEG) introduced in the next section.

Figure 1.11: An example of fNIRS used in a stroke-related clinical study

1.2 Electroencephalography

In 1924, Hans Berger invented the electroencephalography technique and applied in humans [21]. The electroencephalogram detects the electrical variation from the neural activities generated at the cerebral cortex. The basis of EEG signal is from the understanding of the neuronal electrochemical processes. As the basic unit for the human nervous system, neurons undertake six stages from a complete neuron stimulation cycle shown in Figure 1.12. At the resting stage, the member stays at the resting potential at around -70 millivolts. After a stimulus is presented, the graded potential is generated, which opens the sodium or potassium channels. Next is the action potential stage, where depolarisation occurs after the threshold potential is reached. At this stage, the potential difference can be around 100 millivolts. Then, to restore the polarisation of the membrane, repolarisation brings down the member potential to a value that is lower than the previous resting potential. This is called hyperpolarisation, and it is followed by refractory period, where stimulus is absent, and the member prepares for the next circle by returning to the resting potential. By understanding the basis of the signal that EEG collects, we can optimise the design the EEG machine to collect higher quality signals.

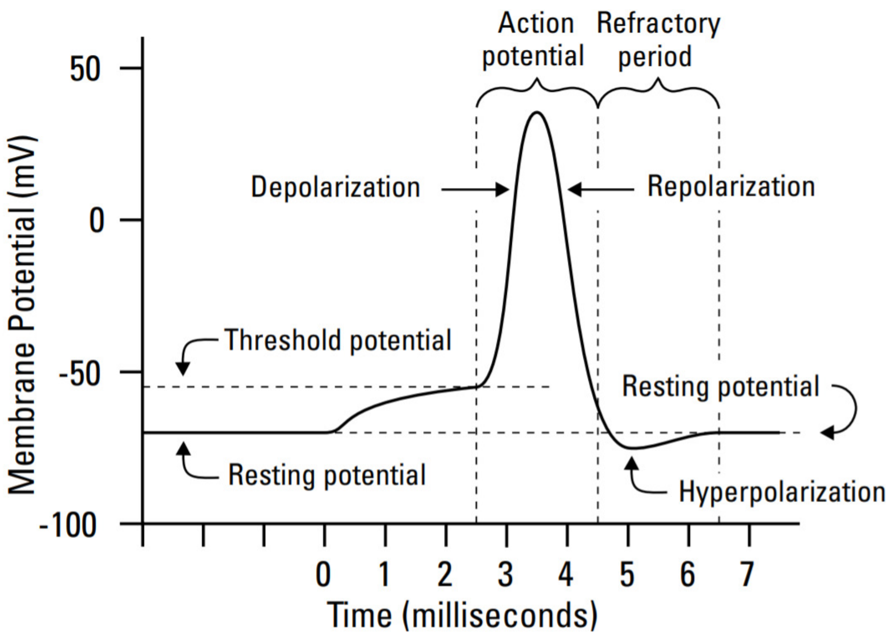

Figure 1.12: The cycle of a neuron's membrane potential

(See:[22])

EEG hardware design is usually discussed under three aspects: recording electrodes and electrode placement. Ag-AgCl electrode demonstrate excellent DC-stability, superior low frequency noise and lowest resistance. This result is in line with the reversible chemical reaction that is responsible for conductive charge transfer:

$$Ag(s) + Cl^{-}(aq) \rightleftharpoons AgCl(s) + e^{-} \tag{1.1}$$

Since EEG has been criticised because of its poor spatial resolution, the placement of the electrodes is even more important to reduce the negative impact. The international 10-20 system is a widely used method to provide a full coverage of the scalp. It uses the bony landmarks to construct lines of sensors in prefrontal, frontal, central, parietal, occipital, and auricular regions shown in Figure 1.13. The standard 10-20 system usually contains 21 seeds including the reference nodes (A1 and A2).

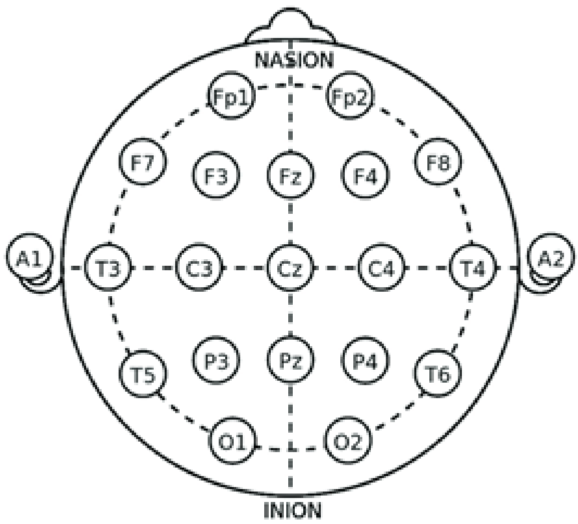

Figure 1.13: The international 10-20 system for EEG sensor placement
(See:[23])

Nowadays, more EEG devices are making innovative sensor placement designs based on the needs. For medical research projects, there are the 10-10 system and other arrangements that increases the number of sensors to 32, 64 and 128 to improve the spatial resolution and detect extremely localised electrical potentials. Whereas some devices focus on the usability and portability of the device. These devices allow the users to move around by applying wireless transmission and reduced number of sensors (e.g. 14 sensors for Emotiv Epoc X). Considering the broad variety of the applications that can provide, both approaches have been tested under different scenarios in this thesis.

Due to the rapid development of the hardware and software of EEG analysis, another phrase,‘Brain-Computer Interface’ (BCI), has become one of most heated topics in both biomedical research and industrial applications.On the 28th of August 2020, Elon Musk's Neuralink chip tested live in pig brain. This news has drawn a lot of attention from the public on how much of potential that the brain research could achieve. In biomedical engineering research, BCI is defined as a computer-based system that collects physiological signals from the brain, processes them, then uses the information gathered as a series of commands to instruct the computer to perform desired tasks[24]. In another word, the brain's signal does not travel to the muscles as human beings normally do. The signal goes to a computer system and is carried out by external tools. The first type of BCI in biomedical engineering is around prostheses development in the early 1970s. However, the development was slow since the hardware and software capabilities. After 2000, reduced cost on the hardware and fast improvement on signal processing and machine learning techniques provided a resourceful environment for BCI to grow. Overall, BCI has been applied in communication, environmental control, assistive devices, and rehabilitation shown in Figure 1.14. This thesis discusses BCI applications in emotion recognition and motor imagery in stroke rehabilitation.

Since the invention, EEG has dramatically developed sensor quality, communication, and signal processing techniques for biomedical engineering projects. The close connection to mechatronics permits hardware improvement over the last few decades. The trend on machine learning and big-data analysis allow EEG research to take a huge leap in noise reduction, feature selection and pattern recognition.

Given the impressed sensitivity in showing rapid changes in neurological reactions, EEG has also been implemented for several clinical practices. The analysis of the neuro-electrical abnormality has produced significant impact on epilepsy detection [26], Alzheimer's disease [27], sensory processing disorders [28], etc.

EEG has been applied in stroke studies for several decades. At first, EEG was mainly used as a diagnostic tool during the acute phase [29]. With the development of CT/PET and fMRI techniques, research projects are shifting EEG into post-stroke rehabilitation stage. EEG can monitor the changes continuously throughout the rehabilitation training. Moreover, several studies examined the differences between the normal and affected hemisphere to gain more information on how the brain undergoes the recovery process after stroke [29] [30].

In this thesis, EEG has been selected as the primary neuroimaging source for brain research for stroke rehabilitation. The reasons are mainly threefold.

First, for pilot studies and clinical trials, EEG is collected using a non-invasion

Figure 1.14: Examples of BCI Applications

(See: [25])

headset that permits the patient to perform rehabilitation training in a specific range and without environment constraints (such as a magnetically shielded room for MEG scan).

Second, high temporal resolution EEG provided, advanced signal processing and machine learning skills allow continuous monitoring and accurate detection and prediction of the brain activities.

Finally, considering the feasibility of the experiment and future clinical applications using our findings in facilities such as rehabilitation clinics or even at home, EEG is a reasonable choice due to ease-of-use, low-risk, and low-cost features. Chapter 2 will discuss how EEG is acquired and the BCI applications using EEG.

1.3 Electromyogram

Currents generated by muscles fibres is a tiny but important signal that can be extracted and analysed for various biomedical studies such as motor neuron disease, neuropathies, or muscular dystrophies. This electrical current is called electromyogram (EMG), which is one of the most important physiological signal studying the human motor functions. Since EMG directly measures the activity of the muscle, it provides the information of how the commands from the motor cortex is executed on the lower end. Two critical properties have made EMG become one of the most significant signal regarding motor function studies [31]. First, EMG is generated before the execution. For upper limb muscles, the EMG signal can be detected 40ms ahead. Secondly, there is a close interaction between EMG signal and EEG signal from the brain. This finding lays the foundation for future applications that would combine signals from different sources. It also presents a promising basis for stroke rehabilitation studies as both the muscles and the brain are investigated at the same time.

To understand how EMG can be used in this thesis, it is necessary to learn the the physiological basis of EMG demonstrated in Figure 1.15. The command of muscle activity is originated from the motor cortex in the brain. The hierarchical structure of the system passes the information from the brain to spinal cord, then to the skeletal muscles. Within the skeletal muscle, the smallest unit is called motor unit (MU), where motoneuron and muscle fibres are presented. The number of MUs per muscle in humans may range from about 100 for a small hand muscle to 1000 or more for large limb muscles.

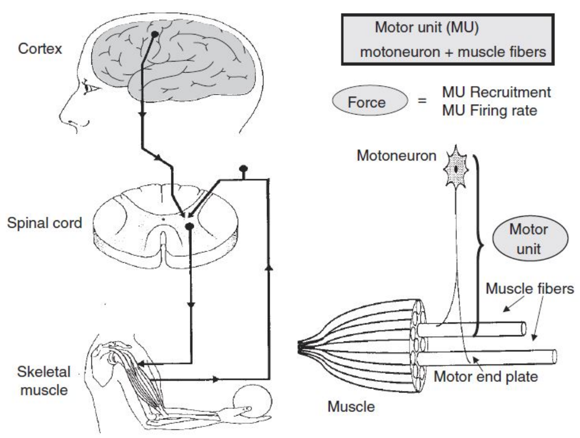

Figure 1.15: A schematic representation of motor control mechanisms

(See:[32])

During muscle contractions, both speed and force can change the motor units recruitment and the activation frequency. The electrical signal detected is based on the total number of MU involved and the activation frequency. Therefore, EMG can directly reflect how strong and how fast the target muscle contracts. It is also important to notice that these two factors are not the only sources that can change EMG signal. Muscle fibre potential, MU discharge synchronisation and fatigue level can also influence EMG patterns.

There are mainly two types of EMG acquisition methods, needle EMG and surface EMG. Needle EMG, illustrated in Figure 1.16, is usually used in clinical practices where clinicians are trying to diagnose any possible muscular skeletal disorders. During a needle EMG, a needle electrode inserted directly into a muscle. This invasion approach is able to gather clearer and faster information from the muscle, however, the main limitation is that invasive EMG requires professional trainings to operate. It is also not portable since the patients usually need to stay at certain position without the freedom to move.

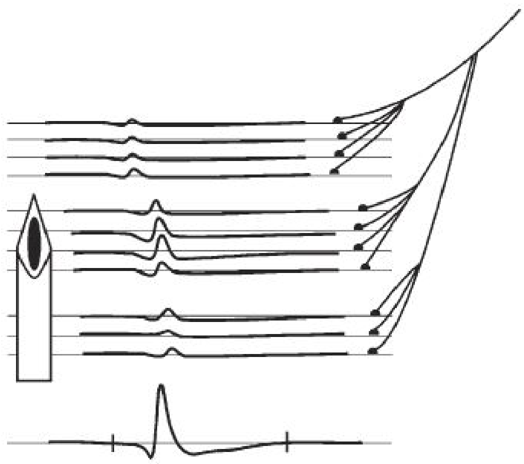

Figure 1.16: An example of needle EMG

(See:[31])

The other approach is surface EMG (sEMG). This approach is more common in research and engineering studies as it is non-invasive and does not require medical doctors to perform signal collection procedures. However, the drawbacks of this method is that sEMG induces more sources of noises in the signal. Therefore, identifying the factors and removing noises is one of the main tasks for sEMG analysis. First, similar with needle EMG, sEMG is mainly affected by the muscle contraction speed and force. Other factors includes the distance between the sensors to the muscles, the impedance of the skin or any other tissues between the skin and the electrode. sEMG signal is also influenced by its hardware quality (amplifiers, electrodes, filters, etc.). The next section introduces several statistical and frequency-based measures to extract information from sEMG signals.

1.4 Stroke Rehabilitation and Wearable Robotics

Stroke is a global health-care problem that is common, serious, and disabling. Only 18% of stroke patients with severe upper extremity paresis regain full arm function [33]. However, arm function is essential to cope with the tasks of daily living. To regain the upper-limb (UL) motor functions, physiotherapists have developed a series of rehabilitation techniques for stroke patients, including motor-skill exercises, mobility training, and constraint-induced therapy. In recent years, technology-assisted rehabilitation is introduced using functional electrical stimulation [34], robotic devices [35], and virtual reality [36]. These rehabilitation strategies have also demonstrated their strengths in several clinical studies [37]. Although the proposed technology-based systems have demonstrated advantages in early research, there are numerous aspects needed to be further investigated to ensure more stable physiological analysis and broader usage in the clinical field [38].

To utilise biological signal for stroke rehabilitation requires an in-depth neurophysiological analysis that reveals biological feedback from the therapies, and more importantly, provides a comprehensive and consistent method to measure the recovery of patients' motor function. With the rapid development of the neuroelectrical devices, there has been an increase in projects using muscle activities of UL in stroke rehabilitation [39] [40]. Surface electromyogram has been used as one of the critical parameters in recent studies. Advantages such as the ability to predict movements, and estimation of the required assistance for rehabilitation therapies illustrate the potential to use sEMG in physiological analysis for stroke [41] [42] [43]. Nevertheless, the long-lasting issues of sEMG such as susceptible easily to various sources of artefact, difficulties in isolating to individual muscles and variations due to physical and environmental states still exist in stroke rehabilitation studies. To overcome such problems, an accurate and stable mapping between sEMG and mechanical parameters is essential. This task has been conducted using healthy participants [44]; however, the unnatural relationship caused by stroke and unpredictable recovery progress of the patient are the top challenges in sEMG applications. Therefore, instead of searching for a suitable model between biological and mechanical input, a similar neuroelectrical signal, electroencephalogram that is collected from the human scalp, has presented a successful example in biomedical research. Modern brain mapping methods have demonstrated the anatomical and functional connection patterns using EEG signal. The organised behaviour of different region of the brain is emphasised to not only establish the relationship between data-driven prospectives and clinical manifestations but also propose a platform to show the commonality of physiological signal in unnatural states between different individuals. Thus, adapting EEG connectivity analysis is a potential solution to apply sEMG in stroke patients who are demonstrating complex neuromuscular feedback.

Rehabilitation is an effective method to recovery after stroke. Rehabilitation often starts right after the patient is out of the critical situation. This thesis aims to develop a rehabilitation system that can used in multiple stages of stroke recovery. Therefore, it is important to first understand the phases of stroke rehabilitation, and the needs at each phase.

According to the Brunnstrom's approach [45], there are seven stages for stroke. First is the flaccidity stage. At this stage, the patient completely lost the capability of move. The paralysis often happens with the acute events that damages the nerves in the brain. The second stage is the appearence of spasticity. This means some muscles of the patients start to perform small, abnormal, and involuntary activities. The next stage of stroke recovery make the spasticity of the muscle at the highest level. Due to the stiffness of the muscle, it is important to perform enough stretching exercises with reasonable rehabilitation activities to reduce the spasticity.

Followed by that, the next stage shows a decreasing trend of the spasticity. This is the stage where the patients start to feel the positive effects of rehabilitation. It is also important to regain the strength and control of the muscles. After regaining the basic movement, the fifth stage is to train the patients to do daily living activities. Once the patients is starting to showing the independence of living, the last two stages are follow-up rehabilitation and returning to normal.

Regarding the technologies used in stroke rehabilitation, this thesis mainly discuss the rehabilitation robots developed in recent years. Although these robots have started in a new era of modern neuromuscular rehabilitation engineering and assistive technology research [46], several concerns have been raised. First, the lack of ergonomic and standardised design leads to issues for transforming the technology from lab to bedside. Some robots present a positive result on healthy subjects; however, stroke patients find these designs are not practical to use in clinical settings. The performance assessment for stroke rehabilitation using robots is also another area that similar works in exoskeleton design have not studied systematically. In this thesis, we present a self-developed upper limb exoskeleton that can be used in multiple stages of stroke recovery with several features to improve the clinical feasibility. A novel EMG-based rehabilitation assessment is also demonstrated, offering a physiological based performance assessment.

1.5 Overview of the Thesis

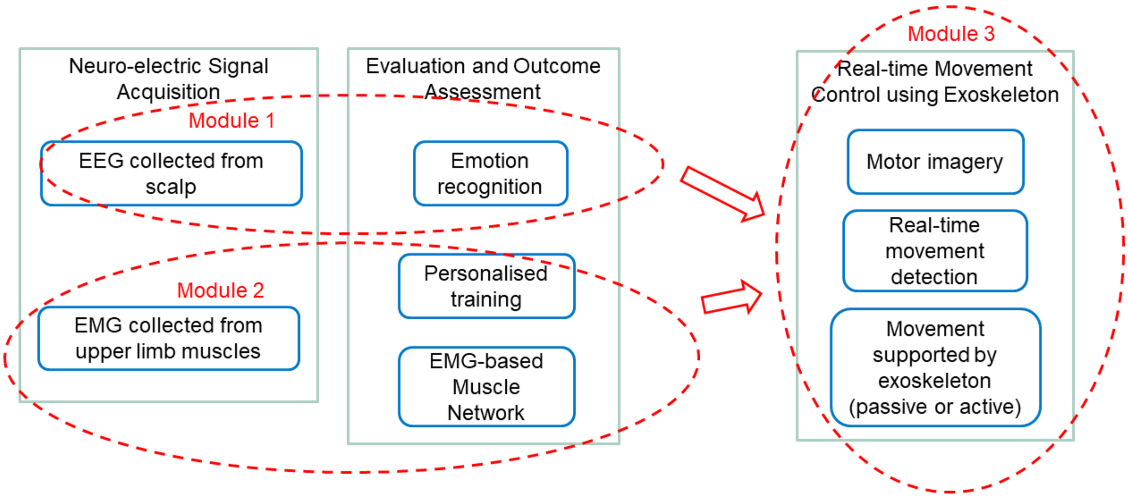

Figure 1.17: A summary of this thesis

In this thesis, 'Multi-mode Stroke Rehabilitation System Using Signal-Controlled Human Machine Interface', a complete robot-based rehabilitation system is offered to improve post-stroke recovery efficiency patients. Three modules are presented in this thesis, shown in Figure 1.17. The first module uses physiological signal to create a Brain-Computer interface application detecting the emotional states during activities. Electroencephalogram is collected as one of the primary physiological sources. The emotional states of the participants are classified during training sessions. The detected emotions provide critical information on the patients' performance. The detected negative emotions, such as fear is used as a safety measure for the system. To create a efficient BCI, three approaches are demonstrated using feature extraction methods and advanced machine learning algorithms to achieve optimised classification accuracy.

The second module of the system acquires electromyogram, which is the muscle's electrical activity. A novel designed EMG connectivity analysis is applied to construct the muscle network of stroke-induced upper limb impairment. EMG-based muscle connectivity reveals the interconnection between different muscle groups during rehabilitation training. This information is used for two purposes in this rehabilitation system. First, it is used as a type of signal processing feature for impaired movement evaluation and detection. Secondly, a personalised training paradigm is constructed for the rehabilitation robot. The EMG feature of the non-affected side of the limb is used as the reference.

Then, when the system detects abnormal EMG connectivity from the affected limb, the robot works as a wearable exoskeleton to guide the impaired limb to perform similarly with the reference. This rehabilitation training method has shown promising results from the feasibility studies and simulations using the previous dataset.

The last module is the design of a hybrid biosignal-based rehabilitation system. First, an upper limb rehabilitation exoskeleton is built using carbon-reinforced 3D printing material. This lightweight, portable, wireless robot is used to support the affected movement for stroke patients. Combined with the findings in previous modules, two human-machine interfaces are developed. First, the emotion classification interface is used in this system during motor imagery (MI) training. During motor imagery training, the system recognises the participant's imagined movement and uses the virtual reality environment as visual feedback. This training is specifically designed for stroke patients at their early recovery stages, where they can hardly perform voluntary limb movements.The robot is served as a motor execution tool to improve the quality of the imaged movement. A real-time movement detection system is implemented when the robot is used as a wearable exoskeleton. The movement detection system, together with the personalised training paradigm developed in the second module offers a customised approach that can improve stroke recovery efficiency.

In the first chapter, this thesis's physiological basis is discussed to present a broad view of the related technologies' history and recent development. The literature review provides a systematical examination regarding neuroimaging techniques, which justifies the selection of the hardware. Hypothesis and research aims are also proposed at the end of the first chapter. The second chapter focuses on the EEG-based brain-computer interfaces. The advanced machine learning algorithms developed have made an impact on analysing internal mental process using neurological signals. The third chapter emphasises on the human motor function. Stroke, an acute neurological dysfunction that can cause severe motor deficits, is introduced in this chapter. Biomedical signal processing skills are applied to explore the unanswered questions in stroke-induced neuromuscular impairments. Next, by merging the BCI and EMG analysis, a multi-mode stroke rehabilitation system is established. Chapter 4 demonstrates a wearable exoskeleton developed at the School of Biomedical Engineering, University of Technology, Sydney. This stroke rehabilitation system has drawn a lot of interest from both the research and industrial fields. One of the ongoing clinical trials is also explained in this chapter. Finally, a summary and future work plan are presented in the Chapter 5.

CHAPTER 2

Emotion Recognition and Brain-Computer Interfaces

2.1 Introduction

Human emotion has been studied by psychologists for more than 200 years to serve as a diagnostic tool for a large number of mental illnesses. Traditionally, psychologists judge the patients' emotion states based on the observations including facial expressions and voice characteristics. Even though to recognise one's emotion is one of the regular tasks for psychologists, there is still a high demand to find an accountable solution for human emotion classification from both research and practical point of view. Especially in the last few decades, the focuses of many scientific and engineering research projects have been oriented to the human body. New terms such as the human-machine interface (HMI) and brain-computer interface require the computer to recognise the emotion states and react to the detected emotions to improve the efficiency of the communication between the machine and human. With the rapid development of human anatomy science and biomedical engineering techniques, researchers have been seeking for an engineering-based approach for emotion classification. Comparing to the psychological method, these approaches share the advantages where data acquisition measures have a solid scientific background that guarantees the accuracy of the collected data, signal processing tools offer a mathematical foundation for the calculation of the original data and machine learning algorithms demonstrate the efficiency of the training and predicting process.

However, the emotion classification systems need further improvement with the challenges including these four areas: (a) to choose the proper method to collect signal and identify the distinction between the emotion states; (b) to reduce the data dimension to perform fast calculation; (c) to extract the correct features to represent the information embedded in the data; (d) to design the learning algorithm to recognise the patterns and accurately classify the emotion based on the training process.

Numerous efforts have been applied in the field of emotion classification from different aspects to overcome the above difficulties. First of all, researchers have studied many sources for emotion classification. Some visible manifestations have been investigated to detect emotion states by used the vector of 12 speech power coefficients to classify six types of basic human emotion[47]. Researchers also have drawn much interest in facial expression, for example, by analysing facial images [48]. Further works have also been done for tracking the characteristics to study of the emotion states [49] [50]. Moreover, combined sources such as facial expression and body gestures have been applied to improve the accuracy [51] [52]. Nevertheless, a significant drawback of using behavioural modalities for emotion detection is the uncertainty that arises in the case of individuals who either are consciously regulating their emotional manifestations or are naturally suppressive [53]. Thus, researchers moved their focus to psychological signals such as electrocardiography (ECG) and electroencephalogram , as these are the involuntary reactions of the human body. Anatomically, it has been confirmed that emotional processes could be represented by EEG activities [54]. Here, it is believed that emotions are generated from the limbic system located in the front lobe of the brain. The limbic system activities can be monitored by EEG signal as it represents the brain activities regarding voltage variation from the human scalp. Many recent projects [55] [56] [57] [58] [59] have been using EEG signal to perform different feature extraction methods and classifier design.

EEG signal can be enormous if it is collected in a long duration of time with high sampling frequency. In the case of human emotion classification, relative long signal collection time and high sampling frequency needed to provide enough resources for different types of human emotion and the adequate number of samples for analysis to detect emotion variations within small time frame. As a result, the computational time would be tedious, and it would limit the application of the system. Researchers have created several methods to compress EEG signal, and sparse representation is one of the most popular choices. A sparse kernel was used to transform EEG signal into the smaller size dataset [60]. Further work has been carried out for determining the sparsity of EEG in Gabor frame [61]. A recently developed method, compressed sensing (CS), has attracted considerable attention in engineering, which offers a framework for compression of finite-dimensional vectors [62]. Zhang et al. [63] argued that current CS algorithms only work well for sparse signals or signals with sparse representation coefficients. Since EEG is neither sparse in the original time domain nor sparse in transformed domains, current CS algorithms cannot achieve good recovery quality. A Block Sparse Bayesian Learning (BSBL) has been further proposed and demonstrated a high result of recovery rate [63].

Followed by data compression, numerous feature extraction methods have been applied for EEG signal. Statistic features involving maximum and minimum value, peak-to-peak, mean, standard deviation have been explored [64] [65]. In the frequency domain, Fourier Transform (FT) analysis has been investigated as well [66][67][68]. Another method, Wavelet Transform (WT), can be used with controllable wavelet size to detect every change of the signal. It also can localise the change in the signal, which could be overlooked if using FT method. Candra et al. [69] addressed several advantages using Discrete WT involving multi-scale zooming and multi-rate filtering. Both relative wavelet energy and relative wavelet entropy used in Candra‚Äôs study showed consistently high quality.

Lastly, a classifier is designed to recognise the feature patterns of human emotion states. There are currently more than a dozen of machine learning algorithms invented and a large number of combinations of them. Finding the suitable algorithm for EEG signal is crucial. Classifiers which include Linear Discriminant Analysis (LDA) [70], k-Nearest Neighbour (kNN) [65], Adaptive Neural Fuzzy Inference Systems (ANFIS) [68], binary linear Fisher‚Äôs Discriminant Analysis (FDA) [71], Hidden Markov Model (HMM) [72] and Support Vector Machine (SVM) [65][69][73] have been utilised. Furthermore, Neural Networks (NN) including deep learning network with principal component-based covariant shift adaption [74] and statistical features back-propagation neural network [75] are also studied in emotion classification projects. The comparison between each algorithm shows that SVM has higher accuracy due to the excellent discrimination performance in binary decision problems [76].

2.2 Material

An online EEG resource, the Database for Emotion Analysis using Physiological signals (DEAP), is selected to be the experimental input dataset. Although invasive methods such as attaching electrode probes directly on the surface of the brain have been developed to collect the electrical movement, considering the objective is to perform emotion classification with easy set-up, a noninvasive process should be preferred. However, non-invasion method, which is collecting the signal from human scalp, introduces a significant amount of noise. Therefore, a high standard electrode placement system and collecting equipment are required. Moreover, to stimulate and record the correct emotion states are also challenging. DEAP dataset has considered both of these factors with a selfassessment questionnaire to maximise the accuracy of the collected EEG signal and the emotion states recorded [77].

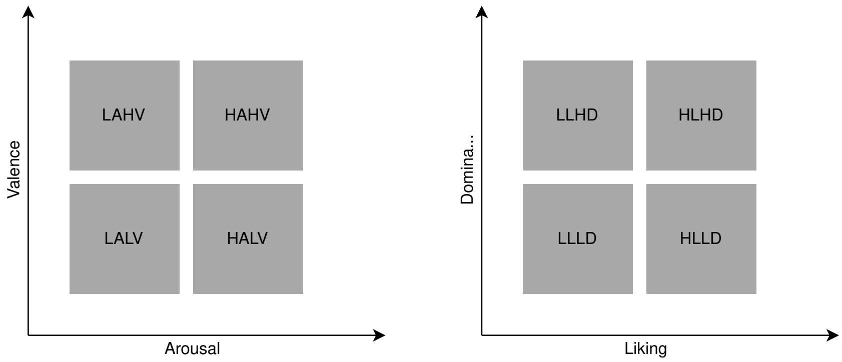

Figure 2.1: 2D Emotion Planes

DEAP dataset contains 32 test subjects to perform EEG signal collection using music video clips to stimulate various emotion states. The 32 participants are asked to sit still, watching 40 music video clips lasting 1 minute. The EEG signal is extracted using the standard 10-20 system, which contains 32 electrodes. The dataset evaluates emotion states using four scales, same as we used later in the classification process, namely valence, arousal, dominance and liking. The emotion is considered from 1–9 in each scale. For instance, number 1 in valence means a deficient valence emotion state, and number 9 in dominance indicates high dominance state. Thus, there is in total four emotion responses for one music video for each. The dataset is downloaded from the official website, and the data file is translated into '.mat' format. For each subject, two matrices record their EEG signal and corresponding emotion states. The first matrix has three dimension, which includes 40 videos labelled from 1 to 40, 32 EEG electrodes as the Geneva order and 60 seconds EEG signal in millivolts. The other matrix indicates the emotion states in four scales, namely valence, arousal, dominance and liking. All four variables are chosen, and two 2D planes are generated based on them. The emotion states are measured on the emotion plane shown below in Figure 2.1 The median value, 5, is used to separate these four areas in both axes.

In the following sections, three approaches are presented to show the improvement of the BCI for emotion recognition from signal processing, feature selection and machine learning algorithm development.

2.3 Solution One: novel parameter with combined support vector machine and hidden Markov model classifier

2.3.1 Methods

The methods overview is demonstrated using a functional block diagram shown in Figure 2.2 The raw signal is collected from the standard 10-20 system, then pass to pre-processing that removes noises and divides the long signal into 6-second segments. The second module uses wavelet analysis to transfer EEG signal from time domain to frequency domain. Three parameters are calculated from each section forming the extracted features. The features enter the combined SVM and HMM classifier and the output is the classified emotion according to arousal-valence plane.

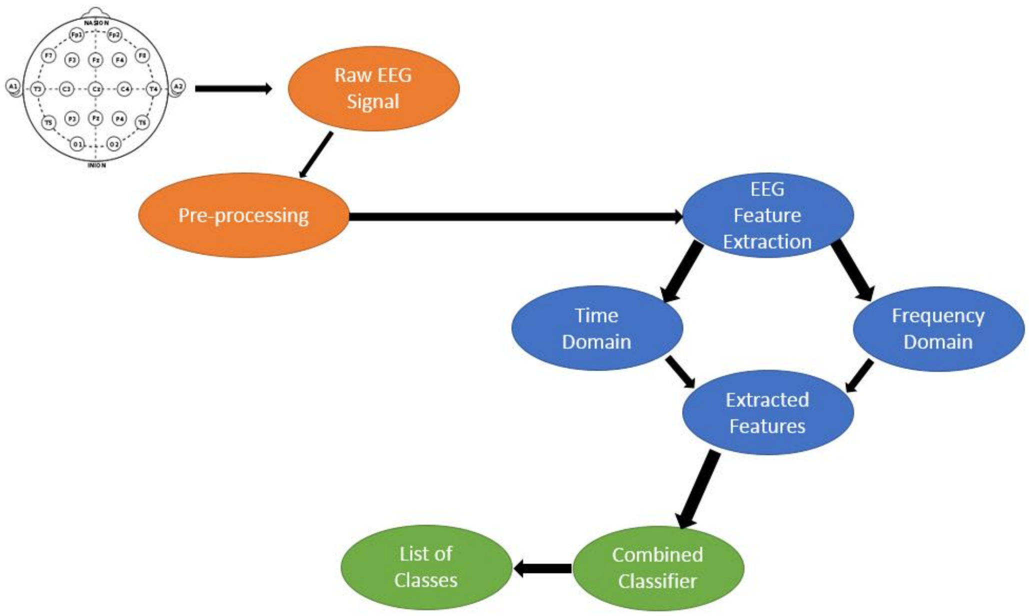

Figure 2.2: Functional Block Diagram

The signal is down-sampled to 128 Hz sample rate. Lower sample rate reduces processing time for the feature parameters calculation. Electrooculography (EOG) is removed in that eye movement is the primary noise source. A bandpass filter is applied to remove noises that are less than 4 Hz or larger than 45 Hz. The noise-free EEG signal is segmented into 6 second time window. Since the sample rate is 128 Hz, after the segmentation, the total number of segments for this solution is $10 \times 32 \times 40 \times 32 = 409600$. All parts will go through the feature extraction process and 30% of the segments are selected to be the learning set for the classifier, and 70% are in the testing set.

DWT is utilised due to the advantages of time-frequency localisation, multiscale zooming, and noise filtering. Since the study focuses on the valence-arousal plane emotion states, the frequency bands chosen are alpha, beta and gamma bands. The specific variables for wavelet transform are determined based on previous studies. The mother wavelet function is Daubechies5 (db5) and the decomposition level is 6 based on the dominant frequency components of EEG signal which are from 8 Hz to 64 Hz.

To start with wavelet analysis, DWT coefficients are calculated. The following equation finds the wavelet coefficients.

$$< f, \psi_{a,b} >= C_{a,b} = \int_{-\infty}^{\infty} (\frac{1}{\sqrt{2^{-j}}}) \psi (\frac{t - 2^{-j} k}{2^{-j}}) \tag{2.1}$$

In equation 2.1, $2^j k$ and 2^j are the time localisation and scale respectively, while $\psi(t)$ denotes the mother wavelet function [69]. DWT coefficients are used in all three features calculation.

The first feature is relative wavelet energy. It is calculated as follows:

$$p_j = \frac{\sum_k^N |C_j(k)|^2}{\sum_j \sum_k |C_j(k)|^2} \tag{2.2}$$

$C_j(k)$ represents the detail coefficients, which indicates that the numerator is the detail wavelet energy. The denominator is the total wavelet energy. The probability p_j reveals the time-scale density of the input data.

The second feature extracted is relative wavelet entropy. It is expressed below:

$$S_{wt}(p|q) = \sum_j p_j \cdot ln(\frac{p_j}{q_j}) \tag{2.3}$$

The variable q_j is used as the reference distribution to give a more accurate value for p_j. Relative wavelet entropy shows the similarity between two probabilities. In this design, the Shannon entropy is utilised.

The third feature used in the study is an innovative approach of joining two features together. DWT coefficients and standard deviation are selected and multiplied to create this variable. This method proposes an ideal circumstance that it includes information from both time domain and frequency domain, which leads to better performance of the classification system. The mathematical notation is shown in equation 2.5.

$$\lambda = C_{a,b} \cdot \sigma^2 \tag{2.4}$$

Firstly, SVM is developed to classify the extracted features. Since SVM is normally for binary classification, in order to classify both valence and arousal axes, two SVMs are established. Radial Basis Function is utilised in the training step. There are three combinations tested in SVM classifier: the innovative variable that joins both time and frequency domain; a bundle of two variables from DWT; and a bundle of all three variables.

While SVMs are large-margin classifiers known for their excellent discrimination performance in binary decision problems, they do not incorporate a model with time, HMM is capable of representing temporal dynamics very efficiently. Thus, a combined model of both SVM and HMM is designed to reach higher accuracy. The general idea is to use SVM output as the input of HMM. However, it is not possible to directly use the output as a probability measure. The output indicates the distance between the sample to the support vectors and the relationship between the output and the class probability is not clear. A sigmoid function is utilised to discover the connection between these two variables shown below:

$$g(h(x), A, B) = \frac{1}{1 + exp(Ah(x) + B)} \tag{2.5}$$

The parameters A and B are calculated by maximum likelihood estimation with $g(h(x), A, B)$. The distance between the support vectors and the optimised plane is used to create the HMM classifier model. Since the classifier only needs to identify whether the input signal is on the higher half or the lower half of the axes, using MATLAB HMM toolbox function, $hmmtrain$ and $hmmdecode$, the class probability is successfully reflected.

2.3.2 Results

Table 2.1: average accuracy for different feature combinations

2D Plane	Innovative Variable Only	Wavelet Variables	All Three Variables
Valence	0.5793	0.5485	0.6021
Arousal	0.6136	0.6182	0.6279

The contribution of the innovative variable for emotion classification is studied. SVM classifier is used with three combinations of the extracted feature shown in Table 2.1. The first set uses the innovative variable only. The second set contains both of the wavelet analysis variables. The last set is a three dimensional matrix including all of the three features. It is worth to note that all 40 music clips and 32 test subjects are taken into the calculation. Since it is a large dataset, average accuracy on valence and arousal planes are used to represent the overall performance. Despite the accuracy of individual parameters is relatively low; the joined three parameter data group is consistently higher than other combinations. On valence axis, the increase of the accuracy of the three parameters test is more than 2% for innovative parameter only and more than 5% for wavelet parameters only. The increase of accuracy confirms that combining time and frequency domain parameters can improve the performance of the classification system.

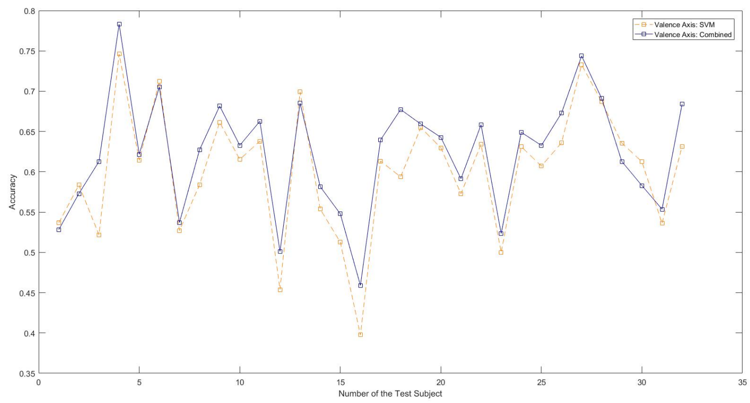

Figure 2.3: Valence Plane Classification Accuracy: all 32 participants are demonstrated on the x-axis. The y-axis indicates the classification accuracy in decimal numbers. The yellow dash line represents the traditional SVM classification, and the blue solid line is accuracy for the novel combined SVM and HMM classifier.

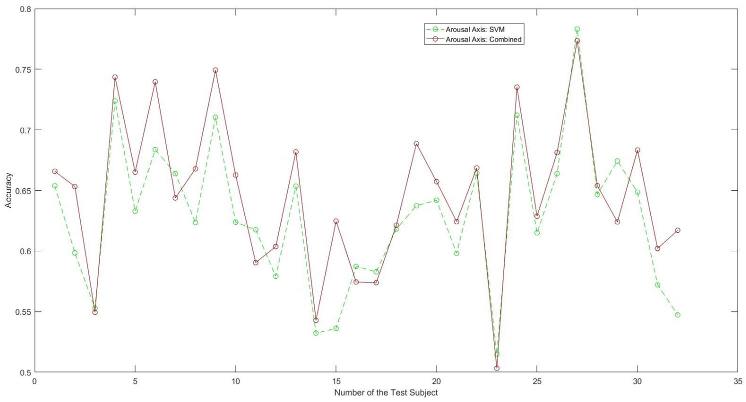

Figure 2.4: Arousal Plane Classification Accuracy: all 32 participants are demonstrated on the x-axis. The y-axis indicates the classification accuracy in decimal numbers. The green dash line represents the traditional SVM classification, and the red solid line is accuracy for the novel combined SVM and HMM classifier.

The SVM classifier and the combined classifier are tested seperately by the three dimentional dataset shown in the last column of Table I. Figure 2.3 and Figure 2.4 demonstrate the average accuracy for each test subject on both valence and arousal plane. As the diagrams shown, the combined SVM and HMM classifier returns higher values constantly in the majority of the cases. This reaffirms the combined classifier methodology, which is to use the property of the support vector of the SVM classifier as the input of the HMM classifier, and as a result, the second classifier finds the hidden information in the features and corrects the classification process.

Figure 2.5 compares the average accuracy for these two classifiers on valence and arousal axis. The blue bars are the average accuracy for SVM classifier and the yellow bars stand for the combined design. The average accuracy on valence axis rises 3.15% and it increases 2.88% on arousal axis. The stable increase of accuracy on both axes illustrates that the combined SVM and HMM classifier contributes in improving the accuracy and the stability of the system.

This approach establishes an innovative design of emotion classification system based on EEG signal. Using DEAP database as the input data, three features, relative wavelet energy, relative wavelet entropy and a novel variable which is the product of standard deviations in time domain and DWT coefficients from frequency domain are calculated respectively. A combined SVM and HMM classifier is also designed aiming to improve the accuracy of the classification. The result indicates that the bundle containing all three features returns the highest accuracy. Comparing the combined classifier with solo

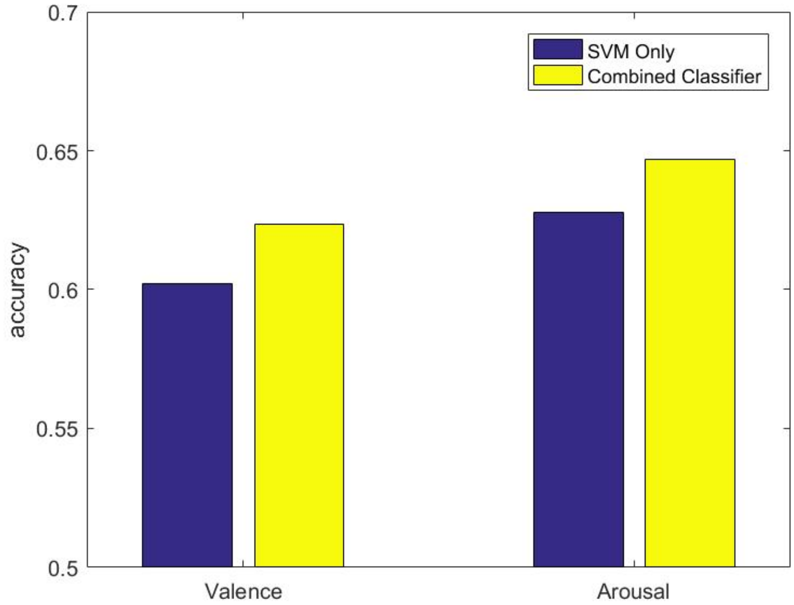

Figure 2.5: Average Accuracy: SVM vs Combined Classifier

SVM classifier, the accuracy increases approximate 3%. It indicates that the combined classifier can optimise the emotion recognition process consistently.

2.4 Solution Two: hybrid fuzzy cognitive map / support vector machine using compressed sensing

2.4.1 Methods

When EEG signal is collected, it is undoubted that the brain activities would cause responses from more than one part of the brain. However, there is yet a clear way to find which part of the brain is working for an individual emotion state, neither to understand how closely related between the extracted features and the result. The vague definition of the acquired signal and the output catalogues has caused serious troubles for the classification. One of the solutions for such situation is to use fuzzy logic. Fuzzy logic provides a foundation for approximate reasoning using imprecise propositions based on fuzzy set theory [78]. A Fuzzy C-Means and Fuzzy k-Means clustering methods have been implemented for classifying the emotions [79]. Additionally, fuzzy cognitive maps (FCMs) are fuzzy models that combine aspects of fuzzy logic, neural networks and non-linear dynamical systems [80]. FCM is firstly studied by Kosko [81]in 1986, then the method has been used in several engineering disciplines. Based on the analysis by Vliet et al.[82], the motivations for using FCM are easy to build and parameterise, flexibility in representation, easy to use and understand, handle complex and dynamic problems. Papageorgiou and Salmeron [83]state that FCM has been used as the classification tool in medicine, business information and agriculture. Salmeron [84] designed a three layer FCMbased classifier for artificial emotions forecasting. FCMs are capable of revealing the inter-relationship between their input states. Nevertheless, fuzzy logic is rarely used in emotion classification, nor in the field of EEG signal processing and analysis. FCM is able to find the inter-relationship between the features, and the relationship would help to select the feature according to the significance. Therefore, combining both algorithms together would improve the accuracy. If a hybrid classifier could merge the merits of both SVM and FCMs, the classification system would reduce the uncertainty of the EEG signal and produce higher accuracy.

In this section, we propose a FCM-based classification algorithm. A simple FCM structure graph is shown in Figure 2.6. C1 to C5 represent each node or state of the system. The connection between each individual is demonstrated as the weight matrix W. Therefore, at each step, the new values of each node depends on the activation function, which is a sigmoid function in this section. The vector state is calculated as:

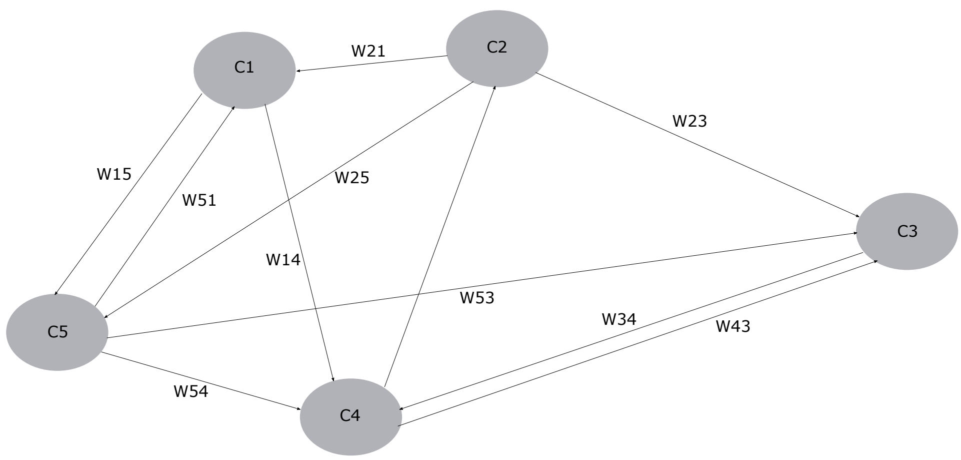

Figure 2.6: An example of Fuzzy Cognitive Map

$$c_i^{t+1} = f(c_i^t + \sum_{j=i}^{n} W_{ji} \cdot c_j^t) \tag{2.6}$$

After an inference process, the FCM reaches either one of two states following some iterations. It settles down to a fixed pattern of node values, the so-called hidden pattern or fixed-point attractor.

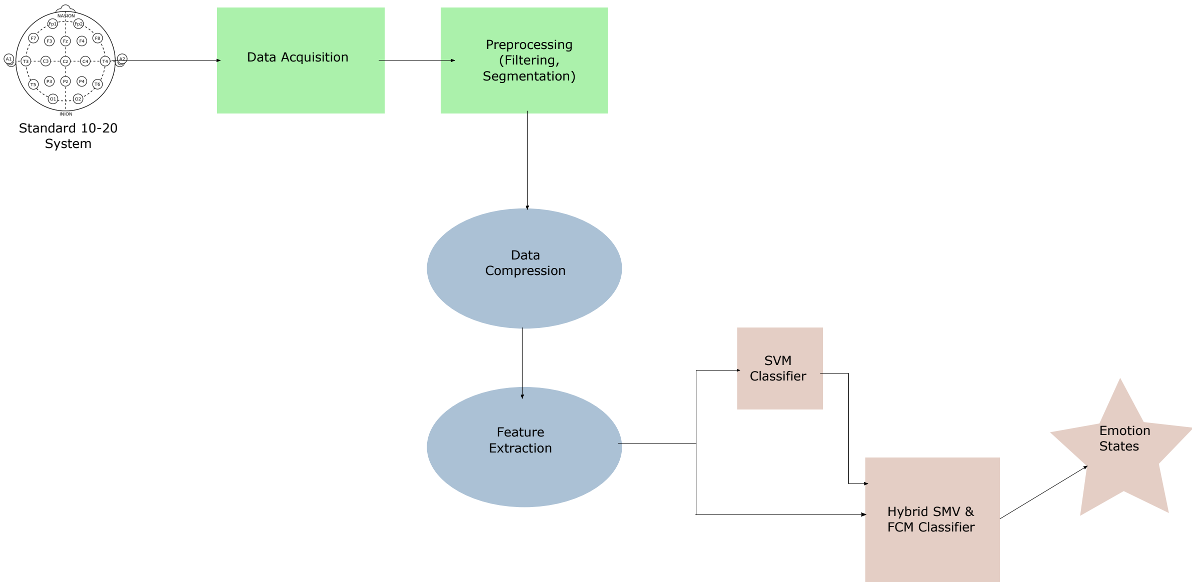

Figure 2.7: Functional Block Diagram

The functional block diagram in Figure 2.7 shows the general development procedures. The study is divided into three modules. Firstly, the raw signal is collected from the standard 10-20 system, then pass to pre-processing that removes noises and segments the long signal into 6-second EEG epochs. The second module uses CS to compress the size of the preprocessed EEG signal into a smaller dimension. Then, WT analysis is used to extract the features form the compressed data. Two parameters are calculated from each segment forming the extracted features. The features enter the last module, classification, which contains an SVM classifier and a hybrid SVM and FCM classifier. The output of the SVM classifier is also used as the input of the hybrid one. Finally, the output is the classified emotion according to the arousal-valence plane and the dominance-liking plane.

Compressed sensing (CS) is initially defined to compress a large data $\mathbf{x}$ with the length N into a much smaller matrix by a random matrix, denoted by Φ, i.e.,

$$\mathbf{y} = \Phi\mathbf{x}, \tag{2.7}$$

where $\mathbf{y}$ is the compressed data, and Φ is the sensing matrix with the size of $M \times N$. However, EEG signal cannot directly use this equation due to the lack of zero in the input signal. The success of CS highly depends on the assumption that most of the input data are zero. An alternative approach is utilised. A dictionary matrix is calculated initially, then the equation becomes:

$$\mathbf{y} = \Phi\mathbf{D}\mathbf{z}, \tag{2.8}$$

where $\mathbf{D}$ has the dimension of $M \times M$ and $\mathbf{z}$ is sparse. In this equation, the CS algorithms recover $\mathbf{z}$ first, and then recover the original signal $\mathbf{x}$. In this section, the EEG epoch contains 768 samples, which is the input data for CS. Using equation 1.9, the compressed data only has 192 samples in each segment.

DWT is utilised due to the advantages of time-frequency localisation, multiscale zooming, and noise filtering. Alpha, beta and gamma bands are studied. The specific variables for wavelet transform are determined based on previous studies. The wavelet used is Daubechies5 (db5) and the decomposition level is 6 because the dominant frequency components of EEG signal is between 8 Hz to 64 Hz.

Figure 2.8 demonstrates the relationship between SVM and FCM. It is the core concept of how to design hybrid SVM and FCM classifier. This study uses MATLAB as the programming language. The architecture of the hybrid SVM and FCM classifier is represented in Fig.4. The extracted features, which are relative wavelet energy and relative wavelet entropy, are firstly entered the SVM classifier. These wavelet features formulate the first layer of the hybrid classifier. The output of the SVM classifier combined with these two features forms a ten-node hidden layer. The sigmoid function is utilised as the activation function. After the system converges, the output layer shows the stable state of the nodes. This process also calculates the weight matrix of the hybrid classifier. The weight matrix reveals the connections between the hidden layer and the output layer, as well as the relationship within the output nodes. A defuzzification method is applied to transform the value of the nodes into scales of the human emotion states. Since the states of each node are within -1 and +1, the low scale emotion are the negative values, and vice versa.

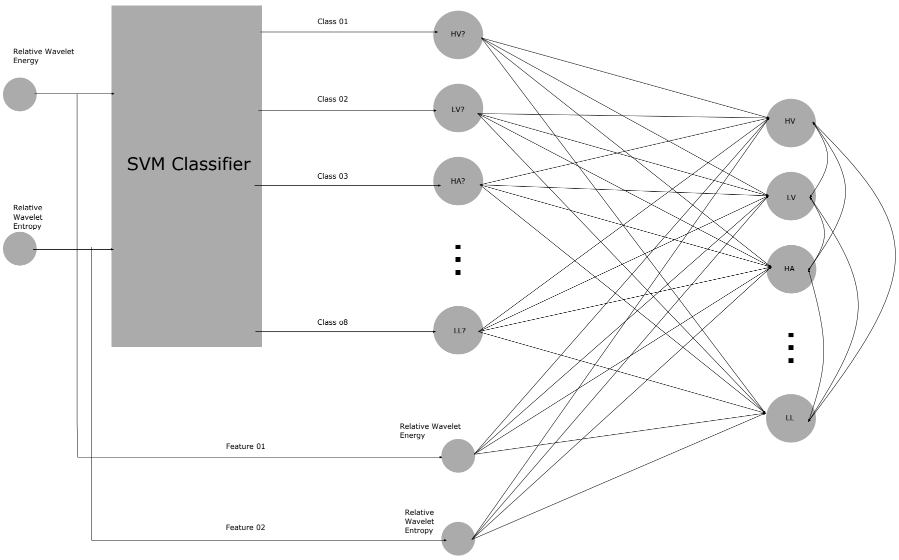

Figure 2.8: Hybrid SVM & FCM Classifier. First two features are relative wavelet energy and relative wavelet entropy, entering the SVM classifier. The output of the SVM classifier together with these two feature establish the FCM, which presents the final output of the classified emotions.

2.4.2 Results

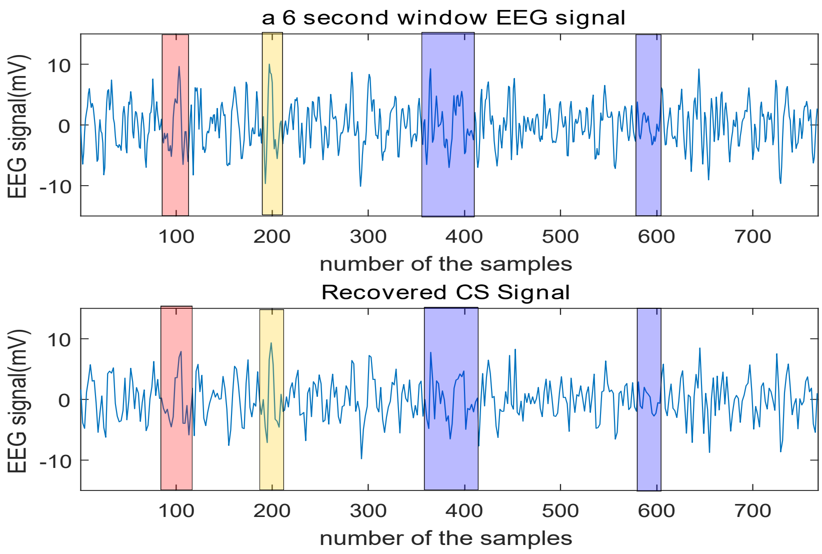

Figure 2.9: A Segment of EEG and its recovered signal from CS

Figure 2.9 demonstrates a random chosen EEG signal segment in its original form and recovered form. The initial 6-second section consists of high frequency noise and 768 number of samples. CS method uses equation 1.9, where $\mathbf{D}$ is the inverse db5 WT matrix, and Φ is a sparse binary matrix, to reduce the noise and the size of the data. It is clear that EEG peaks and valleys have preserved from the CS process. For example, around sample number 100 and 200, highlighted in red and yellow, the peaks are consistent with little distortion. At the same time, the recovered data is smoother, such as the blue highlighted areas that are from sample number 360 to 410, and sample number 580 to 605. The overall presentation of the recovered signal contains the major activities of the original one. The compression process reduces the size of the data into one-fourth of its original size based on equation 2.7, without losing critical information.

Two types of classifiers are tested using the compressed data. A single SVM with Radial Basis Function is first implemented to examine the 6-second EEG epochs and to identify the emotion states from the four planes. Then, A hybrid SVM and FCM classifier is designed to serve the same task. Lastly, the hybrid classifier uses the output of each epoch to recognise the overall emotion states for the music videos. This process is considered as the revised process of the segmentation in preprocessing. As the continuous EEG signal with the same emotion reaction is separated into 10 sections, the last classifier merges the results of the epochs for the same videos and calculate the overall scale on the emotion planes. Figure 2.10 shows the accuracy of the three classifiers for the 32 test subjects on the valence-arousal plane. When the classifiers are tested on the EEG epochs, the hybrid SVM and FCM, which is the red line, is always higher than the single SVM classifier, which is the green line. This is because the hybrid classifier adds the fuzzy logic after the SVM classifier. By doing such, the connectivities within the emotion states and the features can be mapped, and it will correct previous errors by the SVM classifier. A similar trend can be viewed on the dominance-liking plane as well, which is shown in Figure 2.11.

The last classifier designed is shown on both Figure 2.10 and Figure 2.11 using the blue line. The hybrid classifier (videos) merges the result of ten predictions to form one outcome. The accuracy is expected to be higher than the previous ones. The result from all four planes justifies the assumption; however, in each plane, there are a few test subjects showing low accuracy using the last classifier. In Figure 2.10, test subject 4 and 9 are showing much lower accuracy comparing with the epoch methods. Test subject 7 has the same tendency on the dominance-liking plane. This classifier demonstrates the characteristic of emphasising the accuracy of the results. In another word, the third

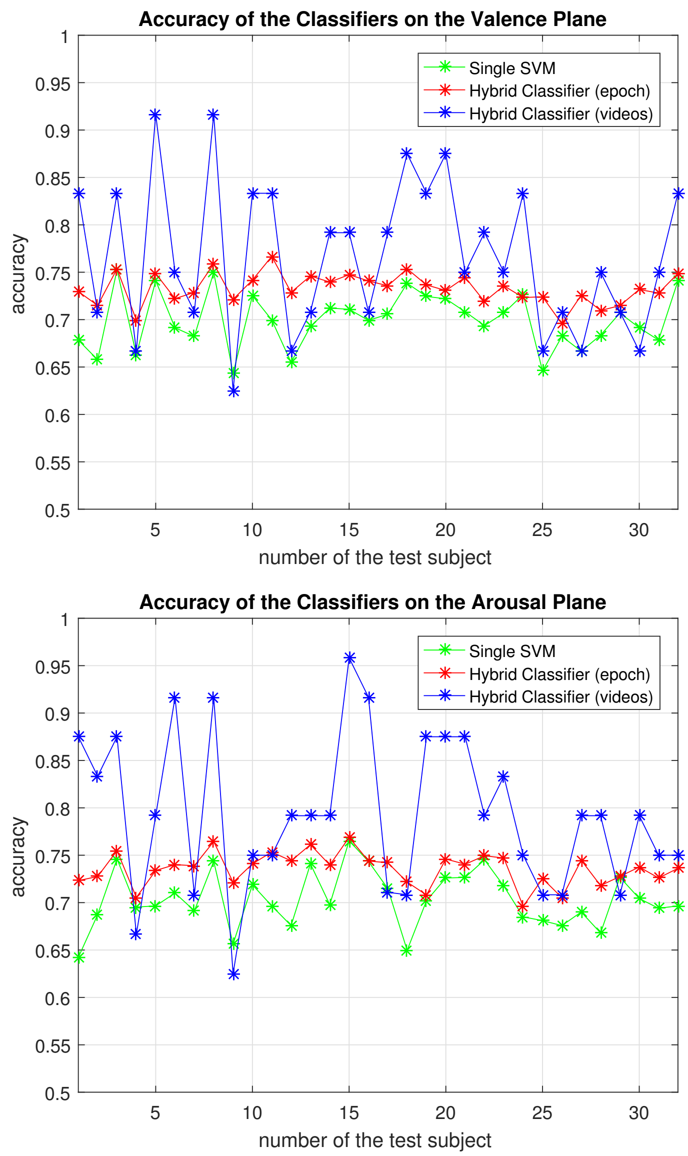

Figure 2.10: Accuracy on Valence-Arousal Plane

classifier can improve the result to a higher accuracy if the previous classifiers can successfully recognise the correct emotion; on the other hand, if the previous classifiers perform poorly, the accuracy of the third classifier would be even lower, because one music video represents one kind of emotion and only one kind. In another word, one music video clip corresponds to a fixed number of four emotion scales. Therefore, if the input for the third classifier is the mean value of each music video. The accuracy will increase if the majority of the window segments recognise the right emotion. However, in some cases like participant 7, the accuracy drops. The possible reason is that the emotion

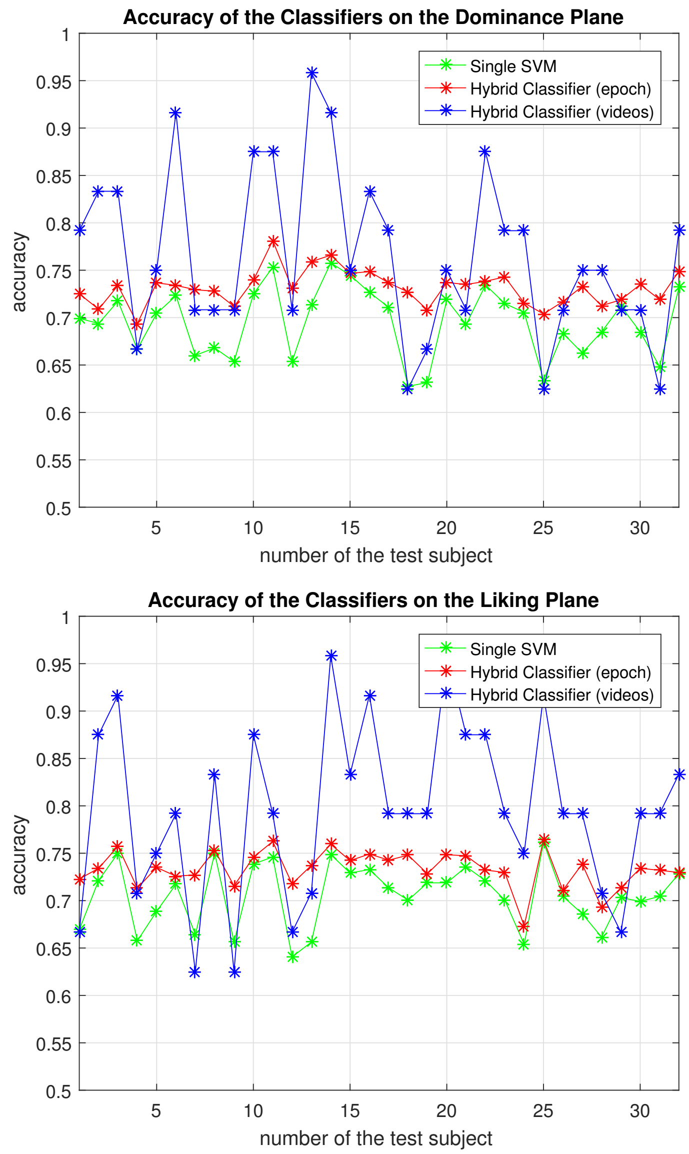

Figure 2.11: Accuracy on Dominance-Liking Plane

experiencing by the participant does not match the standard emotional response.

The average accuracy for all 32 test subjects is calculated and presented in Figure 2.12. The hybrid classifier using videos as a whole has the highest accuracy, which is at 78.39%. Comparing with the single SVM classifier, the hybrid one has a consistent 3.23% increase in accuracy. The dominance plane has the largest improvement, which is 3.63%, and the liking plane has the smallest rise, which is 2.77%. The overall accuracy of the hybrid SVM and FCM classifier for epoch testing is 73.32%, and for video testing is 78.03%. From the confusion matrix shown in Table 2.2, although the third classifier

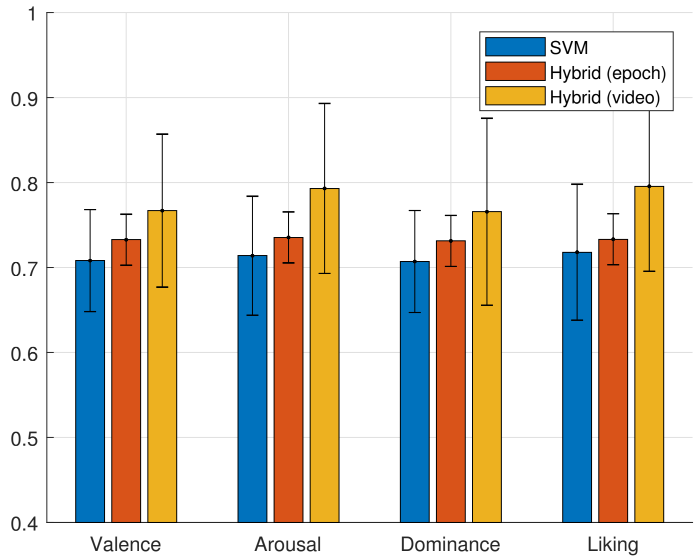

Figure 2.12: Average Accuracy with standard deviation on four Emotion Planes. Blue bar represents classical SVM classifier. Red bar represents hybrid SVM and FCM classifier using epoch. Yellow bar represents hybrid SVM and FCM classifier using video.

has the highest accuracy, it has the highest standard deviation error; however, the classifier of the epoch testing has a much smaller error range than the other two classifiers. Therefore, even though the average accuracy of the videos testing classifier is higher, the system appears to be less stable than the epoch testing hybrid classifier.

	Sensitivity(%)	Specificity(%)	Accuracy(%)
Classifier 1: SVM	71.33 ± 9.4	69.45 ± 9.6	71.17 ± 7.2
Classifier 2: Hybrid (epoch)	72.81 ± 5.3	73.59 ± 5.4	73.32 ± 3.6
Classifier 3: Hybrid (video)	77.37 ± 11.9	78.64 ± 13.2	78.03 ± 11.7

Table 2.2: Confusion matrix for the three designed classifiers

This method proposed a complete human emotion classification system using EEG signal. Due to the large size of the dataset, a series of preprocessing techniques are used, and advanced CS algorithm is designed for EEG signal to reduce the dimension. Wavelet analysis is then implemented to extract the distinctive features. A hybrid classifier which combines SVM and FCM is used to reveal the connection between each state and eventually to classify the emotion states. CS have successfully reduced the size of the EEG signal four times smaller without losing critical information. The hybrid classifier demonstrates consistent improvement comparing with the single SVM classifier, which is 3.34% of the increase in valence axis, 3.19% in arousal axis, 3.63% in dominance axis, 2.77% in liking axis and overall of 3.23%. When considered one piece of 60-second video as a whole, the accuracy can reach 95.83%, with an average of 78.03%. The future work can investigate the connectivity between each EEG electrode using similar methods. With a more comprehensive understanding of the connectivity of the human brain, many brain-related research projects can be benefited from the results, and possible breakthroughs can be expected.

2.5 Solution Three: joint EEG and facial expression features

2.5.1 Methods

First, it is important to notice that for many clinical and engineering project, emotion can be highly correlate to satisfactory or performance. Nonetheless, the previous models of the human emotions is not sufficient to represent the satisfactory level of the product or service. Figure 2.13 categorises 9 basic customer emotions into the 'Negative Neutral Positive (NNP)' scale. According to Feldman's model, these discrete emotion states are placed on the arousal-valence plane. This section utilises the 'NNP' model combined with the arousal-valence plane to adopt both aspects of affective design feedback recognition and the numerical representation from the engineering perspective.

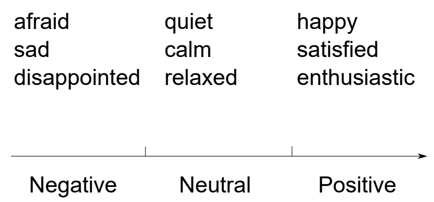

Figure 2.13: Emotion Model: Negative Neutral Positive

The functional block diagram are shown in Fig 2.14. A combination of EEG signals and facial images is applied in this work to classify the affective status of the participants comprehensively. First of all, the data about videos and EEG signals are collected from DEAP dataset. Next, the preprocessing for EEG signal is to remove the noise and segment the long signal into 6-second EEG epochs. The size of preprocessed EEG signal should be compressed into a smaller dimension by CS. Meanwhile, the preprocessing for the videos is to crop picture per second and change the picture to gray-scale. After the preprocessing, WT analysis is used for the compressed EEG signal and LBP is used for the cropped facial gray-scale image to extract the features. At last, the features are the input of classifier and the output is the classified emotion according to the arousal-valence plane and “Negative Neutral Positive" model.

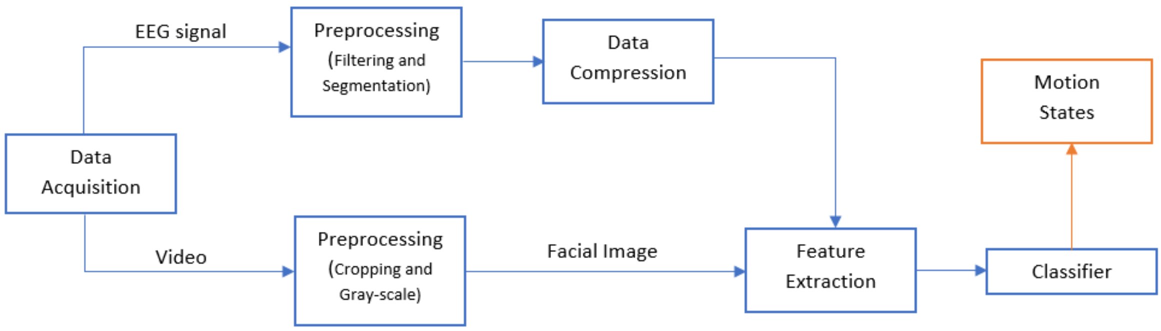

Figure 2.14: Functional block diagram.

For the 22 participants, we have 874 videos totally and each video lasts one minute. We use a auto-screenshot software to obtain the facial image for every second from all the videos. In that case, we got 52440 images of 510×640 pixels. Figure 2.15 shows some examples of these images.

Because of the uncertain position of the crop area and in order to acquire a accurate feature, we have to crop a detail image according to a fixed distance between two eyes from the original pictures. The image should be changed to gray-scale due to LBP's gray-scale invariance.

LBP is widely used in facial expression recognition and a powerful method to describe the texture of image. The cropped image could be divided into cells(e.g. $a \times a$ pixels for each cells). Then compare each pixel with its eight neighbour pixels by circle in a cell, write ‘0’ when the value of center pixel is greater than neighbour's and write ‘1’ when it is smaller. An 8-digit binary number will be given after that. So with 8 surrounding pixels there will be 256 possible combination, called Local Binary Patterns. This histogram is seen as a 256-dimensional feature vector. The basic LBP operator described is a fixed 3×3 neighbourhood. A more formal description of LBP operator is given as:

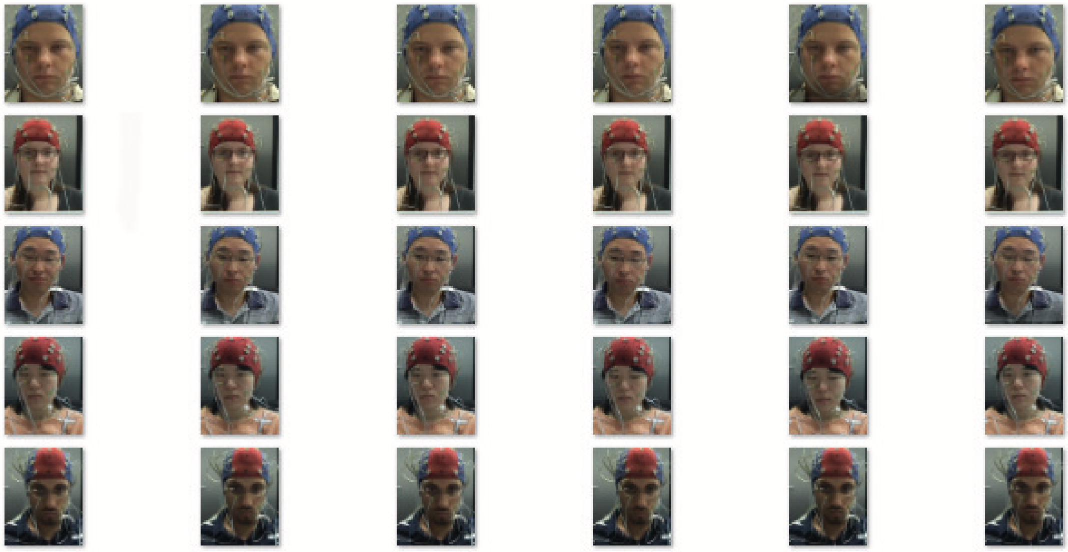

Figure 2.15: The sample facial image after auto-screenshot from the videos.

$$LBP(x_c, y_c) = \sum_{p=0}^{P-1} 2^p s(i_p - i_c) \tag{2.9}$$

(x_c, y_c) is the central pixel with intensity i_c and i_p is the intensity of the neighbour pixel. s is a sign function defined as:

$$s(x) = \begin{cases} 1, & \text{if} \quad x \geq 0 \\ 0, & \text{else.} \end{cases} \tag{2.10}$$

Different types of curved edges has been coded by the binary number of LBP which is shown in Figure 2.16.

The position of the neighbour (x_p, y_p) of a given point (x_c, y_c), $p \in P$ can be calculated by :

$$x_p = x_c + R\cos(\frac{2\pi p}{p}) \tag{2.11}$$

$$y_p = y_c - R\sin(\frac{2\pi p}{p}) \tag{2.12}$$

R is the radius of the circle, which indicates the distance from the centre to the neighbour points. P is the number of sample points, which illustrates the total number

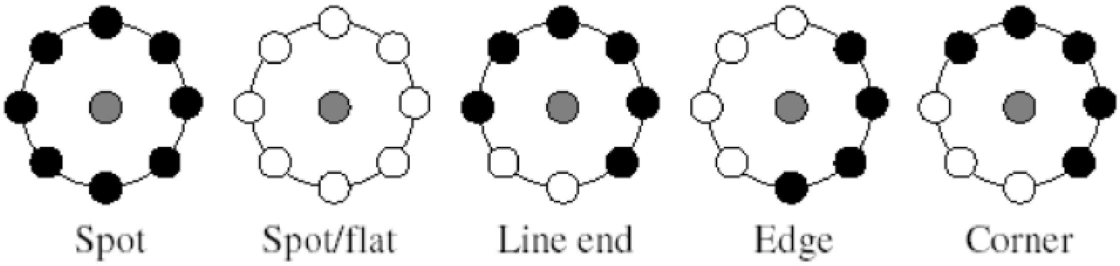

Figure 2.16: Examples of texture primitives which can be detected by LBP (white circles represent ones and black cirlces zeros).

(See: [85])

of circularly symmetric neighbours for one centre point. This operator is an extension to original LBP codes and it's called Extended LBP or Circular LBP. The LBP algorithm is executed by Matlab function 'extractLBPFeatures'. An 1×10 feature vector is obtained for each cropped facial expression image. Therefore, the dimension of feature matrix is 52440×10.

The developed hybrid classifier utilises both EEG features and facial expression features to determine the responses of the test subjects. This study is a subject dependent experiment.

2.5.2 Results

Figure 2.17 represents the accuracy of the classifiers from valence plane. The single SVM classifier, which is the green line, stays at lowest accuracy in most cases. It also fluctuates along the mean value largely comparing with the other two lines. This indicates that the single SVM classifier is less stable than the hybrid classifier. It is also important to notice that for Participant 19, the classification accuracy on the valence plane is lower than others, and the single SVM returns a higher percentage than the hybrid one. This reason for this outlier is that this participant identifies his emotion feedback on the questionnaire is around the median number 5. In this emotion model, the median number is used to separate the classes. Therefore, although the emotion identified by Participant 19 is neural, such as 4.5-5.5 on valence plane, the emotion model divides the emotion into either positive or negative. On the valence plane, the hybrid classifier with EEG features only returns a stable classification accuracy shown as the red line; nonetheless, the combined EEG and facial expression features demonstrates the highest

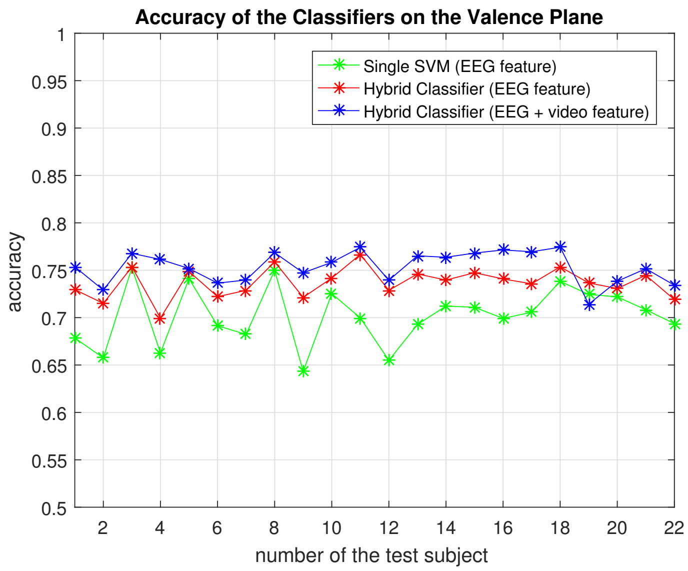

Figure 2.17: Accuracy on Valence Plane

accuracy. The highest accuracy is close to 80% and there are more than half of the test subjects showing over 75% accuracy.

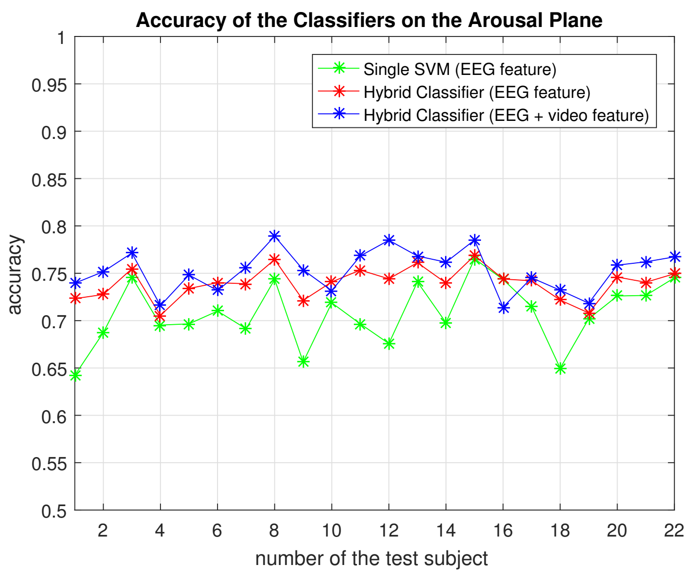

Figure 2.18: Accuracy on Arousal Plane

The average accuracy on the arousal plane has the similar trends as the valence plane shown in Figure 2.18. The single SVM is the most inaccurate and unstable classifier. However, even though there are certain test subjects showing that combined features give higher accuracy, for subject 16, the accuracy is significantly lower than the EEG feature only classifier. These predictions of the classifiers reaffirm that in some situations, facial expressions can be consciously regulated by individuals and become misleading for emotion classification.

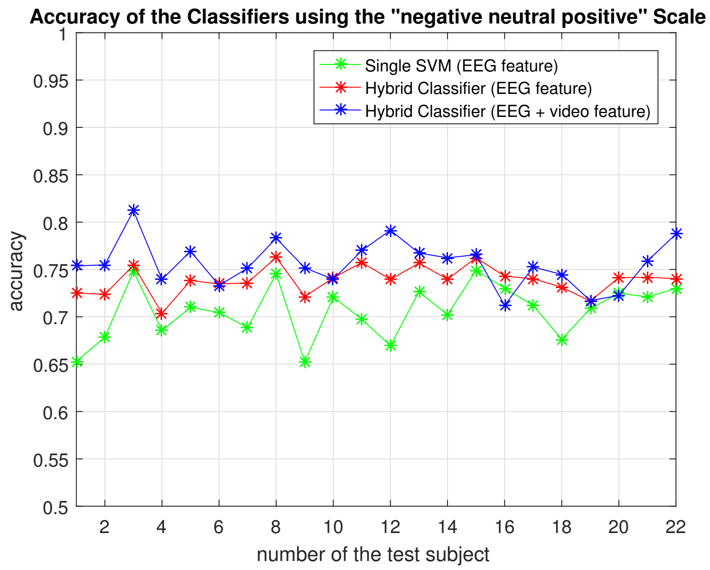

Figure 2.19: Accuracy on 'Negative Neutral Positive' Plane

The 'Negative Neutral Positive' plane is specifically designed for the purpose of providing feedback for an affective system. Figure 2.19 illustrates the subject dependent classification accuracy based on this model. The general trend consists with the previous arousal-valence model; nevertheless, the hybrid classifier with both EEG and facial expression features demonstrates high accuracy. Test subject 2 has over 80% accuracy and three other subjects show accuracy that is very close to this number. As well, Subject 19, which is considered as a special case using the valence-arousal plane model, shows a steady classification accuracy using NNP model. This finding explains that the 'Negative Neutral Positive' model not only gives the intuitive expression of the emotion feedback, but also improve the accuracy of the classifiers.

The bar chart shown in Figure 2.20 compares the overall accuracy for each of the classifier in all three planes. The lowest overall accuracy is always the single SVM classifier and the highest is the hybrid combine feature classifier. The increases of the accuracy are over 5% for all three planes. The largest increase from EEG feature only to combined features occurs on the valence plane, which is 1.68%. The highest overall accuracy is 75.64%, which is on the "Negative Neutral Positive" plane. Thus, the third

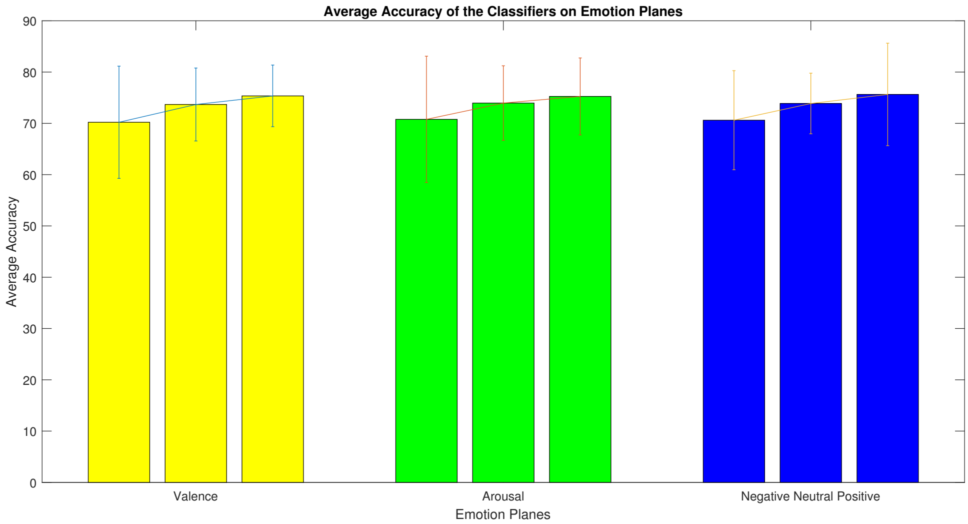

Figure 2.20: Average Accuracy on Three Different Emotional Planes. Yellow indicates valence, and green indicates arousal plane. The blue bars use the NNP model.

blue bar has the highest accuracy among all with a reasonably small error range, which indicates that the FCM-SVM classifier with both EEG and facial expression features using the “Negative Neutral Positive" model is the optimal design for affective system feedback recognition.

This last solution offers a hybrid physiological approach to emotional feedback detection of affective system. The physiological method uses EEG signal and facial expression collected from the customers, applied with the state-of-the-art biomedical signal processing techniques such as LBP, CS and wavelet analysis to extract the distinctive features. Various machine learning algorithms and feature selection combinations have been tested using the processed DEAP dataset. The optimal design of the emotion feedback classification is to use an innovative FCM-SVM classifier with both EEG and facial expression features on the “Negative Neutral Positive" plane. The design overcomes the common issues with emotion classification including emotion model definition, feature extraction and machine learning algorithm design. It improves more than 5% accuracy comparing to the stanard SVM classifier. The overall accuracy for this design is 75.64% with the highest accuracy at 81.2%.

CHAPTER 3

Electromyogram and Post Stroke Movement Analysis

3.1 sEMG-based Statistic and Frequency Analysis

Statistic and frequency analysis allow us to explore the hidden information of sEMG signal. It can also reduces the size of the data for later processing methods. Here, we present six statistic analysis methods and two frequency analysis methods that are broadly used in sEMG analysis [86].

First, mean absolute value (MAV) is one of the most used features in statistical analysis. The reason for taking the absolute value is that sEMG signal varies from negative to positive. The rectification process make the signal into all positive numbers, which presents an easier quantitative analysis. The equation for MAV is:

$$MAV = \frac{1}{N}\sum_{i=1}^{N}|x_i| \tag{3.1}$$

Variance of EMG (VAR) is another time domain feature that is used in sEMG analysis. The equation is shown as:

$$VAR = \frac{1}{N-1}\sum_{i=1}^{N}|x_i^2| \tag{3.2}$$

Root mean square (RMS) is a popular feature that is often measured in sEMG projects. It is calculated as Gaussian random process with constant force and non-fatigue level of the muscle. The euqation is shown as follow:

$$RMS = \sqrt{\frac{1}{N}\sum_{i=1}^{N} x_i^2} \tag{3.3}$$

Log detector feature is closely related to the contraction force of the target muscle. The equation is shown as:

$$LOG = \exp\frac{1}{N}\sum_{i=1}^{N} log(|x_i|) \tag{3.4}$$

Waveform length (WL) measures the complexity of the sEMG signal. It is the cumulative length of the EMG signal over time. The equation is:

$$WL = \sum_{i=1}^{N-1} |x_{i+1} - x_i|) \tag{3.5}$$

The last time domain feature is zero crossing (ZC). This parameter calculates the number of times that EMG waveform crosses the zero amplitude. To minimise the impact from noises, a threshold is always set to determine a range of small variations around zero amplitude are all consider as zero for the sign function. The equation for ZC is:

$$ZC = \sum_{i=1}^{N-1} sgn(x_i * x_{i+1} \cap |x_{i+1} - x_i| \geqslant threshold) \tag{3.6}$$

The spectral domain features are mainly used to investigate the level of fatigue and MU recruitment. The frequency domain is based on the Fourier Transform. In recent years, more spectral features are used in continuous monitoring and rehabilitation projects. First, one of the most basic feature is mean power of the EMG power spectrum. The formula is shown as:

$$MNP = \sum_{j=1}^{m} P_j/M \tag{3.7}$$

Power spectrum ratio (PSR) merges the information from peak frequency and frequency ratio. This parameter compares the energy at the maximum of the power spectrum with the total energy of the entire signal. The equation is:

$$PSR = \frac{\sum_{j=f_0-n}^{f_0+n} P_j}{\sum_{j=-\infty}^{\infty} P_j} \tag{3.8}$$

3.2 EMG Connectivity Analysis in Stroke Rehabilitation

In this section, the proposed sEMG-based functional connectivity techniques are primarily adapted from brain connectivity analysis. Since the early 2000s, two functional connectivity techniques have been broadly applied in EEG studies, Directed Transfer Function (DTF) and Partial Directed Coherence (PDC) [87]. DTF can be used to determine the directional influences between any given pair of channels in a multivariate dataset. DTF is an estimator that simultaneously characterizes the direction and spectral properties of the interaction between brain signals and requires only one multivariate autoregressive (MVAR) model to be estimated simultaneously from time series. Another popular estimator, PDC, transforms into the frequency domain as a factorization of the Partial Coherence based on MVAR coefficients [88]. The PDC is of particular interest because of its ability to distinguish direct and indirect causality flows in the estimated connectivity pattern. Furthermore, to adapt the specific features of sEMG and UL movements, a windowing technique shall be included to present the time information. By applying connectivity analysis on EMG signal, the mapping between biological signal and UL postures evolves to a network of the muscle group, where the dependence and information exchange between the muscles can be formulated.

To further investigate the EMG connectivity result, graph theory techniques play a significant role in reducing the complexity and extracting features. The abstract definition of a graph containing nodes and edges can be smoothly transferred into UL muscle groups and the information flows between them. In EMG connectivity, binary directed networks can be constructed by applying DTF and PDC. Measures of functional segregation and integration present the local and global connection within the network. Therefore, basic attributes such as network density, where the sparseness of the network is calculated, and link reciprocity reflects the tendency of paired nodes. The functional integration is computed using the shortest path length that estimates the strength of the connection between each muscle groups. Another measure, clustering index, which is firstly introduced by the famous 'small-world' network paper, is a suitable indicator for functional segregation analysis.

An innovative approach is offered here to analyse the interconnection of upper limb muscle groups based on sEMG signal for stroke rehabilitation. Functional connectivity analysis is adapted from EEG-based techniques to determine the dominance of the individual muscle dynamically. In this dataset, both affected and non-affected sides are processed for comparison during four-force-level gripping activities. This analysis discovers the differences in the physiological connection for paretic extremities by implementing network analysis parameters. Furthermore, the comparison between the paretic side and non-paretic side offers a powerful tool to design a transformational algorithm, where the paretic arm can study the connectivity patterns of the non-paretic arm.

3.2.1 Materials

The experiment was conducted by the faculty of Biomedical Engineering at Sun Yat-sen University. There were eleven subjects after stroke, mean age: 54 ± 15.84 years, three females, eight males, including in this experiment. The subject selection criteria are firstly hemiparesis resulting from a single unilateral lesion of the brain with onset at least one month prior to data collection. Secondly, the patients are able to generate voluntary contractions of both hands. As well, the participants show normal proprioception as indicated by scoring more than 33 on the sensory and proprioception components of the Fugl-Meyer Assessment (FMA). Lastly, the patients have no visual, cognitive or attention defect which prevented following the experimental procedures as indicated by a score of 23 or more on the mini mental state examination (MMSE). In the healthy group, all the participants were righthanded. Informed consent was obtained from all participants. The study was approved by the Ethics Committee of Sun Yat-sen University.Hand and arm motor impairments of the subjects after stroke were assessed using both FMA and Wolf Motor Function Test (WMFT).

The customised grip dynamometer was cylindrical with a diameter of 60 mm and a height of 90 mm, and it was fixed to the experiment table. The dynamometer contained four force sensors placed asymmetrically to measure the grip force and calculate the rotation torque. A 16-bit analogue to digital converter sampled the force data at a rate of 1000 Hz. As well, customised surface EMG sensors were attached on the upper limb muscles , namely biceps brachii, anterior deltoid, posterior deltoid, flexor carpi radialis, extensor carpi radialis, flexor digitorum superficialis and extensor digitorum communis. The EMG signal was also sampled at 1000 Hz.

Both the affected and unaffected hands of the stroke group and the dominant hands of the healthy group were tested. The participants were instructed to sit with their backs straight against the backrest of the chair and rest the arm to be tested on the tabletop. The upper arm was in a neutral adducted position with approximately 15 - 20° of shoulder flexion and 90° of elbow flexion. The dynamometer was grasped with the thumb and the four fingers in opposition. During testing, the forearm of each participant was constrained by a belt to standardize grip position and prevent forearm motion. Each participant was first instructed to apply maximal grip force (MGF) to the dynamometer three times, holding it for 5 seconds each time while an indicator light was illuminated. The largest MGF among the three measurements was used to normalize the grip force for the sub-maximal force level tasks. The visual presentation designed using LabVIEW displayed both the target and the actual force levels. Figure 1 shows the LabVIEW presentation viewed by each participant. The stationary horizontal red lines represented the three target force levels, and the movable horizontal blue bar represented the actual force level produced by the participant in real time. Then, the participants were instructed to apply sub-maximal force to move the blue bar at the red target line and hold it for 5 seconds. The targets were 25%, 50% and 75% of the MGF. A rest period of 30 seconds was provided between each trial to minimize fatigue. Each force target was presented three times for a total of 9 sub-maximal trials with each participant. Both force and EMG signal from paretic and non-paretic sides were saved for off-line analysis.

3.2.2 EMG Connectivity Analysis

We hypothesize that the stroke-related motor outcome measures can be represented from the interaction of neuromuscular signal in stroke rehabilitation therapy. Moreover, the performance UL movements are accompanied by EMG-based functional connectivity patterns that are evaluated using graph theory measures.

Force and EMG signal are collected simultaneously while the stroke patients are performing the gripping exercise. The stored data firstly enters the pre-processing steps, including filtering, rectification and segmentation. Then, the pre-processed data is analysed by two connectivity methods, which are Short-time DFT and Short-time PDC. Since the experiment shows four force groups, the results can be compared between different percentages of MGF, paretic and non-paretic limb and across the patients. The last step is to use the analysis to generalise the critical concepts of the movement support system that can provide the necessary support to complete the rehabilitation exercises.

A fourth-order Butterworth low-pass filter with a cut-off frequency of 20 Hz was used to filter the force signals. Another third-order Butterworth band-pass filter was added to remove the noise from the EMG signal. The lower cut-off frequency was set to 20 Hz and the higher cut-off frequency is 150 Hz. The EMG signal was also rectified to ensure all data are positive for later calculation. Since the experiment carried out for 15 seconds and the patients held the grip sensor for at least 5 seconds, it is critical to include the time information in the analysis. Therefore, a 1-second window with 0.25-second overlap was utilised for EMG segmentation. Similar to the Short-time Fourier Transform, this segmentation process improves the connectivity analysis by adding the time domain.

First, the EMG signal that includes eight muscle groups in total uses MVAR to generate the estimation parameters. The algorithm adopts the linear Kalman filtering approach to update the MVAR parameters for each time sample. Given a univariate time series, its consecutive measurements contain information about the process that generated it. An attempt at describing this underlying order can be achieved by modelling the current value of the variable as a weighted linear sum of its previous values. This is an autoregressive (AR) process and is a very simple, yet effective, approach to time series characterization [89]. The order of the model is the number of preceding observations used and the weights are the parameters of the model estimated from the data that uniquely characterize the time series [90]. Multivariate autoregressive models extend this approach to multiple time series so that the vector of current values of all variables is modelled as a linear sum of previous activities.

Let X be a set of EMG signal. The pre-processed signal can be presented as:

$$X = [X_1(t), X_2(t), X_3(t), ..., X_8(t)]^T \tag{3.9}$$

where t refers to time and the subscripts indicate the number of the muscle groups. There are eight muscle groups, so the total number of the channels is eight.

The MVAR model is transformed in the time-varying system. The general format of the equation is:

$$Y(t) = \sum_{p}^{i=1} Y(t-i)A(i) + E(t) \tag{3.10}$$

where p is the order of the model, $A(i)$ is the 8-by-8 matrix of coefficients defined by the linear Kalman filtering shown above, and $E(t)$ is the vector of white noise.

The model order, p, is calculated from the Bayesian-Schwartz‚Äôs criterion:

$$SC(p) = ln[det(V)] + \frac{ln(N) * p * 8^2}{N} \tag{3.11}$$

where V is the noise $E(t)$ covariance matrix, and N is the total number of the data. Then, to present the same information from the frequency domain:

$$A(\lambda) = \sum_{p}^{r=1} A_r z^{-r}|_{z=e^{-j2\pi\lambda}} \tag{3.12}$$

and $H(\lambda) = A^{-1}(\lambda)$ is the transfer function derived from $Y(t)$.

The normalised DTF represents the ratio between the inflow from the source channel to the destination channel to the sum of all inflows to this channel. The value of the normalised DTF is always from 0 to 1, where 0 means no influence and 1 means the maximum influence [91]. The calculation is shown as:

$$\gamma_{ij}^2(\lambda) = \frac{(|H_{ij}^2(\lambda)|^2)}{\sum_{m=1}^{8}(|H_{im}^2(\lambda)|^2)} \tag{3.13}$$

Where i is the destination channel and j is the source channel that is used to calculate the influences comparing with the total influence from all eight channels. DTF detects the source channel for both direct and indirect flows. To distinguish between the direct and indirect transmissions, PDC is utilised to show the direct relations only in the frequency domain [92]. It is defined as:

$$\pi_{ij}^2(\lambda) = \frac{(|A_{ij}^2(\lambda)|^2)}{\sum_{m=1}^{8}(|A_{im}^2(\lambda)|^2)} \tag{3.14}$$

This function describes the ratio between outflow from the channel j to channel i to all the outflows from the channel j. Both PDC and DTF are necessary for this analysis as they cover different aspects of the connectivity problem. Whereas PDC addresses the immediate direct dynamic frequency domain link between the various time series, DTF exposes the links from one time series to another regardless of the influence pathway, be it immediate or otherwise [93]. DTF shows the existence of the influence of the source channel onto all other channels while it is not influenced by them. As such, PDC portrays immediate direct connectivity, whereas DTF portrays directional signal reachability denoting active indirect interaction. By plotting both of methods against time, the rehabilitation exercise can be analysed regarding the upper limb muscle groups and their interconnection relationship.

3.2.3 Graph Theory Analysis

First, to demonstrate the sparseness of the network, one of the most frequently used parameter is density, denoted by k. The value varies from 0 to 1, where 0 means sparser, and the network has fewer edges and less information is transferred between the nodes

[94]. The calculation for density is shown as:

$$k(M) = \frac{1}{N(N-1)} \sum_{i \neq j} m_{i,j} \tag{3.15}$$

By combining PDC and DTF analysis, we create EMG-based directed connectivity networks for upper limb movements. The information flow in or flow out becomes an important identity needed to be addressed. Moreover, the tendency of forming paired nodes is considered to reveal significance of the information flow in the EMG network. Link reciprocity illustrates the tendency of pairing nodes that can be computed as:

$$\rho(M) = \frac{r(M) - k(M)}{1 - k(M)} \tag{3.16}$$

The following two parameters are broadly used in binary network analysis. The structural properties of the network are demonstrated by the average shortest path length PL and clustering index C. C measures the cliquishness of the neighbourhood (a local property), whereas PL measures the functional integration property between two nodes in the graph (a global property) [95]. The equation for the characteristic path length is shown as:

$$PL = \frac{1}{N(N-1)} \sum_{i \neq j} d_{i,j} \tag{3.17}$$

3.2.4 Discussion

Based on the EMG and force signal extracted from the stroke patients while they are performing the grip exercise, it is possible to address the limitations mentioned at the beginning. Firstly, a new approach of neurophysiological analysis specifically for stroke rehabilitation is established. Using connectivity analysis on EMG signal transforms the upper limb into a system where each node is one group of muscle. The eight nodes in total show a complete system for movement analysis. By differentiating the levels of strength, the interrelationship between the eight muscle groups on the healthy and paralysed arm is clearly shown. The common channels that are displayed in all strength levels show the consistency of the movement. More importantly, the difference of the connectivity is noticed to distinguish how the muscles work to generate higher strength. The more significant analysis is to compare the paretic and non-paretic muscle connectivity. This comparison indicates the internal connection between the muscles after stroke. It is reasonable to assume that similar EMG connectivity would be obtained on both arms for healthy subjects. This analysis shows one of the possible reasons why the stroke-affected arm cannot perform as well as the healthy side from the muscular function point-of-view. Therefore, to recover from the affected motor function, gaining the similar muscle connectivity can reduce the difficulties and time length of the recovery, as the connectivity represents the certain individual movement pattern. This approach overcomes the issue with the learning a 'general' or 'healthy' movement pattern that is developed by other people.

The possible application for this analysis is to design a movement support system for stroke rehabilitation exercises. The system would use the healthy side of the EMG connectivity as the reference. Since the time information is also included in the Short-time DTF and Short-time PDC analysis, it has the potential to track the connectivity changes on the paralysed arm in a real-time situation. The rehabilitation device shall provide the adequate support to transform the connectivity on the paretic side to the reference. Nonetheless, before drawing the conclusion, a few limitations of this study need to be pointed. The experiment needs to be expanded to a larger number of patients and more categories of rehabilitation exercises. As well, DFT and PDC are functional connectivity methods, effective connectivity analysis such as Granger causality shall be considered in the following studies.

3.3 An EMG Connectivity Application: Functional Electrical Stimulation-based Stroke Rehabilitation System

3.3.1 Introduction

Functional Electrical Stimulation (FES), which directly stimulates the affected muscle by applying electrical current [96], also indicates a direct effect on the excitability of the central nervous system [97]. FES has been utilised in a series of fundamental movements, including standing and walking [98] mainly targeting large muscles. However, to make this treatment available for more precise and complex low-level fine movements, Jarc et al. proposed that it is necessary to develop a patient-specific stimulation pattern to cope with varying task demands [99]. Furthermore, to reduce the expertise and labour required to provide instruction and supervision, the stimulation strategy shall embed intelligent technologies such as automating intervention. This goal can be achieved by implementing an analysis of patients' biological data. Therefore, FES is also capable of transferring the recovery process from repeating personal-instructed and practical exercises to a data-driven neurophysiological point-of-view.

Regarding the analysis of neuro-feedback of the rehabilitation, electromyography is the most frequently used parameter since it reveals the electrical activity of a specific muscle that is related to the muscle force [100]. EMG connectivity analysis using MVAR was proposed to analyse the inter-relationship between muscles. Using EMG connectivity analysis, the paretic arm is considered as the abnormal system, and the non-paretic arm is the reference side. The rehabilitation strategy is to control the abnormal system to generate identical EMG connectivity patterns as the reference side.

To implement FES in upper-limb rehabilitation, a permutation representation of the EMG connectivity can be adapted in this circumstance. The permutation network transforms n input terminals to its n output terminals [101]. Moreover, the n-puzzle problem solver can be used here to discover the FES triggering method. The n-puzzle problem consists of the initial state, goal state, path cost and successor function [102]. In the case of automated upper-limb FES strategy, the eight-puzzle solver is ideal since the solver is the largest puzzle can be completely solved [103], and the eight channels can efficiently cover the majority of the superficial muscles on the arms.

In this section, a permutation representation is proposed to describe the EMG connectivity analysis and an 8-puzzle solver is modified as the automated FES control strategy to simulate the transfer from the abnormal to the healthy muscle inter-connection. The following section illustrates the material used in this study and an overview; the EMG connectivity methods, permutation representation and 8-puzzle solver. The stimulation strategy was then applied to an 11-patient database to evaluate the efficiency of the proposed functional electrical stimulation system.

3.3.2 Methods

A third-order Butterworth band-pass filter is used to remove the noise from the EMG signal explained in the previous section. The lower cut-off frequency is set to 20 Hz, and the higher cut-off frequency is 150 Hz. The EMG signal is then rectified, and a 1-second window with 0.25-second overlap is utilised for segmentation. Similar to the Short-time Fourier Transform, this segmentation process improves the connectivity analysis by adding the time domain.

The short-time DTF and PDC analysis reveal a large amount of information regarding the interconnection between the eight muscles. For each time segment, there are seven outflows from one muscle, and there are seven inflows towards one muscle. Therefore, the representation of the connectivity analysis is often a complex matrix; in this case, a 8 x 8 matrix. Since both inflow and outflow are considered, two matrices are shown for each time segment. The complexity of this representation creates obstacles for real-time FES triggering. Thus, the cycle notation of permutation is adopted in this process. The most dominant muscle is firstly determined. In each time frame, DTF and PDC are combined to find the closest connected muscle to the most dominant muscle and treat as the next element in the cycle. This mathematical transformation is a rather conceptual conversion from a high dimensional data to a simple format. A three-dimensional human model using graphic modelling tool Blender is established to visualise the permutation representation of the EMG connectivity more directly and intuitively.

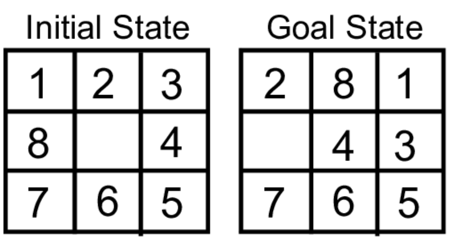

Figure 3.1: An Example of 8-puzzle Problem

The permutation representation of the EMG connectivity reduces the complexity of an 8x8 matrix to an eight-element sequence. In this study, we consider the non-affected side as the reference and the affected side as the abnormal system. Therefore, for each patient, there will be two sequences representing the muscle interconnection. This idea is identical to Eight-puzzle Problem, one of the classic difficulty problem in artificial intelligence [104]. Figure 3.1 is an example of the 8-puzzle problem. The goal is to rearrange the initial state squared tiles to the goal state by moving tiles into the adjacent empty square. An artificial intelligence 8-puzzle solver by MATLAB is designed using the node ordering schemes in Iterative-Deepening A*. As mentioned above, the 8-puzzle has one initial state, which is the paretic arm permutation and one goal state, which is the healthy arm permutation. The solver calculates the simplest path, presents the step-by-step instruction, and offers the cost function, which shows the total number of steps needed to reach the goal state. The simplest path is then selected as the automated FES stimulation strategy.

3.3.3 Results and Discussion

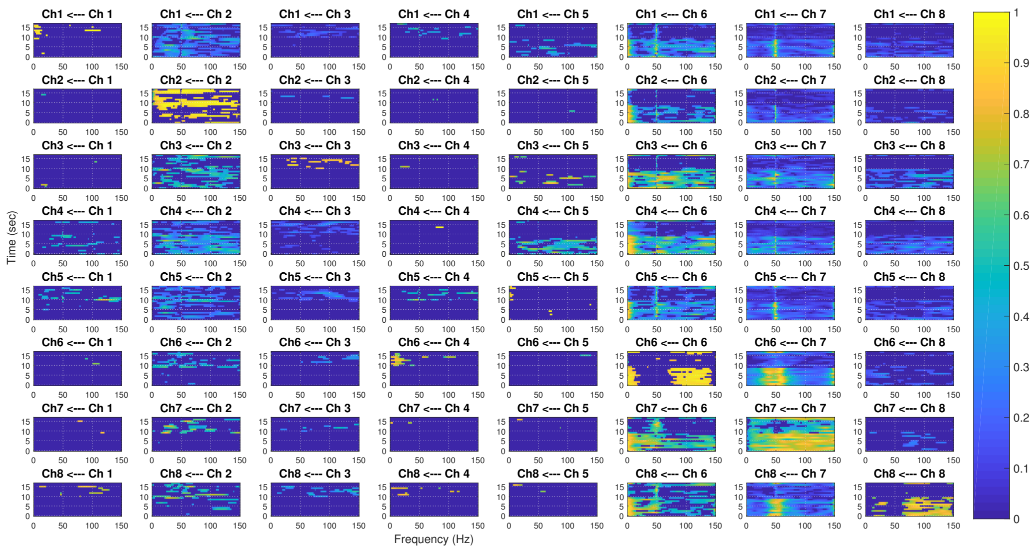

Figure 3.2: Patient 9 Non-paretic Sides 25% MGF DTF Representation Using 8x8 Matrix

The EMG connectivity using DTF and PDC are firstly represented using two 8 x 8 matrices. One example is given in Figure 3.2. In this example, patient number 9 is selected while performing 25% of MGF. Figure 3.2 shows the non-paretic arm, and

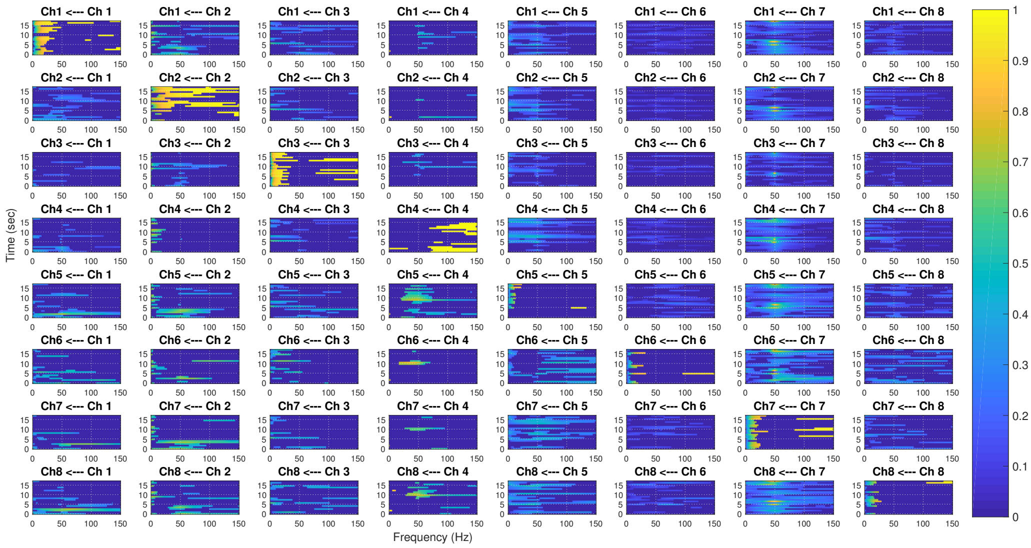

Figure 3.3: Patient 9 Paretic Sides 25% MGF DTF Representation Using 8x8 Matrix

Figure 3.3 indicates the paretic arm connectivity of the DTF analysis. The vertical axis represents time in seconds, and the horizontal axis represents frequency in Hertz. The colour bar on the right indicates that strong influence appears in yellow and weak influence is in dark blue. The most dominant muscles are clear to identify. For the non-paretic side, the DTF shows muscle number 6. On the paretic side, DTF is muscle number 7. This finding proves that the connectivity between muscles has differences between the paretic and non-paretic arm. Moreover, these differences can cause the rehabilitation process to be struggling for the patients. It is important to note that traditional mirroring therapy requires the patient to following the exact movement based on mechanical observation. Nevertheless, in this FES training strategy, we focused on the neuromuscular feedback of the non-paretic arm. Thus, instead of aiming at asking patients to follow specific movement trajectories, the rehabilitation shall be focused on the training the muscles to coordinates with each other in the correct fashion.

Table 3.1: Permutation Format: Cycle Notation

Upper Extremity	Permutation Sequence
Non-affected	(6, 3, 4, 8, 7, 5, 1, 2)
Affected	(7, 8, 4, 5, 1, 2, 6, 3)

To extract the information about the information flow between muscles, the permutation representation is adapted for a clearer understanding. The same example is used to show the cycle notation of the permutation. These matrices shown in Figure 3.2 and Figure 3.3 can be reduced to the format shown in Table 3.1. On the health side, the most dominant muscle number is 3, then muscle number 6 is most connected with muscle number 3. The next element is muscle number 4, and so on. This process is also implemented using MATLAB. This representation reduces the complexity of the original matrix format. The same observation can also be demonstrated using a three-dimensional human model shown in Figure 3.4. It contains the specific muscle names and locations with the corresponding movement animations.

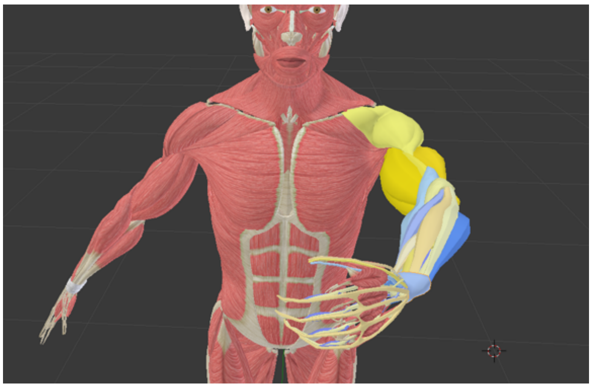

Figure 3.4: Permutation Format: Three-dimensional Human Model

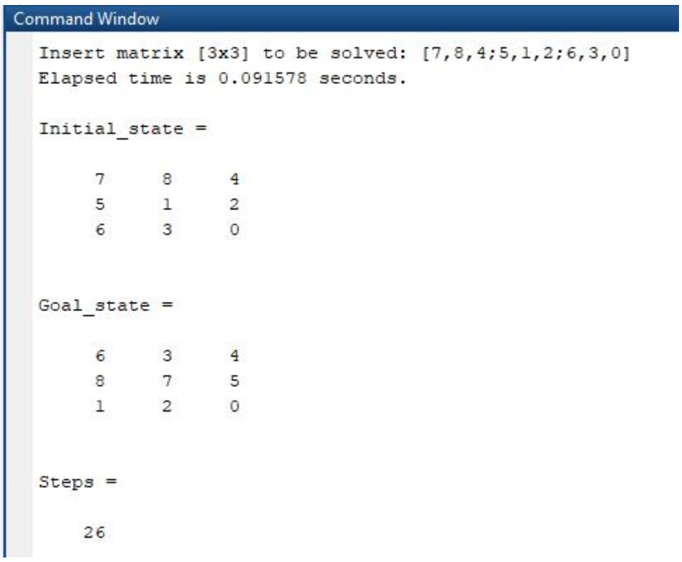

Figure 3.5: 8-Puzzle Solver

Lastly, the 8-puzzle solver is utilised to find the fastest path from the initial state to the goal state. In Figure 3.5, both states are presented in the tradition 8-puzzle format. MATLAB is used in this stage to best move and the cost, which is the total number of the action required. Following the previous example for patient 9, the cost is 26 steps, indicating that the automated stimulation strategy for this particular case requires 26 steps to convert the affected arm EMG connectivity pattern into the normal one. We executed this proposed strategy to all collected data. Since 11 patients performed 12 upper limb movements for each individual, we have in total of 132 trials. The average length of the optimal path is 14.65 ± 3.82 (round up to 11–18) steps, with the minimum steps is 4, and the maximum is 27. Considering a conventional pre-defined FES treatment is usually over 10 minutes, the number of steps is within a reasonable range. Considering the low computational power required, this proposed strategy can be implemented in the current market-available FES devices that are programmable.

3.4 Conclusion

Module 2 presents a novel automated functional electrical stimulation strategy for upper limb stroke rehabilitation. It is developed by simplifying the inter-relationship between muscles to permutation notation. Then, the puzzle-based solver is modified to find the best path from the paretic side to the healthy side of the arm. This best path represents the fastest stimulation strategy to train and support patients' movements. Based on the 11 stroke patients dataset, this automated stimulation strategy requires small computational power to calculate the patient-specific intervention, and the procedure is simple to implement in practical fields.

CHAPTER 4

Hybrid Biosignal-based Rehabilitation System Using A Wearable Robot

4.1 AI Exoskeleton: a Self-developed Rehabilitation Robot

At present, the mainly clinically therapy for post-stroke patients is repetitive, active movement-based rehabilitation which promotes brain plasticity and motor recovery to regain various functions [100]. Many of the improvements are made in the first six months after treatment, but improvement can continue for years [105]. Although rehabilitation can improve the motor function of the affected limb, several concerns and challenges are needed to be addressed.

Firstly, the cost of the physical therapy is high due to the requirements of professional supervisions at specific facilities and hospitals for a long-term. Now in Australia, the number of registered physical therapist members is around 18,000, which is seriously insufficient. As well, patients need to purchase a series of rehabilitation devices to meet the different demands along the recovery process. The annual cost of outpatient stroke rehabilitation is approximately 24,500 AUD [104], which could last for several years. The financial burden would discourage patients from receiving proper rehabilitation training.

Secondly, as the age group of stroke incidence is getting younger [106], the traditional rehabilitation methods such as motor-skill exercises, mobility training, and constraint-induced therapy appears to be a lack of pleasure and efficiency for younger patients. Especially, when young workers are the targeted patients, their goals are returning to independent daily life and work as soon as possible. Thus, new technologies with better interactions are demanded.

One approach to overcome the above issues is robotics. Since the 1960s, robot technology has been developed with the characteristics of precision, controllability, and lack of fatigue [107]. Due to these advantages, since the 1980s, the research of rehabilitation robots has begun to attract attention. Rehabilitation robots can assist physiotherapists in rehabilitation training to free physiotherapists from high-intensity physical labour. By using the high-precision sensors attached to robots for monitoring and evaluating the training process, the physiotherapists can accurately grasp the recovery of patients' motor function, so as to develop a corresponding training program, make training more targeted and scientific. Furthermore, robotic devices have the advantages of possible independent training, where professional human power is not necessary during the training if proper safety measures have been considered.

In order to design a rehabilitation program for helping young post-stroke patients return to work, a further challenge is to provide individualised rehabilitation goals and management plans based on patients' own requirements [108]. However, most of the current rehabilitation robots cannot make real-time adjustments according to the patient's consciousness. It is easy for patients to rely on the machine to passively complete the training [109]. Since stroke can affect both upper and lower extremities motor function at different severity, rehabilitation robots need to cover different motor functions on both arms and legs. As shown in the research in [110], the majority of the young patients are blue-collar workers, therefore both gross and fine motor functions are required to be included in their rehabilitation. As well, a new technology, Virtual Reality (VR), demonstrates the advantages of mimic real working environment and the higher level of engagement. Thus, a robotic-based full-body rehabilitation system with lower costs, improved recovery efficiency and enjoyment shall be developed to assist young stroke survivors to return to work.

This section introduce a self-developed multi-mode robotic rehabilitation system (MRRS) with multiple training modes and functions for aiding young post-stroke patients to finish their personal-designed training programs based on their needs for returning to work.

First, an upper-limb exoskeleton is going to be developed for rehabilitation exercises such as gripping. The upper-limb exoskeleton would use the functional connectivity analysis on surface electromyography to discover the movement pattern of the health side of the arm and use this information as the reference to train the paretic arm. By doing such, the exoskeleton uses the patients' own movement characteristics, so it would be easier for them to regain the movement abilities.

VR is introduced in this project as the main visual feedback method for rehabilitation exercises. Actual working environments is developed using VR. To evaluate the rehabilitation system and ensure the safety of the training, the project also aims to use electroencephalogram of the patients to detect the fatigue level and emotion states, as well as to classify the whether the movement is passive or active.

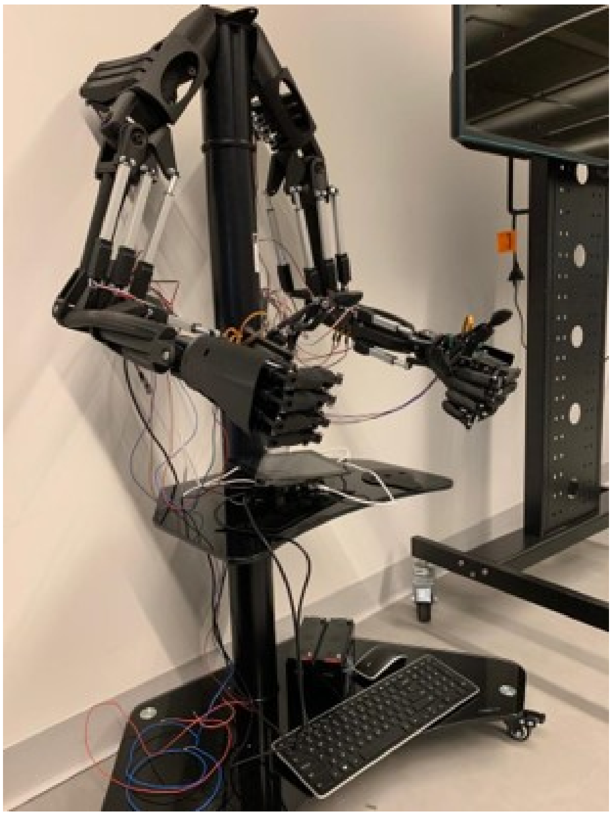

Figure 4.1: AI Exoskeleton

Figure 4.1 shows the design our AI exoskeleton that can be used in various stages of stroke rehabilitation. It uses 3D printed material as the main frame of the robot. Carbon-reinforced material ensures rigidity of the robot, at the same time, offers a lightweight design. Regarding the hand, shown in Figure 4.2, there are six linear actuators to perform flexion and extension of the fingers and thumbs. The additional actuator allows the thumb to rotate.The hand is able to perform several hand gestures, including basic movement such as pinch gripping, shown in Figure 4.3, and complex movements such as holding a cup, shown in Figure 4.4.

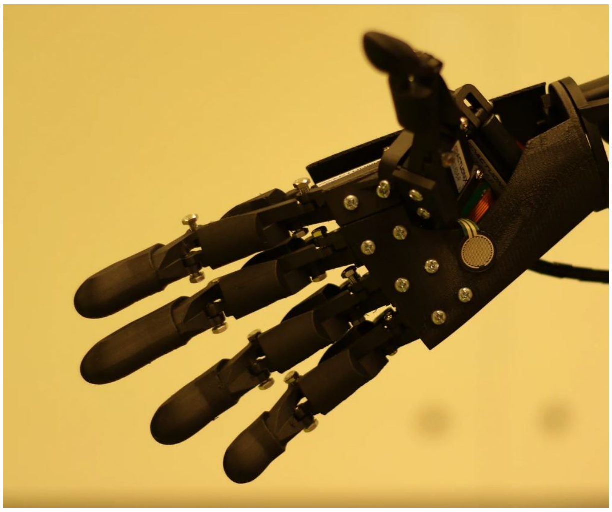

Figure 4.2: Hand section of the AI Exoskeleton

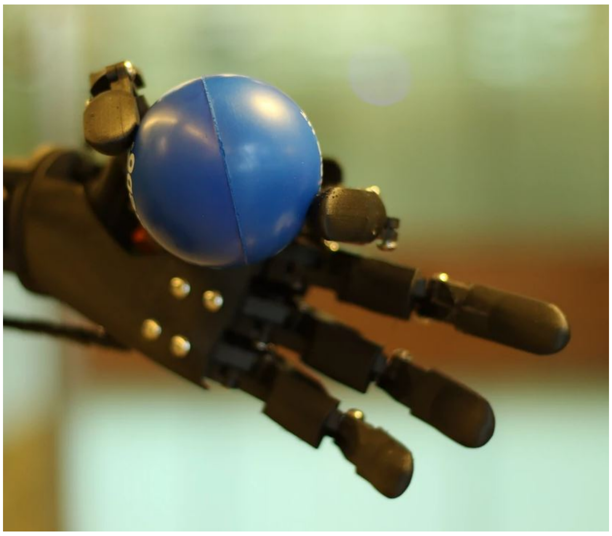

Figure 4.3: AI Exoskeleton performing pinch grip

On each side of the robot, the forearm consists of 5 actuators. There are 4 actuators on the upper arm and 3 actuators around the shoulder area. In total 12 actuators permits wrist, elbow and shoulder joints to perform like-human movements. The robot has in total 14 degree-of-freedom on the fingers, thumb, wrist, elbow, and shoulder joints. The wrist is able to rotate using the actuators shown in Figure 4.5. The elbow produce flexion and extension, and the shoulder joints are connected to the middle support piece and

Figure 4.4: AI Exoskeleton holding a cup

offers abduction, adduction, horizontal flexion and extension with the actuators shown in Figure 4.6. The mechanical design on these joints provide users a natural movement wearing the exoskeleton. Additional features such as wireless communication, low power consumption and touch-screen GUI are also implemented on the robot to optimise the users experience. The following section explains how we use the previously discussed techniques with EMG and EEG in this rehabilitation robot to help patient recover.

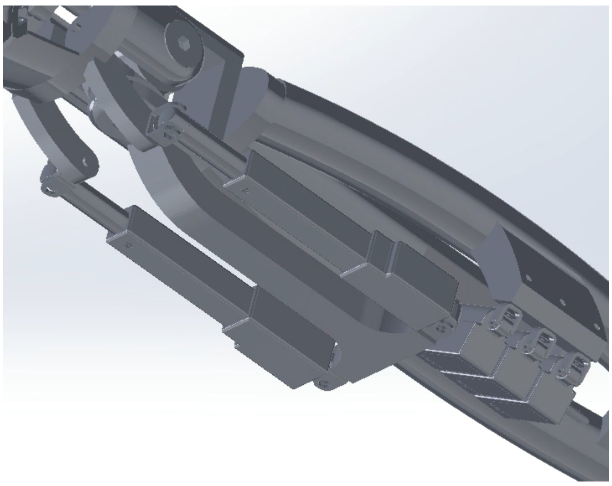

Figure 4.5: AI Exoskeleton: wrist and forearm with actuators

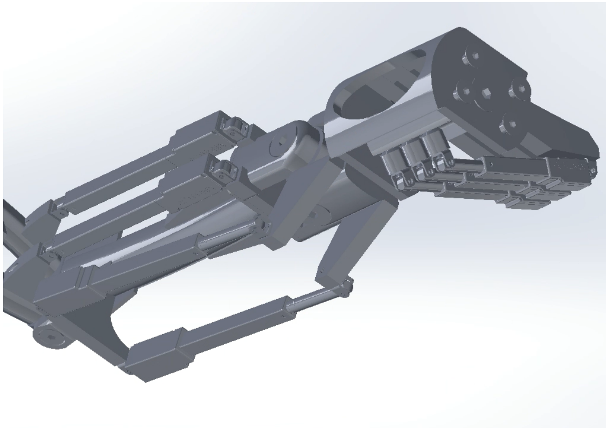

Figure 4.6: AI Exoskeleton: elbow, upper arm and shoulder with actuators

4.2 Virtual Reality-based Motor Imagery

Motor imagery (MI) can be defined as the covert cognitive process of imagining a movement of your own body (-part) without actually moving that body(-part) [111]. Motor images are endowed with the same properties as those of the (corresponding) motor representations, and therefore have the same functional relationship to the imagined or represented movement and the same causal role in the generation of this movement. At the cortical level, a specific pattern of activation, that closely resembles that of action execution, is observed in areas devoted to motor control. Jeannerod [112] laid the foundation that motor imagery and mental training can be used to enhance the neurological feedbacks for actual motor functions. Since 2000, MI has been applied in brain-computer interface (BCI) [113], neurologic rehabilitation [114], and psychological evaluation [115]. In recent years, since the rapid development of neuroelectric measurement devices and BCI-related machine learning algorithm, MI and its medical applications have become one of the most significant practical implementations [99]. However, there still are challenges applying this technology in the clinical field. Two main issues are the quality / vividness of the imaginary action and the satisfactory level of the technology-based rehabilitation paradigm.

The first challenge in MI is the quality of the imagined actions. Until today, this issue remains as the major practical obstacle. To properly address this problem, the first step is to differentiate the motor or kinesthetic imagery from visual imagery [116]. The critical difference is that MI is not the virtual environment imagined in a third person's view but introspective kinesthetic feelings of moving the limb in a first person's view. To ensure the first person's view, the latest technology, immersive VR, offers a possible solution. Vourvopoulos et al. [117] demonstrated that VR-induced motor imagery training paradigms improved rehabilitation efficiency. This interactive training environment requirement can be addressed adequately by immersive virtual reality technology. By implementing VR-based MI in stroke rehabilitation, the rehabilitation process can start as early as the patients gain the conscious of practising motor acts in their heads. Moreover, the MI exercises can be easily modified to become a home-based training with minimal safety concerns. Nevertheless, as VR technology is still at the early stage, how to design the visual training instructions during MI in order to produce better event-related desynchronization patterns is still unclear [118].

The level of engagement and satisfaction is an important factor that often neglected by the researchers and engineers who develop these rehabilitation systems. So far, there is yet a systematic research project investigating the technology-induced stroke rehabilitation methods. Nonetheless, the concerns of the user's experience have raised as more physiotherapists and clinicians have reported that the drop-out rate is increasing. Therefore, to overcome these two issues, this paper presents a virtual reality-induced motor imagery rehabilitation protocol that focuses on the high-repetitiveness of the acts and their functionality. It also proposes a novel systematic Participant Engagement and Satisfaction Survey (PESS) to access the user's experience of the designed training protocol.

Due to the impact from the COVID-19 restrictions on laboratory use and conduction of the clinical trials, the VR-based MI study cannot be started as planned. Here, we mainly discuss the designed experimental protocol.

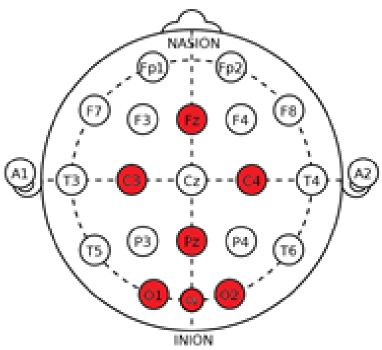

Figure 4.7: EEG sensor placement (in red) for MI experiment

This motor imagery training protocol offers an innovative stroke rehabilitation intervention using quantitative methods to assess the quality of the VR-induced MI training strategies. For VR-based training, OSVR HDK2 open-source head-mounted display set was selected in this proposed experiment. Together with the HDK2 set, a 7-channel Electroencephalogram pad is also attached on the straps of the VR headset. EEG signal is recorded to analyze the quality of the imagination using mental task classification tools. EEG is acquired at a sampling frequency of 256 Hz [110]. The following sensor locations are selected based on the standard 10-20 system: C3, C4, Fz, O1, O2, Oz, and Pz. Figure 4.7 demonstrates the exact locations of the EEG sensors that are highlighted in red on the 10-20 system. To capture activity relating to MI, three electrodes should be placed above the sensorimotor cortex at C3, C4 and Fz. To capture activity relating to stimulation response, four electrodes should be placed over the parietal-occipital region at O1, Oz, O2 and Pz. Since the headset straps are firmly secured to ensure the VR google staying on the user, the EEG sensors are also stabilised by this set-up.

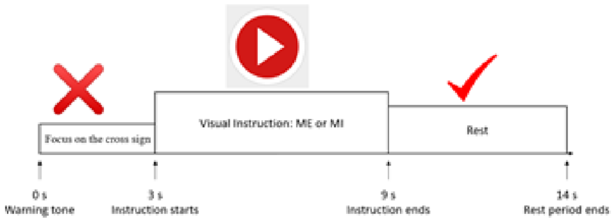

Figure 4.8: Timeline for the ME/MI trial

There are three fundamental rehabilitation acts: extend the left arm straight out (left arm lateral raise to shoulder height), extend the right arm straight out (right arm lateral raise to shoulder height), raise both arms horizontally in front of the body (both arms anterior raise to shoulder height). There are also three functional rehabilitation acts: drinking water from a cup and putting the cup back, using a spoon to drink soup from a plate, and buttoning and unbuttoning the shirt.

Figure 4.9: An example of the visual cue: a computer-based movement instruction

In order to evaluate the vividness of VR-induced training, it is necessary to establish a control group that is given the movement instructions based on computer-based animations. Therefore, this proposed rehabilitation protocol includes two phases. The first phase is a randomized motor execution (ME) / motor imagery (MI) experiment using three-dimensional human model animations as visual instruction. This instruction is shown on a computer screen. Figure 4.8 shows the action sequence for each trial on a time scale. To ensure focus, each trial begins with participants gazing at a cross sign at the center of the screen for 3 seconds, and a 1 second warning tone is presented at the beginning. Then, randomly, one of the animation cues appears for 6 seconds, during which time the participants are instructed to follow the movement as long it is present on the computer screen. One of the visual cue examples is shown in Figure 4.9. The instructions illustrate the type of the movement the participant shall perform, and whether it is ME (move the arms) or MI (without moving the arms). In the end, there is a 5-second resting period to avoid fatigue. Phase one repeats this sequence 30 times, and there is a 2-minute for every 10 trials. After finishing 30 trials, a Kinesthetic and Visual Imagery Questionnaire (KVIQ) is completed to evaluate the vividness of MI. This data is used as the reference for the later EEG-based vividness analysis. The engagement and satisfaction survey is completed by the participants.

Figure 4.10: VR-based movement instruction: drinking water from a cup

Phase two of the experiment is to use immersive VR as the visual instruction for MI. Similar procedures are followed, and the animated visual cue is replaced by the first-person VR instruction. Figure 4.10 demonstrates an example of first-person VR instruction. In this example, the VR environment shows an arm is reaching to a glass of water in front of the participant. The height of the arm and the distance of the glass are designed using realistic measures. We used a 360-degree camera (HUAWEI 360 Panoramic VR Camera) to record the training movements; therefore, the users feel more sensible to watch an actual human arm performing exercises at the same level of their own arms. Thirty trials are conducted in Phase two as well. After phase two, the participants complete another KVIQ and PESS to assess the vividness of MI using the VR-assisted method.

The designed survey is listed in the APPENDIX section. The first section of PESS contains 16 evaluation questions targeting the movement instructions, physical and mental feelings of the training protocol. Question 1-3 focus on the clarity of the visual instructions. Question 4-6 are related to the required movements. Question 7-9 discover the focus and rest set-up of the trials. Question 10-12 gather the information of the comfortableness of the devices used in this protocol. Lastly, question 13-16 ask the participants overall experiences. In this section, we use 1 point as 'Strongly Disagree' and 5 points as 'Strongly Agree' for statistical analysis. The statistics can clearly indicate the success and inadequacy of this training scheme. The second section lists four open-ended questions to gather more systematic reviews. It is important to note that immersive VR environment can be overwhelming for some patients; therefore, this survey can provide the additional information to improve the design. In cases where patients are not suitable for VR-based therapy, the exoskeleton can also used as a visual feedback by executing the imagined activities.

4.3 Human-Machine Interface: Upper Limb Movement Prediction

In the upper-limb movement prediction module, the first step is to acquire sEMG data during rehabilitation exercises. The choices of exercise should expand to a wider range as the rehabilitation system aims to provide as many types of movement assists as possible [96]. These exercises shall also be selected depending on the previous working environment of the patients. The following basic exercises are selected based on the recommendation of physiotherapists: cane leaning, circle movement, straight push, punching movement, pushing movement, unweighted bicep curls, weighted bicep curl, open arm movement and side arm raise [119].

EMG signal is then analysed using functional connectivity method, which is derived from EEG connectivity, to differentiate the interconnection of muscles. Studies [120] have shown that the comparison between the paretic side and non-paretic side can offer a powerful tool to design the transformation algorithm. As the goal is to provide movement assist, the most effective strategy is to control the paretic arm to do the same routine as the non-paretic arm. The paretic arm muscle group is treated as the abnormal system, and the non-paretic muscle group is considered as the reference. A mapping is created to transform the abnormal system into the reference. The mapping utilises the permutation and advanced machine learning algorithms to minimise the workload.

Two standard exercises are required for all patients, gripping exercise and moving target exercise for 1 hour per day, 3 days a week. Each exercise lasts 1 minute and repeats 20 times. The patient shall grip or move the handle at the tip of the exoskeleton, which in turn moves the cursor or playing rehabilitation games using Virtual Reality (VR) technology as the visual feedback. VR is introduced in exoskeleton module as this method presents users with opportunities to engage in activities within environments that appear, to various extents, similar to real-world objects and events [121]. Moreover, specific working environment and skills can be designed using VR. Then, the exoskeleton arms are placed on both paretic and non-paretic arms. Movement support is given on the paretic arm to assist the patients to reach the exercise target.

4.4 Fatigue and Safety: an Application for Emotion Classification

VR is considered to be the optimal feedback method for the three modules mentioned above, as this technology provides the capability to create an environment in which the intensity of feedback and training can be systematically manipulated and enhanced in order to create the most appropriate, individualized motor learning paradigm [122]. The VR environment is developed based on individual requirements in order to offer higher motivation and enhance visual, auditory and haptic feedback [123].

To evaluate the training process and ensure the safety of the patients, EEG is acquired to serve the following purposes. First, real-time fatigue level [107] and emotion detection [124] is implemented to show the mental state of the patients. When negative feelings are detected, measures such as reducing workload and difficulties, encouragement and incentives would increase the communication between the patients and the robot, resulting in higher motivation.

4.5 A Clinical study: EMG analysis and Upper Limb Fugl-Meyer Assessment

4.5.1 Intruduction

During rehabilitation process, evaluation of motor function is essential for understanding the mechanisms of motor control and motor learning. Multiple clinical scales are available to determine the functional ability and motor function in individuals with hemiparesis [125]. An assessment scale that is robust, easily administered, reliable and capable of reflect changes over time can reveal precise evaluation of the impairment and become a powerful tool for optimal prediction and evaluation [126]. The Fugl-Meyer Assessment (FMA) developed and introduced in 1975 by Fugl-Meyer et al. [127], which was the first quantitative instrument for evaluation of hemiparetic patients. FMA is the most widely used standardized clinical scale for evaluation of sensorimotor function after stroke. Furthermore, upper limb FMA can be used in every stage of stroke recovery to investigate the motor function of the patient. Clinically, together with FMA, the Brunnstrom Approach is also broadly used to evaluate the current degree of hemiplegia and develop an appropriate rehabilitation strategy [128]. Nevertheless, with the rapid development of the non-invasive electro-physiological devices in recent years, the limitations of the traditional assessment tools have been revealed, which are highly based on the observation of the physiotherapists and lack of the neurological basis for the rehabilitation process.

To overcome this limitation and discover the changes on the neuromuscular level of upper-limb stroke rehabilitation, surface electromyogram is an ideal source of physiological signal for the analysis. In 2018, a novel approach of sEMG decoding system is proposed ‚Äì EMG functional connectivity analysis ‚Äì that have been validated on a dataset consisting of eleven stroke patients performing gripping rehabilitation exercises. The EMG functional connectivity analysis, which is adapted from electroencephalogram connectivity analysis, can unveil the direction of the information flow between the upper extremity muscles. The previous study demonstrates that the muscle activity and connectivity can be different for the same participant at different strength levels. Secondly, the different connectivity patterns across the patients shows that, each individual has a unique movement behaviour and muscle activation pattern. Lastly, large the connectivity pattern differences appear when comparing between the affected and non-affected arm. However, the previous study only focused on one type of upper limb motion, which can be considered as inclusive at certain degree. Therefore, to track the recovery process while collecting EMG data becomes essential in this study. In this clinical study, we propose a seven-week plus one follow-up visit experiment that collects sEMG signal on both affected and non-affected arms while perform upper limb FMA activities. We aim to discover the neurological basis of the upper limb muscle recovery process and establish an EMG-based quantitative assessment tool for stroke-related motor function impairment and recovery prediction.

4.5.2 Experimental Protocol

From mid 2020, by collaborating with Shanghai Jiao Tong University, a clinical trial in China is established to explore the EMG variations during stroke rehabilitation. This experiment is a two-month weekly collection plus one follow-up visit experiment that collects sEMG signal on both affected and non-affected arms while performing UL-FMA activities. The study aims to discover the neurological basis of the upper limb muscle as patients recover, and to establish an EMG-based quantitative assessment tool for stroke-related motor function impairment. We also aim to predict recovery based on EMG functional connectivity using machine learning.

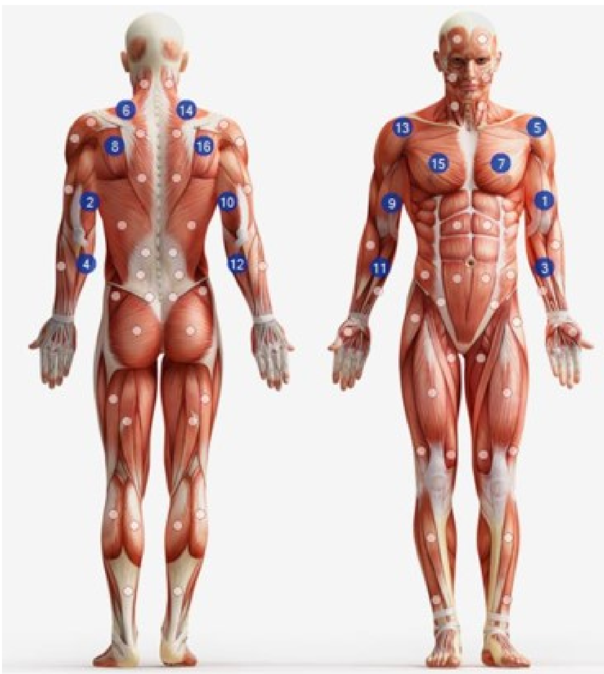

Figure 4.11: EMG sensor location for the EMG-FMA experiment

This is an ongoing experiment, where patients are evaluated by occupational therapists every week using modified UL-FMA. EMG sensors are attached on both arms during assessment. At this stage, five participants are recruited and four weeks of data has been processed as the primary data analysis phase. The demographic details of the patients are shown in the Appendix section. In this experiment, 16 EMG sensors from Cometa wireless PicoEMG system is used to collect both EMG and IMU signal. Eight muscle groups on each arm are studied, namely, biceps brachii, triceps brachii, flexor carpi radialie, extensor carpi ulnaris, posterior deltoid, upper trapezius, pectoralis major, and infraspinatus. The sensor locations are shown in Figure 4.11.

At this stage, we have completed the primary data analysis for the first four weeks. All five patients have shown positive results regarding their recovery. For each participant, the significant findings and predictions are listed in the following paragraphs.

4.5.3 Results and Discussion

4.5.3.1 Patient 1

The overall FMA upper limb score for Patient 1 has increased over the last 4 weeks, from less than 40 to 50. The stacked bar chart divides the UL-FMA activities into seven categories shown in Figure 4.12. Category 1 (C1) is volitional movement within synergies (flexor) in navy. Category 2 (C1) is volitional movement within synergies (extensor) in organe. Category 3 (C1) is volitional movement mixing synergies in yellow. Category 4 (C1) is volitional movement within little or no synergies in purple. Category 5 (C1) includes movements on wrists in green. Category 6 (C1) are motions related to hands in blue. Category 7 (C1) is coordination and speed in maroon. Figure 4.12 shows there are major rises in C1, C3 and C6. It is also worth noting that although there are fluctuations between weeks (especially week 2), none of the categories falls consistently. Later, C3 movements are further analysed by EMG signals to indicate the improvement, and EMG connectivity analysis is utilised to discover C7, where the FMA scores stay at a lower range through the four weeks.

In Figure 4.13, two muscles are selected, namely flexor carpi radialis and upper trapezius. The first two graphs demonstrate the EMG magnitude changes between week 1 and week 4. The non-affected side EMG is also included as a reference. The RMS values for the EMG signals are also calculated. Flexor carpi radialis is presenting an increasing trend, which further proves Patient 1 is recovering well. However, the upper trapezius

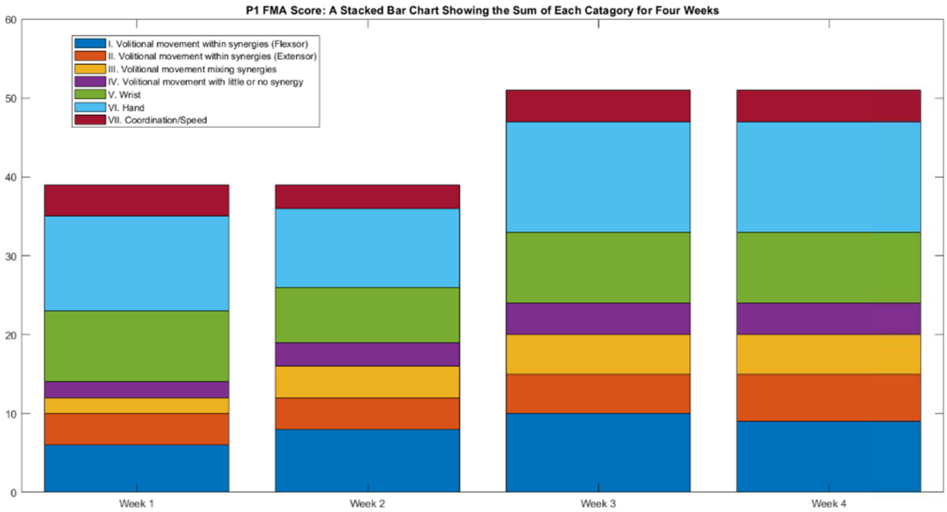

Figure 4.12: Patient 1 FMA score. Category 1 (C1) is volitional movement within synergies (flexor) in navy. Category 2 (C1) is volitional movement within synergies (extensor) in organe. Category 3 (C1) is volitional movement mixing synergies in yellow. Category 4 (C1) is volitional movement within little or no synergies in purple. Category 5 (C1) includes movements on wrists in green. Category 6 (C1) are motions related to hands in blue. Category 7 (C1) is coordination and speed in maroon.

RMS values state there is a decreasing trend. The reason for this observation is that upper trapezius is the major muscle for movement 12. When other muscles cannot be customarily activated, the major muscle over activates. Therefore, the fatigue level of the major muscle increases rapidly; in turn, the difficulty of the movement increases.

In Figure 4.14 and Figure 4.15, the relatively low score (w1: 4, w2: 3, w3: 4, w4: 4) movement is analysed by EMG connectivity method, short-term directed transfer function. The significant nodes in the affected network are Ch7 and Ch4, whereas the non-affected network has Ch 7 and Ch 1 as the significant nodes. A future suggestion is that more therapies targeting biceps brachii can be considered during coordination and speed exercises.

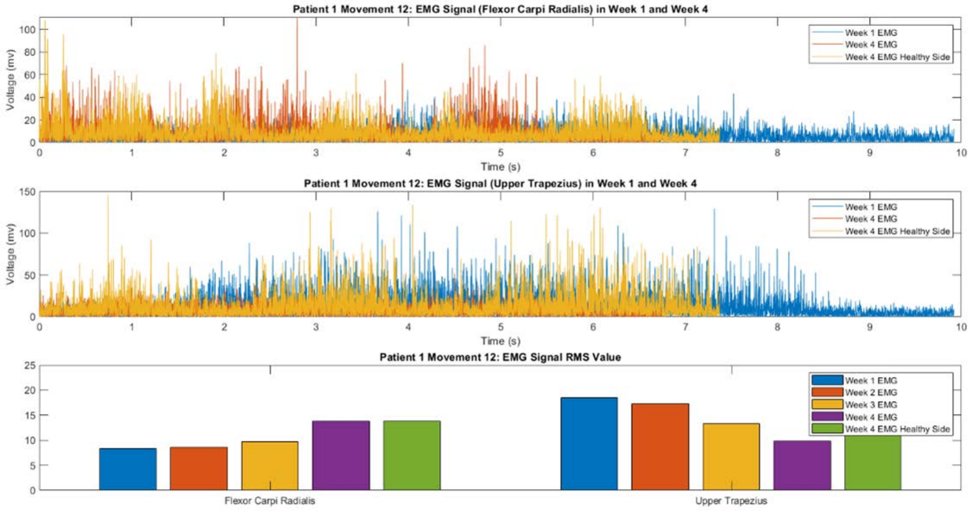

Figure 4.13: Patient 1 Movement 12 EMG Analysis

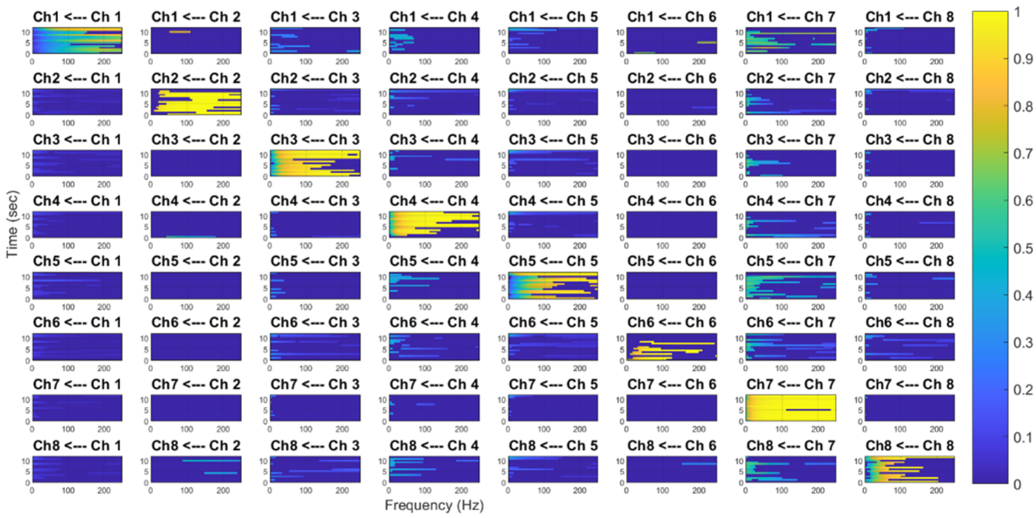

Figure 4.14: Patient 1 Movement 28 Affected Side EMG Connectivity

4.5.3.2 Patient 2

Patient 2's overall FMA upper limb score has increased over the last 4 weeks, from less than 20 to almost 40. Figure 4.16 shows there are major rises in C3, C4 and C6. Later, C6 movements are further analysed by EMG signals to demonstrate the improvement, and EMG connectivity analysis is utilised to discover C7, where the FMA scores stay at

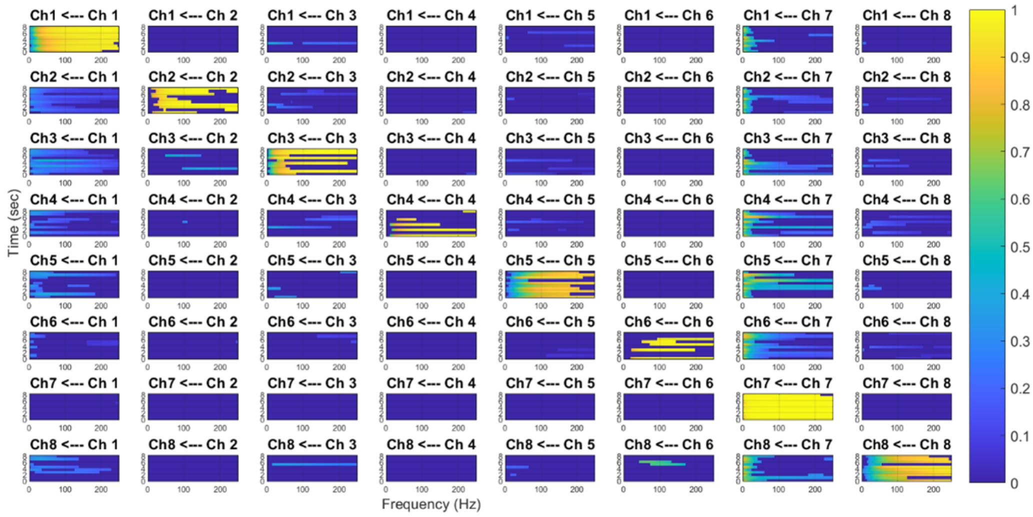

Figure 4.15: Patient 1 Movement 28 Non-affected Side EMG Connectivity

almost zero throughout the four weeks.

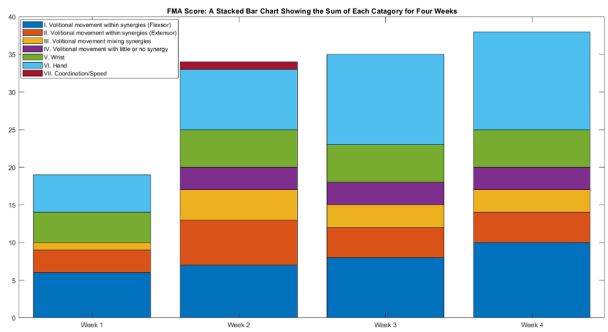

Figure 4.16: Patient 2 FMA score

In Figure 4.17, two muscles are selected, namely biceps brachii and posterior deltoid. The first two graphs demonstrate the EMG magnitude changes between week 1 and week 4. The non-affected side EMG is also included as a reference. The RMS values for the EMG signals are calculated. Biceps brachii serves as one of the major muscles in movement 23. The RMS values clearly state the low activation level in the first week, which score 1 for FMA upper limb test. It is important to note that although patient 2 had score 2 in the following weeks, and the activation level is relatively stable; comparing to the activation level of the healthy side for posterior deltoid, the non-affected muscle is approximately four-fold higher. A suggestion is to continue work on the deltoid region in future therapies to prevent fluctuation and/or deterioration.

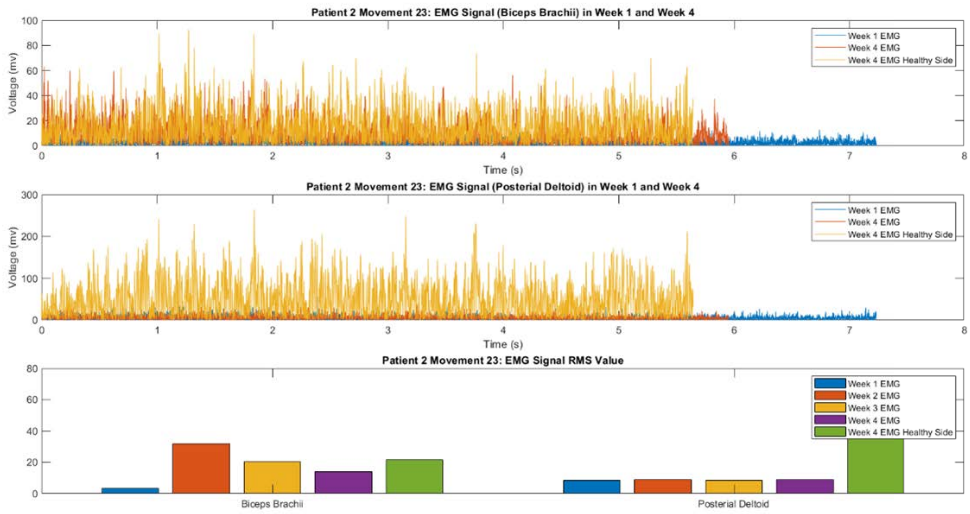

Figure 4.17: Patient 2 EMG Analysis for Movement 23

Figure 4.18 and Figure 4.19 directly present the issue of the upper limb muscle networks during movement 28. The affected network only has one significant node that is Ch7. However, the non-affected side shows a rather sparse network that information is exchanged through Ch7, Ch 4, Ch 2 and Ch 1. In future therapies, the coordination of multiple muscle regions including upper arm, forearm and chest region shall be focused.

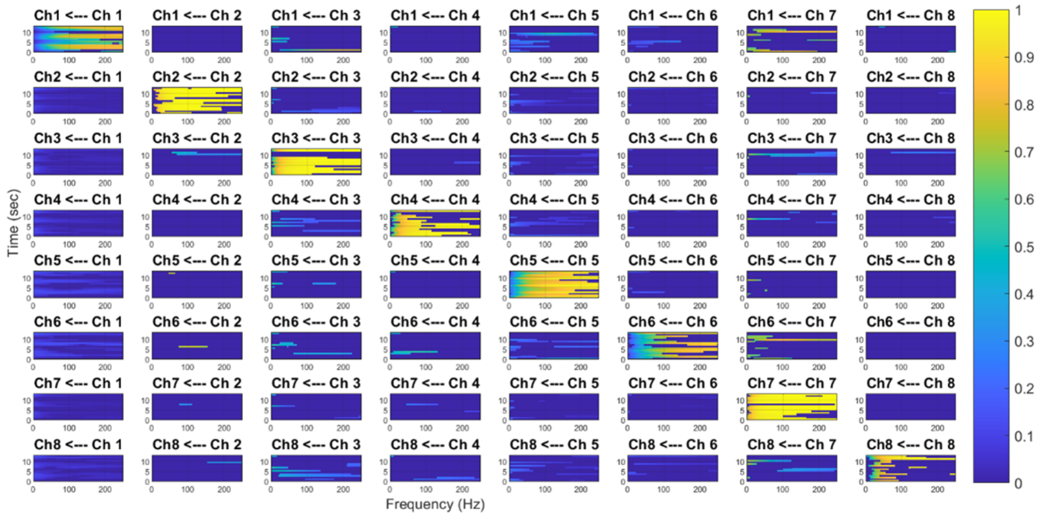

Figure 4.18: EMG Connectivity analysis on Movement 28. Affected Arm.

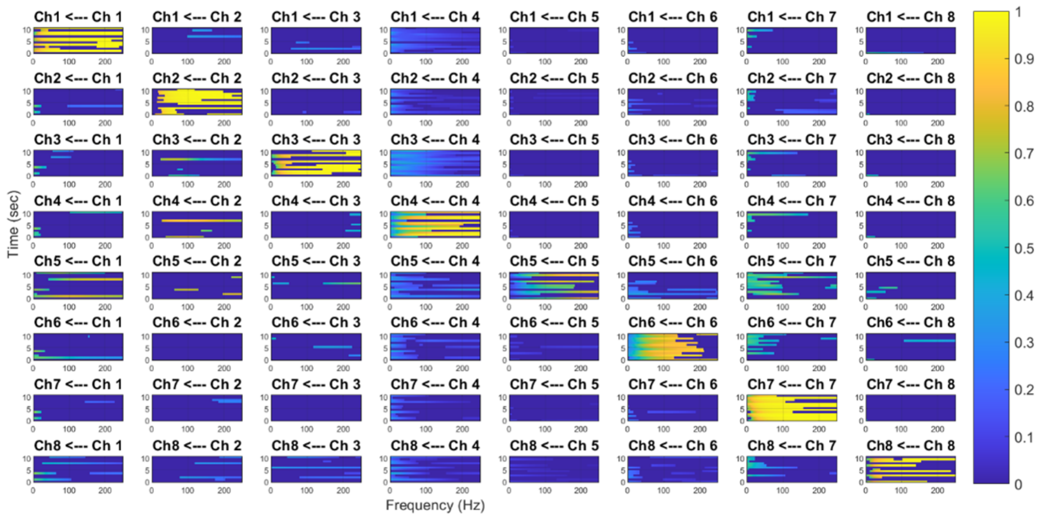

Figure 4.19: EMG Connectivity analysis on Movement 28. Non-affected Arm.

4.5.3.3 Patient 3

Patient 3's overall FMA upper limb score has increased approximately 5-8 points over the last 4 weeks. Figure 4.20 demonstrates there are steady rises in C1 and C3. It is worth noting that C6 remained at zero for the first two weeks, showed a spike in week 3 and returned to a low value in week 4. Later, C1 movements are further analysed by

EMG signals to show the improvement, and EMG connectivity analysis is utilised to discover the variation of C6, and further discuss the human error introduced by FMA.

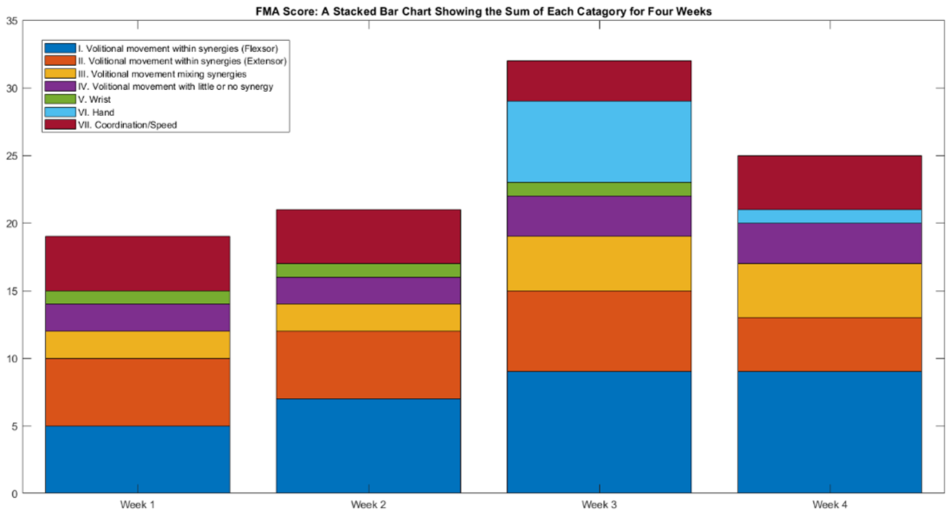

Figure 4.20: Patient 3 FMA score

Two muscles are selected, infraspinatus and posterior deltoid, to analyse movement 2 of C1. Figure 4.21 demonstrate the EMG magnitude changes between week 1 and week 4. The non-affected side EMG is also included as a reference. The RMS values for the EMG signals are also calculated. Infraspinatus serves as a support muscle, shows a recovery trend, but it is far from the activation level on the healthy side. As a result, the major muscle is over-activated to compensate for the loss of the support from other muscles, showing in posterior deltoid. A suggestion is to focus on the support muscle regions, which can reduce the load from the major muscles, in turn, minimise the fatigue effect.

Figure 4.22 and Figure 4.23 are the muscle networks from week 3 and week 4, indicating similar sparseness and motifs for movement 21. On the other hand, Figure 4.24 is the healthy side muscle network has a completely different information exchange system for the same movement. This finding indicates that the sudden spike in week 3 can be human error, where the FMA assessor made an incorrect judgement. This also reveals that by evaluating in three-level, 0, 1 and 2, is not efficient enough for upper limb movements that can be considered as small variations in terms of displacement and joint angles. Thus, EMG-based analysis shall be utilised in such circumstances. A suggestion is to activate Ch 5. posterior deltoid in coordination and speed exercises.

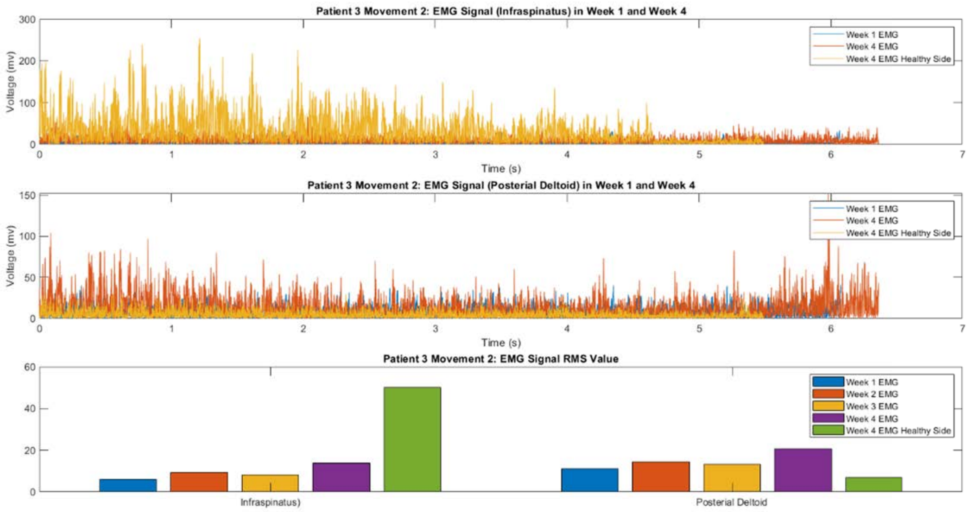

Figure 4.21: Patient 3 Movement 2 EMG Analysis

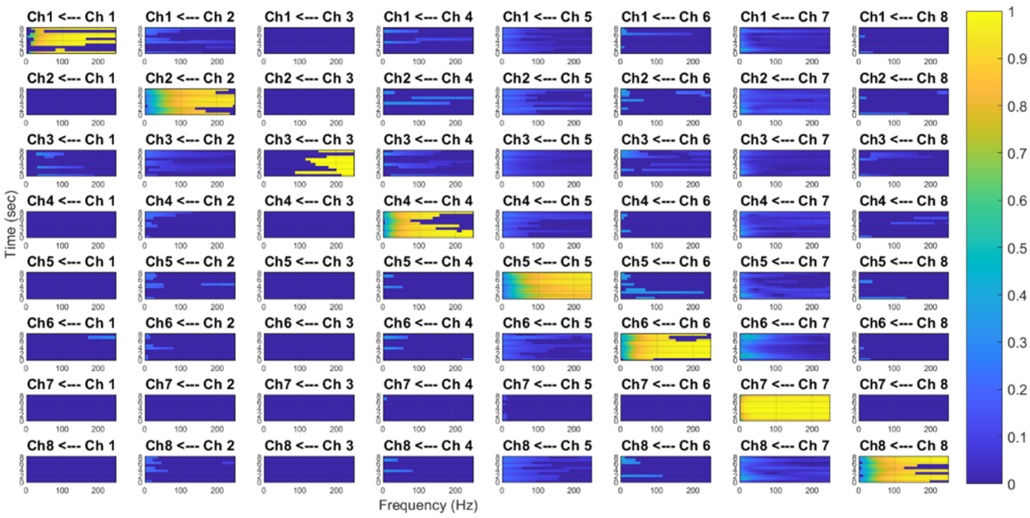

Figure 4.22: EMG Connectivity analysis on Movement 21. Affected Arm Week 3.

4.5.3.4 Patient 4

Patient 4 has a high FMA score in all four weeks, showing slight fluctuations in week 2 and week 3, shown in Figure 4.25. However, the motor functions are considered in a high standard in most categories. In this analysis, movement 17 from C5 is isolated for further discussion, since C5 appears as the worst category for patient 4, averaging 6.25

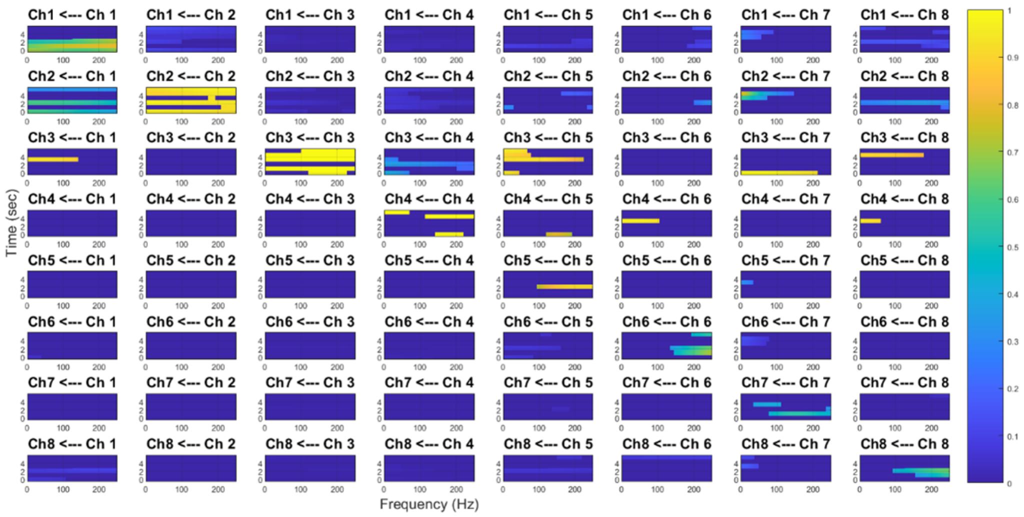

Figure 4.23: EMG Connectivity analysis on Movement 21. Affected Arm Week 4.

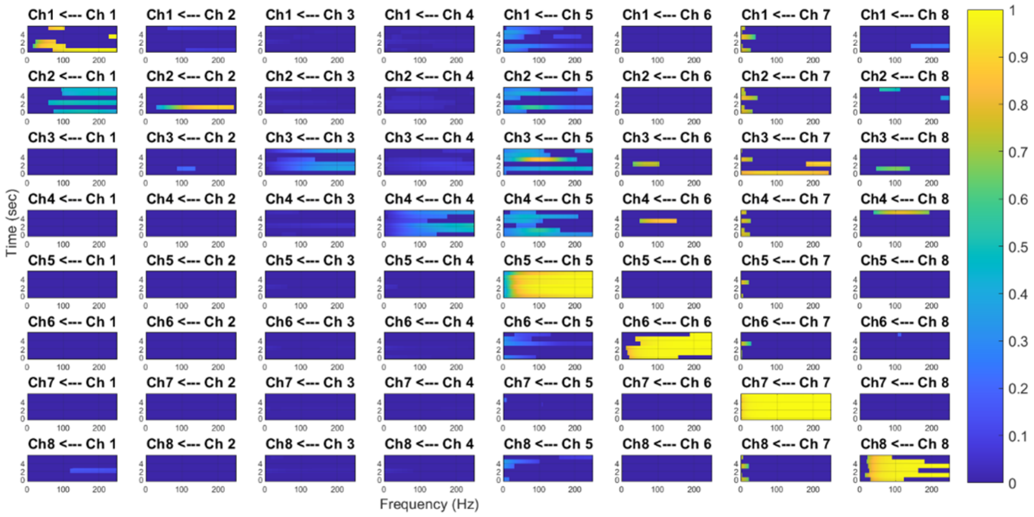

Figure 4.24: EMG Connectivity analysis on Movement 21. Non-affected Arm Week 4.

out of 10.

In Figure 4.26, two muscles are selected, namely extensor carpi ulnaris and upper trapezius, to investigate the muscle activation levels using EMG signal. The first two graphs demonstrate the EMG magnitude changes between week 1 and week 4 for movement 17. The non-affected side EMG is also included as a reference. The RMS values for the EMG signals are presented in the third graph. The RMS values for

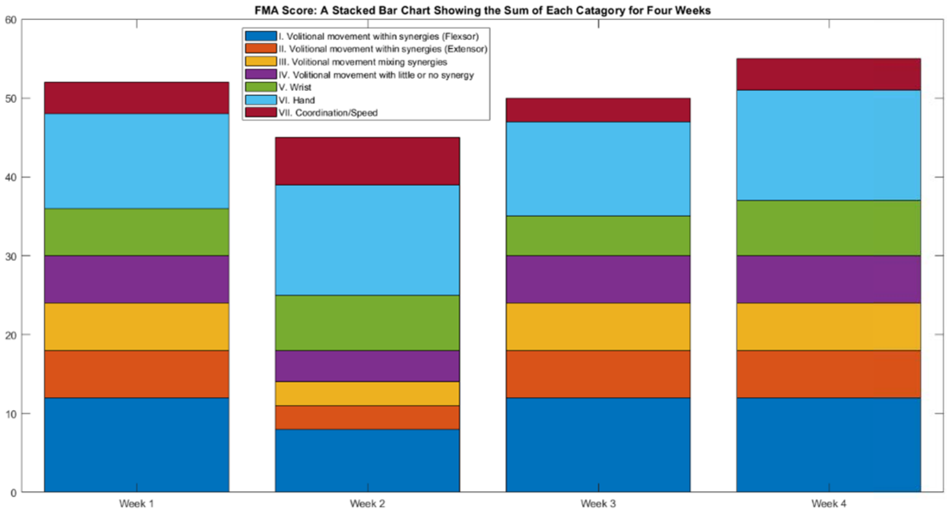

Figure 4.25: Patient 4 FMA score

extensor carpi ulnaris show a steady increasing trend over the last four weeks, and it is closing to the level on the healthy side. This indicates that the current rehabilitation therapy for extensor muscle groups is sufficient. The upper trapezius muscle presents over-activation on the affected side comparing to the non-affected arm. However, the upper trapezius muscle is not considered the major muscle in this activity. The suggestion is during the daily rehabilitation therapies, it is necessary to explain and guide patient 4 to show which muscle regions are major and which are support. The coordination of muscles during wrist exercises needs to be emphasized.

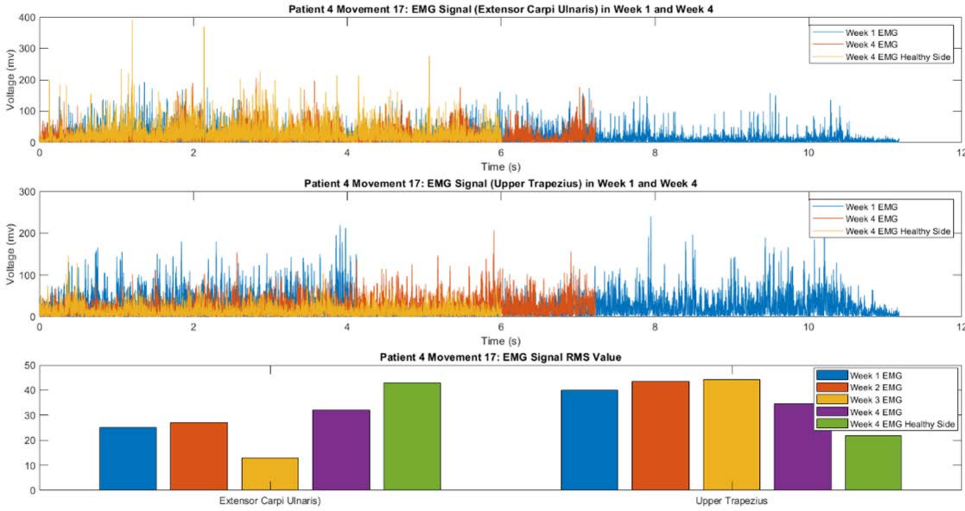

Figure 4.26: Patient 4 Movement 17 EMG Analysis

4.5.3.5 Patient 5

The overall FMA upper limb score has made an impressive rise over the last four weeks, from less than mid-30 towards mid-50. Figure 4.27 shows there are major rises in C1, C3 and C4. At the same time, C5 remains at a similar status. Further analysis includes EMG statistic analysis for C4 movement 13 and frequency domain connectivity analysis for C5 movement 19.

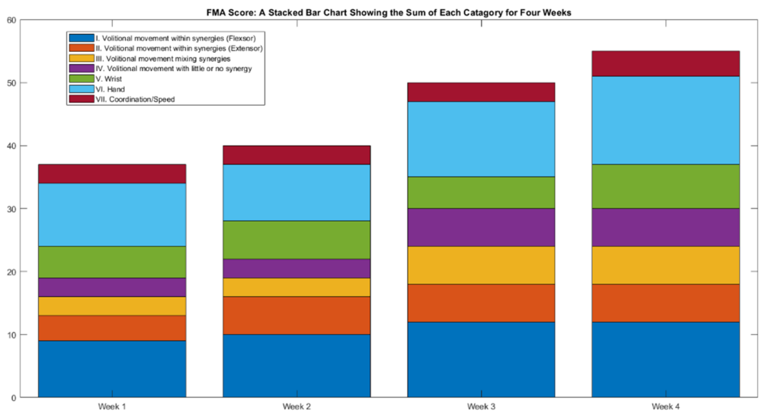

Figure 4.27: Patient 5 FMA score

Figure 4.28, Figure 4.29, Figure 4.30, and Figure 4.31 show the affected side EMG connectivity for movement 19 over the past four weeks. Although FMA and statistical EMG analysis could not express the changes, the functional connectivity and the muscle network has demonstrated the progress. The affected side network demonstrated high sparseness in week 1. Then, the significant nodes were adjusting from Ch 8 (week 1, 2), Ch 7 (week 2), and Ch 3 (week 3), to two nodes Ch 7 and Ch 1 (week 4). This proves that this connectivity transformation corresponds to the network pattern on the healthy side, shown in Figure 4.32. This trend indicates that although the progress is not showing on FMA or statistical EMG analysis, patient 5 is recovering and forming the correct information exchange network on the affected arm. Suggestions are to continue the current therapy and focus on the biceps brachii training during elbow and wrist exercises.

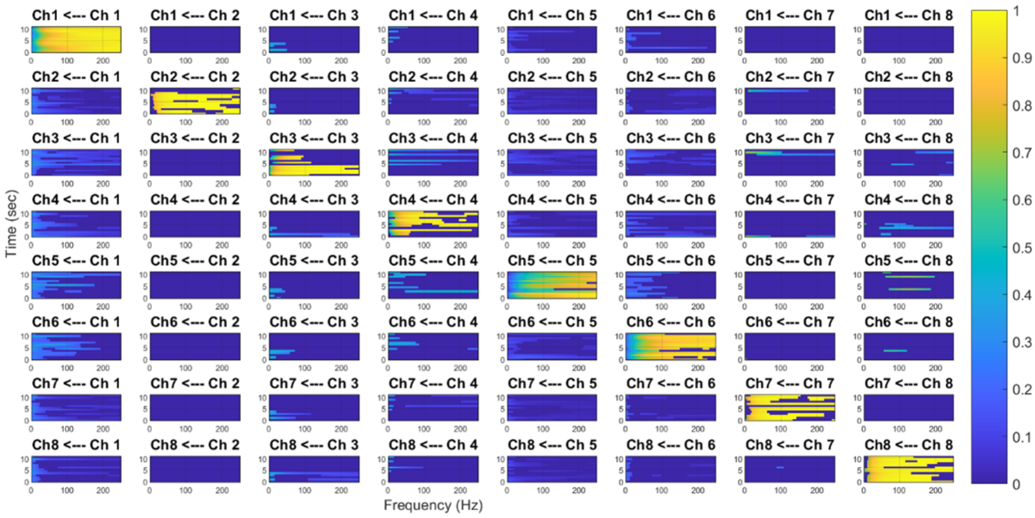

Figure 4.28: EMG Connectivity analysis on Movement 19. Affected Arm Week 1.

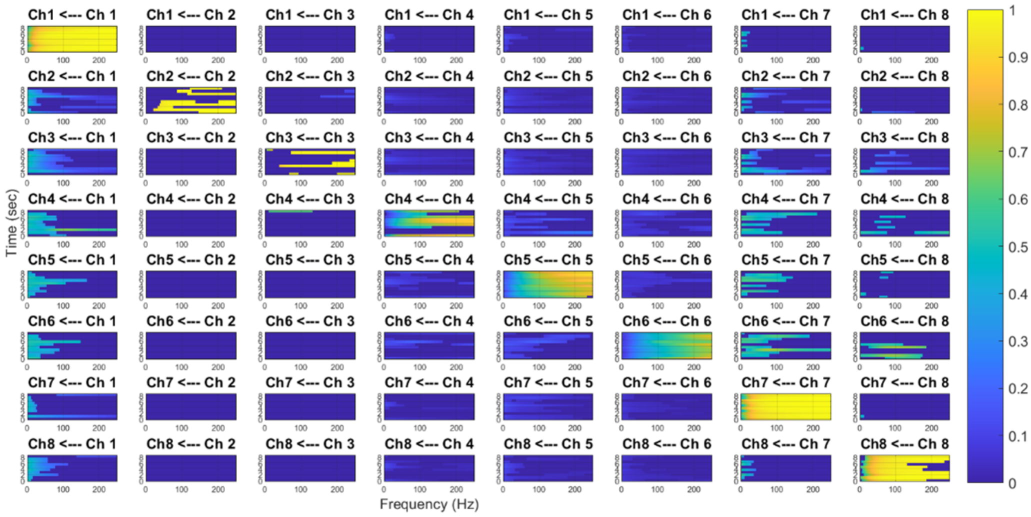

Figure 4.29: EMG Connectivity analysis on Movement 19. Affected Arm Week 2.

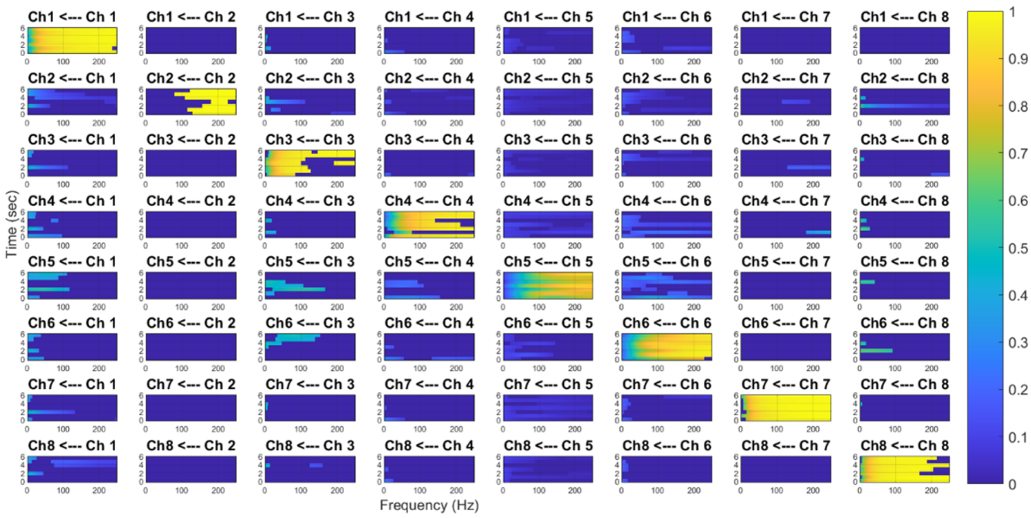

Figure 4.30: EMG Connectivity analysis on Movement 19. Affected Arm Week 3.

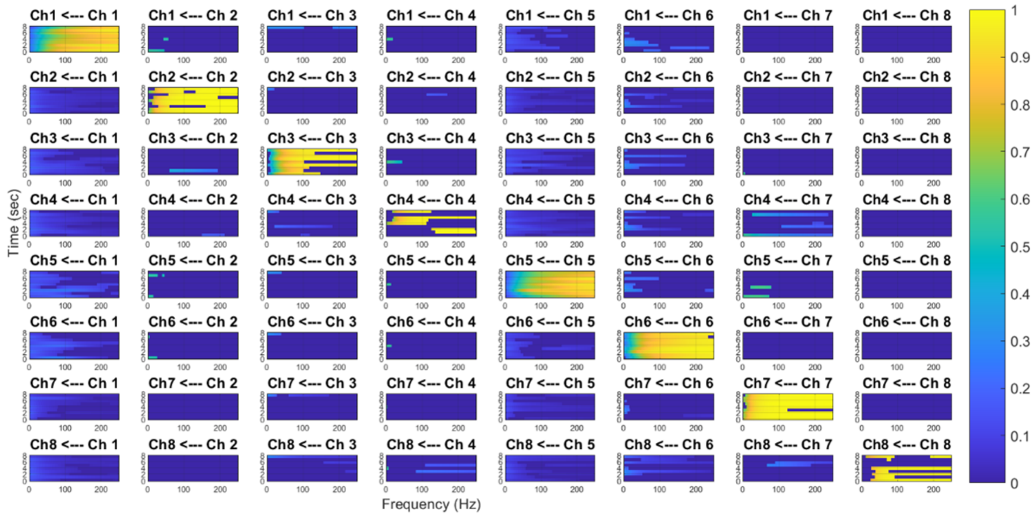

Figure 4.31: EMG Connectivity analysis on Movement 19. Affected Arm Week 4.

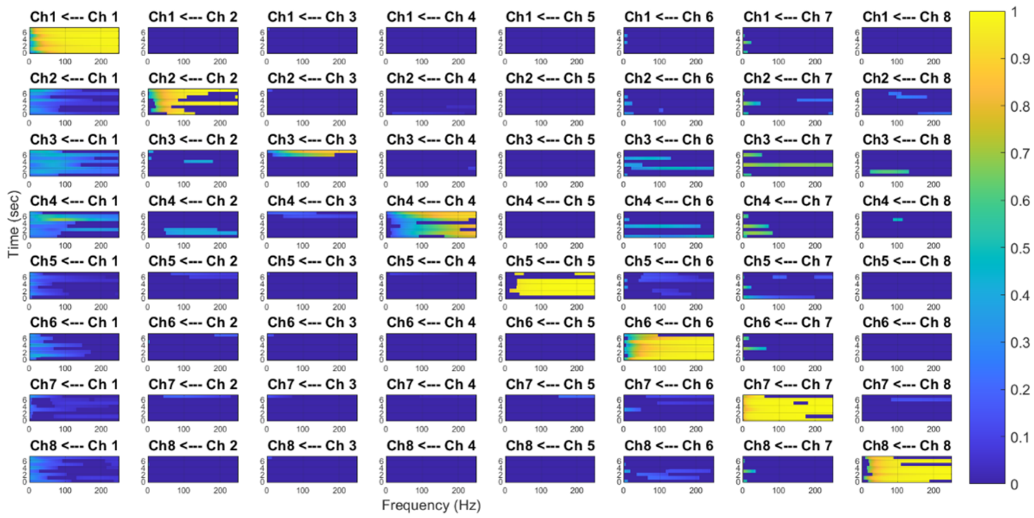

Figure 4.32: EMG Connectivity analysis on Movement 19. Non-affected Arm Week 4.

4.6 Conclusion

In this chapter, Module 3 is presented by introducing the self-developed exoskeleton. This upper limb exoskeleton provides 14 degree of freedom on both extremities. This 3D printed robot is light and portable with user-friendly operating system. Furthermore, this thesis emphasises the human-machine interfaces implemented in this system to provide rehabilitation therapies at different stages of stroke recovery. This robot-based stroke rehabilitation system offers two types of training mode, motor imagery and movement support, with over 30 different activities. First, at early stages of stroke recovery, the motor imagery mode uses EEG signal collected from the wireless headset using 14 seeds to identify the motion intent without physically moving the limbs. The feedback of the imagined activities are demonstrated with VR technology. This therapy improves the neuroplasticity of the affected regions brain. After the stroke survivors start to regain some voluntary motor functions, the movement support mode provides the assist-as-needed during upper limb training in real-time. Moreover, a performance assessment tool using EMG connectivity is presented and verified in an ongoing clinical study. The primary results show that EMG connectivity analysis discovers the physiological changes of the affected extremities and provides a systematical method to analyse the link between anatomic and statistical connection between the muscle groups.

CHAPTER 5

SUMMARY AND FUTURE WORK

5.1 Summary

To conclude, the stroke rehabilitation system is developed to meet the different enquires at several recovery stages. At early stages of the post-stroke recovery process, patients cannot perform voluntary movements. Under these scenarios, we utilise the neurological information extracted from the brain to conduct motor imagery training. Patients are instructed to picture movements in the head without actually moving their arms. Using the human-machine interface explained in Chapter 2 and Chapter 4, the rehabilitation system detects the intent of the movement, and execute it on the robot as the feedback for the patients. Also, the neurological signal from the brain, electroencephalogram, is also continuously monitoring the mental state of the patient. It is not only an evaluation measurement for the designed training sessions, but also a part of the protection scheme that can adjust or stop the training if there is a negative emotion detected.

Three modules are presented in this thesis. Module 1 analyses neuroelectrical signal from the brain to detect psychological variations during upper limb activities. Module 2, explained in Chapter 3, offers another mode of rehabilitation training, where stroke patients are able to perform slight movement on their affected side. In this case, EMG signal is processed using the novel developed functional connectivity methods to generate the upper limb muscle network. This network reveals the inter-relationship between the upper limb muscle groups. By comparing the muscle network of the impaired arm to the non-affected side, a personalised training scheme is proposed. Function electrical stimulation method is simulated using this training scheme. Furthermore, the robotic system can also use this interface between muscle and machine to guide the abnormal movement using the robitc arms.

Module 3 evaluates the practical significance of this thesis that is presented in Chapter 4, where an upper limb exoskeleton is constructed at the Centre for Health Technologies Lab at the University of Technology, Sydney. By combining with EEG and EMG signals as the input, this system is able to monitor, evaluate and perform real-time movement instructions during different stages of the stroke recovery. This robot can improve the rehabilitation efficiency by providing personalised training programs. As the sources of the input are physiological signals and the automatic human-machine interfaces are applied, this system is capable of reducing the load of the physiotherapists. Additionally, the possibility of home rehabilitation presented in this rehabilitation system presents an enormous potential for tele-health market. Under the impact of COVID 19, receiving rehabilitation treatment at home is a tremendous benefit not only to the post-stroke patients, but also to the community as a whole.

5.2 Future Work

Despite the multi-mode stroke rehabilitation system has been constructed, the research and practical work for this system is not finished. The future work is mainly in two areas, machine learning algorithm development and conducting clinical trials.

First, the machine learning algorithms are currently used as pattern recognition and real-time detection. With the latest data received from the clinical trial in Shanghai, a new approach is discussed: the prediction of stroke recovery based on early EMG signals. This study will provide a deep insight into the physiological changes based on different types of stroke events. The correlation between the damage in the brain and the impact on the muscle will also be emphasized.

Another approach using machine learning is to use the state-of-the-art algorithms such as transfer learning and reinforcement learning to investigate how the patient adapts the machine. This will further present the effort on how to design the human-machine interface to minimise the effort required to use the system.

Last but not least, clinical studies with larger groups are necessary for validating the theories and methodologies presented in this thesis. Luckily, the AI Exoskeleton system has attracted attentions from several hospitals and research institutes in Australia, China, and India. Although the current COVID 19 situation has made clinical ever more challenging than before, the discussion with these hospitals and institutes is going well. Learning from the current clinical trial in Shanghai, it is highly possible to start a larger group clinical trial in Sydney and Melbourne in 2021.

APPENDIX

A

APPENDIX

Participant Engagement and Satisfaction Survey

Please rate your satisfaction	Strongly Agree	Agree	Neutral	Disagree	Strongly Disagree
1. The experiment procedure was clearly explained					
2. The instructions given were easy to follow					
3. The length of the instruction video was adequate					
4. I can understand what the required movements are					
5. I can perform the three fundamental movements					
6. I can perform the three functional movements					
7. I can keep my focus during the entire experiment					
8. I did not experience any muscle fatigue					
9. I did not experience any motion sickness or nauseated					
10. The VR headset does not restrict my normal movement					
11. The straps of the VR headset does not create uncomfortableness of the head					
12. I did not feel pain on the scalp after wearing the VR headset					
13. The training module was engaging					
14. The training module was interesting					
15. The training module was a useful upper limb exercise					
16. Overall, I was satisfied with the training protocol					

Open-ended questions:

1. If you were satisfied with this experiment, please indicate why you feel this way.
2. Would you like to do this type of training again? Was there anything about this experience that would make you think twice before doing it again?
3. What would influence whether you would/would not engage virtual reality training again?
4. Is there anything else that you would like to tell me about your experience with virtual reality training?

Bibliography

[1] V. C. Scanlon and T. Sanders, *Essentials of anatomy and physiology*. FA Davis, 2018.

[2] "Lobes of the brain," Jul 2018. [Online]. Available: https://qbi.uq.edu.au/brain/brain-anatomy/lobes-brain

[3] N. B. Cant and L. E. White, "Overview of the human brain," 2017. [Online]. Available: https://web.duke.edu/brain/lab01/lab01.html

[4] Q. B. Institute, "The limbic system, university of queensland," https://qbi.uq.edu.au/brain/brain-anatomy/limbic-system, Jan 2019, (Accessed on 01/15/2021).

[5] R. Kötter and N. Meyer, "The limbic system: a review of its empirical foundation," *Behavioural brain research*, vol. 52, no. 2, pp. 105–127, 1992.

[6] D. Keltner and J. J. Gross, "Functional accounts of emotions," *Cognition & Emotion*, vol. 13, no. 5, pp. 467–480, 1999.

[7] "Motor cortex (section 3, chapter 3) neuroscience online: An electronic textbook for the neurosciences | department of neurobiology and anatomy - the university of texas medical school at houston," https://nba.uth.tmc.edu/neuroscience/m/s3/chapter03.html, (Accessed on 01/15/2021).

[8] J. N. Sanes and J. P. Donoghue, "Plasticity and primary motor cortex," *Annual review of neuroscience*, vol. 23, no. 1, pp. 393–415, 2000.

[9] E. Salmon, C. B. Ir, and R. Hustinx, "Pitfalls and limitations of pet/ct in brain imaging," in *Seminars in nuclear medicine*, vol. 45, no. 6. Elsevier, 2015, pp. 541–551.

[10] "Computed tomography (ct or cat) scan of the brain | johns hopkins medicine," https://www.hopkinsmedicine.org/health/treatment-tests-and-therapies/computed-tomography-ct-or-cat-scan-of-the-brain, (Accessed on 01/15/2021).

[11] E. C. Camargo, G. González, R. G. González, and M. H. Lev, “Unenhanced computed tomography,” in *Acute Ischemic Stroke*. Springer, 2006, pp. 41–56.

[12] M. E. Mullins, “Acute stroke imaging with spect, pet, xenon-ct, and mr spectroscopy,” in *Acute Ischemic Stroke*. Springer, 2006, pp. 199–208.

[13] S. P. Singh, “Magnetoencephalography: basic principles,” *Annals of Indian Academy of Neurology*, vol. 17, no. Suppl 1, p. S107, 2014.

[14] G. Vecchiato, L. Astolfi, F. De Vico Fallani, J. Toppi, F. Aloise, F. Bez, D. Wei, W. Kong, J. Dai, F. Cincotti *et al.*, “On the use of eeg or meg brain imaging tools in neuromarketing research,” *Computational intelligence and neuroscience*, vol. 2011, 2011.

[15] D. Vu, R. G. González, and P. W. Schaefer, “Conventional mri and mr angiography of stroke,” in *Acute Ischemic Stroke*. Springer, 2006, pp. 115–137.

[16] J. P. Hornak, “The basics of mri, 2008,” *URL http://www. cis. rit. edu/htbooks/mri/index. html*, vol. 68, 2008.

[17] R. Weber, J. M. Mangus, and R. Huskey, “Brain imaging in communication research: A practical guide to understanding and evaluating fmri studies,” *Communication Methods and Measures*, vol. 9, no. 1-2, pp. 5–29, 2015.

[18] N. Naseer and K.-S. Hong, “fnirs-based brain-computer interfaces: a review,” *Frontiers in human neuroscience*, vol. 9, p. 3, 2015.

[19] “Wireless fnirs - cortech solutions, inc.” https://cortechsolutions.com/product-category/nirs-fnirs/nirs-fnirs-wireless-mapping/, (Accessed on 01/15/2021).

[20] M. M. Plichta, M. J. Herrmann, C. Baehne, A.-C. Ehlis, M. Richter, P. Pauli, and A. J. Fallgatter, “Event-related functional near-infrared spectroscopy (fnirs): are the measurements reliable?” *Neuroimage*, vol. 31, no. 1, pp. 116–124, 2006.

[21] A. S. Jacks and N. R. Miller, “Spontaneous retinal venous pulsation: aetiology and significance,” *Journal of Neurology, Neurosurgery & Psychiatry*, vol. 74, no. 1, pp. 7–9, 2003.

[22] R. F. Kratz, *Biology for dummies*. John Wiley & Sons, 2017.

[23] G. M. Rojas, C. Alvarez, C. E. Montoya, M. de la Iglesia-Vayá, J. E. Cisternas, and M. Gálvez, "Study of resting-state functional connectivity networks using eeg electrodes position as seed," *Frontiers in neuroscience*, vol. 12, p. 235, 2018.

[24] Y. Li, J. Pan, F. Wang, and Z. Yu, "A hybrid bci system combining p300 and ssvep and its application to wheelchair control," *IEEE Transactions on Biomedical Engineering*, vol. 60, no. 11, pp. 3156–3166, 2013.

[25] M. Tangermann, K.-R. Müller, A. Aertsen, N. Birbaumer, C. Braun, C. Brunner, R. Leeb, C. Mehring, K. J. Miller, G. Mueller-Putz *et al.*, "Review of the bci competition iv," *Frontiers in neuroscience*, vol. 6, p. 55, 2012.

[26] N. Kannathal, M. L. Choo, U. R. Acharya, and P. Sadasivan, "Entropies for detection of epilepsy in eeg," *Computer methods and programs in biomedicine*, vol. 80, no. 3, pp. 187–194, 2005.

[27] A. Tsolaki, D. Kazis, I. Kompatsiaris, V. Kosmidou, and M. Tsolaki, "Electroencephalogram and alzheimer,Äôs disease: clinical and research approaches," *International journal of Alzheimer,Äôs disease*, vol. 2014, 2014.

[28] P. L. Davies and W. J. Gavin, "Validating the diagnosis of sensory processing disorders using eeg technology," *American Journal of Occupational Therapy*, vol. 61, no. 2, pp. 176–189, 2007.

[29] S. Giaquinto, A. Cobianchi, F. Macera, and G. Nolfe, "Eeg recordings in the course of recovery from stroke." *Stroke*, vol. 25, no. 11, pp. 2204–2209, 1994.

[30] G. Pellegrino, L. Tomasevic, M. Tombini, G. Assenza, M. Bravi, S. Sterzi, V. Giacobbe, L. Zollo, E. Guglielmelli, G. Cavallo *et al.*, "Inter-hemispheric coupling changes associate with motor improvements after robotic stroke rehabilitation," *Restorative neurology and neuroscience*, vol. 30, no. 6, pp. 497–510, 2012.

[31] R. Merletti and P. J. Parker, *Electromyography: physiology, engineering, and non-invasive applications*. John Wiley & Sons, 2004, vol. 11.

[32] M. Al-Faiz and Y. I. Al-Mashhadany, "Human arm movements recognition based on emg signal." 2009.

[33] A. M. Stewart, C. G. Pretty, M. Adams, and X. Chen, "Review of upper limb hybrid exoskeletons," *IFAC-PapersOnLine*, vol. 50, no. 1, pp. 15 169–15 178, 2017.

[34] N. Jarrassé, T. Proietti, V. Crocher, J. Robertson, A. Sahbani, G. Morel, and A. Roby-Brami, “Robotic exoskeletons: a perspective for the rehabilitation of arm coordination in stroke patients,” *Frontiers in human neuroscience*, vol. 8, p. 947, 2014.

[35] G.-x. Pan, H.-q. Fu, X.-f. Zhang, and F.-l. Ma, “Research on bionic mechanism of shoulder joint rehabilitation movement,” in *Wearable Sensors and Robots*. Springer, 2017, pp. 181–194.

[36] H. Yu, I. S. Choi, K.-L. Han, J. Y. Choi, G. Chung, and J. Suh, “Development of a upper-limb exoskeleton robot for refractory construction,” *Control Engineering Practice*, vol. 72, pp. 104–113, 2018.

[37] D. Sui, J. Fan, H. Jin, X. Cai, J. Zhao, and Y. Zhu, “Design of a wearable upper-limb exoskeleton for activities assistance of daily living,” in *2017 IEEE International Conference on Advanced Intelligent Mechatronics (AIM)*. IEEE, 2017, pp. 845–850.

[38] C.-L. Koh, S.-L. Pan, J.-S. Jeng, B.-B. Chen, Y.-H. Wang, I.-P. Hsueh, and C.-L. Hsieh, “Predicting recovery of voluntary upper extremity movement in subacute stroke patients with severe upper extremity paresis,” *PLoS One*, vol. 10, no. 5, p. e0126857, 2015.

[39] D. J. Smit, C. J. Stam, D. Posthuma, D. I. Boomsma, and E. J. De Geus, “Heritability of ‘small-world’ networks in the brain: A graph theoretical analysis of resting-state eeg functional connectivity,” *Human brain mapping*, vol. 29, no. 12, pp. 1368–1378, 2008.

[40] A. Sarasola-Sanz, N. Irastorza-Landa, E. López-Larraz, C. Bibián, F. Helmhold, D. Broetz, N. Birbaumer, and A. Ramos-Murguialday, “A hybrid brain-machine interface based on eeg and emg activity for the motor rehabilitation of stroke patients,” in *2017 International conference on rehabilitation robotics (ICORR)*. IEEE, 2017, pp. 895–900.

[41] F. S. Sarfo, U. Ulasavets, O. K. Opare-Sem, and B. Ovbiagele, “Tele-rehabilitation after stroke: an updated systematic review of the literature,” *Journal of Stroke and Cerebrovascular Diseases*, vol. 27, no. 9, pp. 2306–2318, 2018.

[42] T. Särkämö, "Music for the ageing brain: Cognitive, emotional, social, and neural benefits of musical leisure activities in stroke and dementia," *Dementia*, vol. 17, no. 6, pp. 670–685, 2018.

[43] M. Gandolfi, C. Geroin, C. Tomelleri, I. Maddalena, A. Picelli, N. Smania, A. Waldner *et al.*, "Feasibility and safety of early lower limb robot-assisted training in sub-acute stroke patients: a pilot study." *European journal of physical and rehabilitation medicine*, vol. 53, no. 6, pp. 870–882, 2017.

[44] Y. Zhou, Y. Fang, J. Zeng, K. Li, and H. Liu, "A multi-channel emg-driven fes solution for stroke rehabilitation," in *International Conference on Intelligent Robotics and Applications*. Springer, 2018, pp. 235–243.

[45] T.-J. Su, K.-L. Lo, J. S.-H. Tsai, W.-A. Yeh, and C.-F. Kuo, "A brunnstrom stage evaluation system with fuzzy-accelerometer," *Applied Sciences*, vol. 9, no. 18, p. 3718, 2019.

[46] M. A. Gull, S. Bai, and T. Bak, "A review on design of upper limb exoskeletons," *Robotics*, vol. 9, no. 1, p. 16, 2020.

[47] T. L. Nwe, F. S. Wei, and L. C. De Silva, "Speech based emotion classification," in *Proceedings of IEEE Region 10 International Conference on Electrical and Electronic Technology. TENCON 2001 (Cat. No. 01CH37239)*, vol. 1. IEEE, 2001, pp. 297–301.

[48] C. Padgett and G. W. Cottrell, "Representing face images for emotion classification," in *Advances in neural information processing systems*, 1997, pp. 894–900.

[49] J. J.-J. Lien, T. Kanade, J. F. Cohn, and C.-C. Li, "Detection, tracking, and classification of action units in facial expression," *Robotics and Autonomous Systems*, vol. 31, no. 3, pp. 131–146, 2000.

[50] T. Hu, L. C. De Silva, and K. Sengupta, "A hybrid approach of nn and hmm for facial emotion classification," *Pattern Recognition Letters*, vol. 23, no. 11, pp. 1303–1310, 2002.

[51] T. Baltrušaitis, D. McDuff, N. Banda, M. Mahmoud, R. El Kaliouby, P. Robinson, and R. Picard, "Real-time inference of mental states from facial expressions and upper body gestures," in *Face and Gesture 2011*. IEEE, 2011, pp. 909–914.

[52] H. Gunes and M. Piccardi, “Bi-modal emotion recognition from expressive face and body gestures,” *Journal of Network and Computer Applications*, vol. 30, no. 4, pp. 1334–1345, 2007.

[53] F. Agrafioti, D. Hatzinakos, and A. K. Anderson, “Ecg pattern analysis for emotion detection,” *IEEE Transactions on affective computing*, vol. 3, no. 1, pp. 102–115, 2011.

[54] G. L. Ahern and G. E. Schwartz, “Differential lateralization for positive and negative emotion in the human brain: Eeg spectral analysis,” *Neuropsychologia*, vol. 23, no. 6, pp. 745–755, 1985.

[55] M. Li and B.-L. Lu, “Emotion classification based on gamma-band eeg,” in *2009 Annual International Conference of the IEEE Engineering in medicine and biology society*. IEEE, 2009, pp. 1223–1226.

[56] Y.-P. Lin, C.-H. Wang, T.-P. Jung, T.-L. Wu, S.-K. Jeng, J.-R. Duann, and J.-H. Chen, “Eeg-based emotion recognition in music listening,” *IEEE Transactions on Biomedical Engineering*, vol. 57, no. 7, pp. 1798–1806, 2010.

[57] M. Murugappan, N. Ramachandran, Y. Sazali *et al.*, “Classification of human emotion from eeg using discrete wavelet transform,” *Journal of biomedical science and engineering*, vol. 3, no. 04, p. 390, 2010.

[58] X.-W. Wang, D. Nie, and B.-L. Lu, “Emotional state classification from eeg data using machine learning approach,” *Neurocomputing*, vol. 129, pp. 94–106, 2014.

[59] Y. Liu, O. Sourina, and M. K. Nguyen, “Real-time eeg-based human emotion recognition and visualization,” in *2010 international conference on cyberworlds*. IEEE, 2010, pp. 262–269.

[60] Q. Yuan, W. Zhou, S. Yuan, X. Li, J. Wang, and G. Jia, “Epileptic eeg classification based on kernel sparse representation,” *International journal of neural systems*, vol. 24, no. 04, p. 1450015, 2014.

[61] S. Aviyente, “Compressed sensing framework for eeg compression,” in *2007 IEEE/SP 14th workshop on statistical signal processing*. IEEE, 2007, pp. 181–184.

[62] Y. C. Eldar and G. Kutyniok, *Compressed sensing: theory and applications*. Cambridge university press, 2012.

[63] Z. Zhang, T.-P. Jung, S. Makeig, and B. D. Rao, "Compressed sensing of eeg for wireless telemonitoring with low energy consumption and inexpensive hardware," *IEEE Transactions on Biomedical Engineering*, vol. 60, no. 1, pp. 221–224, 2012.

[64] M. Islam, T. Ahmed, S. S. Mostafa, M. S. U. Yusuf, and M. Ahmad, "Human emotion recognition using frequency & statistical measures of eeg signal," in *2013 International Conference on Informatics, Electronics and Vision (ICIEV)*. IEEE, 2013, pp. 1–6.

[65] P. C. Petrantonakis and L. J. Hadjileontiadis, "Emotion recognition from eeg using higher order crossings," *IEEE Transactions on information Technology in Biomedicine*, vol. 14, no. 2, pp. 186–197, 2009.

[66] Y. Yuankui and Z. Jianzhong, "Recognition and analyses of eeg & erp signals related to emotion: from the perspective of psychology," in *Proceedings. 2005 First International Conference on Neural Interface and Control, 2005.* IEEE, 2005, pp. 96–99.

[67] R.-N. Duan, J.-Y. Zhu, and B.-L. Lu, "Differential entropy feature for eeg-based emotion classification," in *2013 6th International IEEE/EMBS Conference on Neural Engineering (NER)*. IEEE, 2013, pp. 81–84.

[68] R. M. Ravindran, "Classification of human emotions from eeg signals using filtering and anfis classifier," in *Second International Conference on Current Trends In Engineering and Technology-ICCTET 2014*. IEEE, 2014, pp. 113–119.

[69] H. Candra, M. Yuwono, R. Chai, A. Handojoseno, I. Elamvazuthi, H. T. Nguyen, and S. Su, "Investigation of window size in classification of eeg-emotion signal with wavelet entropy and support vector machine," in *2015 37th Annual international conference of the IEEE Engineering in Medicine and Biology Society (EMBC)*. IEEE, 2015, pp. 7250–7253.

[70] A. Bhardwaj, A. Gupta, P. Jain, A. Rani, and J. Yadav, "Classification of human emotions from eeg signals using svm and lda classifiers," in *2015 2nd International Conference on Signal Processing and Integrated Networks (SPIN)*. IEEE, 2015, pp. 180–185.

[71] D. Oude Bos, "Eeg-based emotion recognition-the influence of visual and auditory stimuli," *Capita Selecta (MSc course)*, 2006.

[72] C. A. Torres-Valencia, H. F. Garcia-Arias, M. A. A. Lopez, and A. A. Orozco-Gutiérrez, "Comparative analysis of physiological signals and electroencephalogram (eeg) for multimodal emotion recognition using generative models," in *2014 XIX Symposium on Image, Signal Processing and Artificial Vision*. IEEE, 2014, pp. 1–5.

[73] W.-L. Zheng, B.-N. Dong, and B.-L. Lu, "Multimodal emotion recognition using eeg and eye tracking data," in *2014 36th Annual International Conference of the IEEE Engineering in Medicine and Biology Society*. IEEE, 2014, pp. 5040–5043.

[74] S. Jirayucharoensak, S. Pan-Ngum, and P. Israsena, "Eeg-based emotion recognition using deep learning network with principal component based covariate shift adaptation," *The Scientific World Journal*, vol. 2014, 2014.

[75] T. Y. Chai, S. S. Woo, M. Rizon, and C. S. Tan, "Classification of human emotions from eeg signals using statistical features and neural network," in *International*, vol. 1, no. 3. Penerbit UTHM, 2010, pp. 1–6.

[76] M. F. Valstar and M. Pantic, "Combined support vector machines and hidden markov models for modeling facial action temporal dynamics," in *International workshop on human-computer interaction*. Springer, 2007, pp. 118–127.

[77] S. Koelstra, C. Muhl, M. Soleymani, J.-S. Lee, A. Yazdani, T. Ebrahimi, T. Pun, A. Nijholt, and I. Patras, "Deap: A database for emotion analysis; using physiological signals," *IEEE transactions on affective computing*, vol. 3, no. 1, pp. 18–31, 2011.

[78] G. Chen and T. T. Pham, *Introduction to fuzzy systems*. CRC Press, 2005.

[79] M. Murugappan, M. Rizon, R. Nagarajan, S. Yaacob, I. Zunaidi, and D. Hazry, "Eeg feature extraction for classifying emotions using fcm and fkm," *International journal of Computers and Communications*, vol. 1, no. 2, pp. 21–25, 2007.

[80] M. Glykas, *Fuzzy cognitive maps: Advances in theory, methodologies, tools and applications*. Springer, 2010, vol. 247.

[81] B. Kosko, "Fuzzy cognitive maps," *International journal of man-machine studies*, vol. 24, no. 1, pp. 65–75, 1986.

[82] M. van Vliet, K. Kok, and T. Veldkamp, "Linking stakeholders and modellers in scenario studies: The use of fuzzy cognitive maps as a communication and learning tool," *Futures*, vol. 42, no. 1, pp. 1–14, 2010.

[83] E. I. Papageorgiou and J. L. Salmeron, "A review of fuzzy cognitive maps research during the last decade," *IEEE Transactions on Fuzzy Systems*, vol. 21, no. 1, pp. 66–79, 2012.

[84] J. L. Salmeron, "Fuzzy cognitive maps for artificial emotions forecasting," *Applied Soft Computing*, vol. 12, no. 12, pp. 3704–3710, 2012.

[85] A. Hadid, M. Pietikainen, and T. Ahonen, "A discriminative feature space for detecting and recognizing faces," in *Computer Vision and Pattern Recognition, 2004. CVPR 2004. Proceedings of the 2004 IEEE Computer Society Conference on*, vol. 2. IEEE, 2004, pp. II–II.

[86] A. Phinyomark, P. Phukpattaranont, and C. Limsakul, "Feature reduction and selection for emg signal classification," *Expert systems with applications*, vol. 39, no. 8, pp. 7420–7431, 2012.

[87] S. Haufe, V. Nikulin, and G. Nolte, "Identifying brain effective connectivity patterns from eeg: performance of granger causality, dtf, pdc and psi on simulated data," *BMC Neuroscience*, vol. 12, no. 1, pp. 1–2, 2011.

[88] M. F. Pagnotta and G. Plomp, "Time-varying mvar algorithms for directed connectivity analysis: Critical comparison in simulations and benchmark eeg data," *PloS one*, vol. 13, no. 6, p. e0198846, 2018.

[89] J. Chiang, Z. J. Wang, and M. J. McKeown, "A generalized multivariate autoregressive (gmar)-based approach for eeg source connectivity analysis," *IEEE Transactions on Signal Processing*, vol. 60, no. 1, pp. 453–465, 2011.

[90] A. Atyabi, F. Shic, and A. Naples, "Mixture of autoregressive modeling orders and its implication on single trial eeg classification," *Expert systems with applications*, vol. 65, pp. 164–180, 2016.

[91] F. Babiloni, F. Cincotti, C. Babiloni, F. Carducci, D. Mattia, L. Astolfi, A. Basilisco, P. M. Rossini, L. Ding, Y. Ni *et al.*, "Estimation of the cortical functional connectivity with the multimodal integration of high-resolution eeg and fmri

data by directed transfer function," *Neuroimage*, vol. 24, no. 1, pp. 118–131, 2005.

[92] L. Astolfi, F. Cincotti, D. Mattia, M. G. Marciani, L. A. Baccala, F. de Vico Fallani, S. Salinari, M. Ursino, M. Zavaglia, L. Ding *et al.*, "Comparison of different cortical connectivity estimators for high-resolution eeg recordings," *Human brain mapping*, vol. 28, no. 2, pp. 143–157, 2007.

[93] A. Omidvarnia, M. Mesbah, J. M. O'Toole, P. Colditz, and B. Boashash, "Analysis of the time-varying cortical neural connectivity in the newborn eeg: A time-frequency approach," in *International Workshop on Systems, Signal Processing and their Applications, WOSSPA*. IEEE, 2011, pp. 179–182.

[94] D. B. West *et al.*, *Introduction to graph theory*. Prentice hall Upper Saddle River, 2001, vol. 2.

[95] D. J. Watts and S. H. Strogatz, "Collective dynamics of ‚Äòsmall-world‚Äônetworks," *nature*, vol. 393, no. 6684, pp. 440–442, 1998.

[96] P. H. Peckham and J. S. Knutson, "Functional electrical stimulation for neuromuscular applications," *Annu. Rev. Biomed. Eng.*, vol. 7, pp. 327–360, 2005.

[97] C. T. Freeman, A.-M. Hughes, J. H. Burridge, P. H. Chappell, P. L. Lewin, and E. Rogers, "A model of the upper extremity using fes for stroke rehabilitation," *Journal of biomechanical engineering*, vol. 131, no. 3, 2009.

[98] S. Harkema, Y. Gerasimenko, J. Hodes, J. Burdick, C. Angeli, Y. Chen, C. Ferreira, A. Willhite, E. Rejc, R. G. Grossman *et al.*, "Effect of epidural stimulation of the lumbosacral spinal cord on voluntary movement, standing, and assisted stepping after motor complete paraplegia: a case study," *The Lancet*, vol. 377, no. 9781, pp. 1938–1947, 2011.

[99] A. M. Jarc, M. Berniker, and M. C. Tresch, "Fes control of isometric forces in the rat hindlimb using many muscles," *IEEE Transactions on Biomedical Engineering*, vol. 60, no. 5, pp. 1422–1430, 2013.

[100] B. Sahyudi, W. Khairunizam, M. Majid, S. Vijayam, W. Mustafa, I. Zunaidi, S. Bakar, Z. Razlan, and H. Desa, "Investigation of upper limb movement for vr based post stroke rehabilitation device," in *2018 IEEE 14th International*

Colloquium on Signal Processing & Its Applications (CSPA). IEEE, 2018, pp. 52–56.

[101] A. Waksman, “A permutation network,” *Journal of the ACM (JACM)*, vol. 15, no. 1, pp. 159–163, 1968.

[102] H. Bhasin and N. Singla, “Genetic based algorithm for n-puzzle problem,” *International Journal of Computer Applications*, vol. 51, no. 22, 2012.

[103] A. Reinefeld, “Complete solution of the eight-puzzle and the bene t of node ordering in ida*,” in *International Joint Conference on Artificial Intelligence*. Citeseer, 1993, pp. 248–253.

[104] H. Shi, “Searching algorithms implementation and comparison of eight-puzzle problem,” in *Proceedings of 2011 International Conference on Computer Science and Network Technology*, vol. 2. IEEE, 2011, pp. 1203–1206.

[105] M. Kellmann, M. Bertollo, L. Bosquet, M. Brink, A. J. Coutts, R. Duffield, D. Erlacher, S. L. Halson, A. Hecksteden, J. Heidari *et al.*, “Recovery and performance in sport: consensus statement,” *Int J Sports Physiol Perform*, vol. 13, no. 2, pp. 240–245, 2018.

[106] J. E. Sullivan, B. E. Crowner, P. M. Kluding, D. Nichols, D. K. Rose, R. Yoshida, and G. Pinto Zipp, “Outcome measures for individuals with stroke: process and recommendations from the american physical therapy association neurology section task force,” *Physical therapy*, vol. 93, no. 10, pp. 1383–1396, 2013.

[107] A. Vourvopoulos, A. L. Faria, M. S. Cameirao, and S. B. i Badia, “Rehabnet: A distributed architecture for motor and cognitive neuro-rehabilitation,” in *2013 IEEE 15th International Conference on e-Health Networking, Applications and Services (Healthcom 2013)*. IEEE, 2013, pp. 454–459.

[108] T. Mulder, “Motor imagery and action observation: cognitive tools for rehabilitation,” *Journal of neural transmission*, vol. 114, no. 10, pp. 1265–1278, 2007.

[109] A. R. Fugl-Meyer, L. Jääskö, I. Leyman, S. Olsson, and S. Steglind, “The post-stroke hemiplegic patient. 1. a method for evaluation of physical performance.” *Scandinavian journal of rehabilitation medicine*, vol. 7, no. 1, p. 13, 1975.

[110] M. Jeannerod, “Mental imagery in the motor context,” *Neuropsychologia*, vol. 33, no. 11, pp. 1419–1432, 1995.

[111] C.-Y. Chen, C.-W. Wu, C.-T. Lin, and S.-A. Chen, "A novel classification method for motor imagery based on brain-computer interface," in *2014 International Joint Conference on Neural Networks (IJCNN)*. IEEE, 2014, pp. 4099–4102.

[112] A. J. Coutts and R. Duffield, "Validity and reliability of gps devices for measuring movement demands of team sports," *Journal of science and Medicine in Sport*, vol. 13, no. 1, pp. 133–135, 2010.

[113] B. E. Maki and W. E. McIlroy, "Cognitive demands and cortical control of human balance-recovery reactions," *Journal of Neural Transmission*, vol. 114, no. 10, pp. 1279–1296, 2007.

[114] L. A. Frey-Law, J. M. Looft, and J. Heitsman, "A three-compartment muscle fatigue model accurately predicts joint-specific maximum endurance times for sustained isometric tasks," *Journal of biomechanics*, vol. 45, no. 10, pp. 1803–1808, 2012.

[115] A. Park, J. Clare, V. Spicer, P. L. Brantingham, T. Calvert, and G. Jenion, "Examining context-specific perceptions of risk: exploring the utility of ‚Äúhuman-in-the-loop‚Äù simulation models for criminology," *Journal of experimental criminology*, vol. 8, no. 1, pp. 29–47, 2012.

[116] L. Peternel, N. Tsagarakis, D. Caldwell, and A. Ajoudani, "Robot adaptation to human physical fatigue in human–robot co-manipulation," *Autonomous Robots*, vol. 42, no. 5, pp. 1011–1021, 2018.

[117] F. Schettini, A. Riccio, L. Simione, G. Liberati, M. Caruso, V. Frasca, B. Calabrese, M. Mecella, A. Pizzimenti, M. Inghilleri *et al.*, "Assistive device with conventional, alternative, and brain-computer interface inputs to enhance interaction with the environment for people with amyotrophic lateral sclerosis: a feasibility and usability study," *Archives of physical medicine and rehabilitation*, vol. 96, no. 3, pp. S46–S53, 2015.

[118] S. M. Harrison, R. C. Whitton, C. E. Kawcak, S. M. Stover, and M. G. Pandy, "Evaluation of a subject-specific finite-element model of the equine metacarpophalangeal joint under physiological load," *Journal of Biomechanics*, vol. 47, no. 1, pp. 65–73, 2014.

[119] M. Pantic and L. J. M. Rothkrantz, "Automatic analysis of facial expressions: The state of the art," *IEEE Transactions on pattern analysis and machine intelligence*, vol. 22, no. 12, pp. 1424–1445, 2000.

[120] P. S. Holmes and D. J. Collins, "The pettlep approach to motor imagery: A functional equivalence model for sport psychologists," *Journal of applied sport psychology*, vol. 13, no. 1, pp. 60–83, 2001.

[121] K. K. Ang, C. Guan, K. S. G. Chua, B. T. Ang, C. Kuah, C. Wang, K. S. Phua, Z. Y. Chin, and H. Zhang, "A clinical study of motor imagery-based brain-computer interface for upper limb robotic rehabilitation," in *2009 annual international conference of the IEEE engineering in medicine and biology society*. IEEE, 2009, pp. 5981–5984.

[122] A. S. Aghaei, M. S. Mahanta, and K. N. Plataniotis, "Separable common spatio-spectral patterns for motor imagery bci systems," *IEEE Transactions on Biomedical Engineering*, vol. 63, no. 1, pp. 15–29, 2015.

[123] M. Vijayan and P. H. Reddy, "Stroke, vascular dementia, and alzheimer‚Äôs disease: molecular links," *Journal of Alzheimer's Disease*, vol. 54, no. 2, pp. 427–443, 2016.

[124] S. Liang, K.-S. Choi, J. Qin, W.-M. Pang, Q. Wang, and P.-A. Heng, "Improving the discrimination of hand motor imagery via virtual reality based visual guidance," *Computer methods and programs in biomedicine*, vol. 132, pp. 63–74, 2016.

[125] A. Lazaric, "Transfer in reinforcement learning: a framework and a survey," in *Reinforcement Learning*. Springer, 2012, pp. 143–173.

[126] T. S. Braver, J. L. Paxton, H. S. Locke, and D. M. Barch, "Flexible neural mechanisms of cognitive control within human prefrontal cortex," *Proceedings of the National Academy of Sciences*, vol. 106, no. 18, pp. 7351–7356, 2009.

[127] A. E. Leeper, K. Hsiao, M. Ciocarlie, L. Takayama, and D. Gossow, "Strategies for human-in-the-loop robotic grasping," in *Proceedings of the seventh annual ACM/IEEE international conference on Human-Robot Interaction*, 2012, pp. 1–8.

[128] A. P. Buccino, H. O. Keles, and A. Omurtag, “Hybrid eeg-fnirs asynchronous brain-computer interface for multiple motor tasks,” *PloS one*, vol. 11, no. 1, p. e0146610, 2016.